Dopamine and Serotonin Metabolism in Parkinsonian Models

Carmen de la Fuente Barrigon
UCL Great Ormond Street Institute of Child Health

Thesis submitted for the degree of Doctor of Philosophy (PhD) awarded by University College London (UCL).

Funded by Marie Skłodowska-Curie Actions of the European Union's Seventh Framework Programme (FP7).

APRIL 2018

I, Carmen de la Fuente Barrigon confirm that the work presented in this thesis is my own. Where information has been derived from other sources, I confirm that this has been indicated in the thesis.

Signed .....

Date .....

Dedico esta tesis a los pilares de mi vida.
A mis padres, Tomás y Marisa.
A mi hermana, Paloma.
A mi amor, Francesco.
Por vuestros sacrificios, paciencia, amor y apoyo
incondicionales que me hacen ser quien soy hoy.

Abstract

Parkinson's disease (PD) is a neurodegenerative disorder caused by loss of dopaminergic neurons in the substantia nigra. Different pathogenic mechanisms have been implicated, including loss of mitochondrial complex I function and dysfunction of lysosomal glucocerebrosidase (GBA1) (Neumann et al., 2009; Schapira et al., 1990). Also, it has been hypothesised that serotonin metabolism could be affected in these patients due to the number of enzymes shared by both pathways (Albizu et al., 2011). This thesis considers the potential involvement of complex I and GBA1 in PD using HPLC analysis of changes in the extracellular levels of the metabolites of dopamine and serotonin, and the expression and activity of the enzymes of the dopamine pathway. Using SH-SY5Y cells, complex I deficiency was modelled using rotenone, and GBA1 deficiency was modelled using conduritol B epoxide (CBE). Inhibition of mitochondrial complex I or GBA1 significantly increased extracellular concentrations of 3,4-dihydroxyphenylacetic acid (DOPAC) and 5-hydroxyindoleacetic acid (5-HIAA), direct products of the degradation by monoamine oxidase (MAO) of dopamine and serotonin respectively. These results suggest increased MAO activity, providing evidence for the involvement of impaired complex I or GBA1 activity in the dopamine deficiency seen in PD. As MAO produces hydrogen peroxide as a side-product, its increased activity could enhance the oxidative stress present in PD (Dias et al., 2013). Therefore, intracellular GSH levels were quantified to determine whether the antioxidant mechanisms were affected, but no changes were observed. In addition to the main project, I collaborated with a number of groups to study monoamine metabolism in parkinsonian models. Also, the glycoprofile of cerebrospinal fluid (CSF) of patients with and without impaired dopamine metabolism was studied to explore the possibility of using glycans as pathologic biomarkers.

Impact statement

This thesis has improved understanding in Parkinson's Disease (PD) pathogenic mechanisms. This has been achieved by demonstrating a common effect on dopamine metabolism when mitochondria or lysosomes are affected in a cellular model.

Parkinson's disease (PD) is the second most common neurodegenerative disorder and it is caused by loss of dopaminergic neurons in the substantia nigra. Although different mechanisms have been implicated in the pathogenesis of PD, e.g. loss of mitochondrial complex I function, dysfunction of lysosomal glucocerebrosidase (GBA1), the triggering cause is still unknown.

At UCL, a project called Training in Neurodegeneration, Therapeutics Intervention and Neurorepair (TINTIN) funded by Marie Curie Actions and European Union Seventh Framework Programme, aimed to research the relationship between two known organelles that are affected in PD and the cause of the disease symptoms, the loss of dopamine in the substantia nigra. To do so, changes in the release of dopamine and its metabolites by a cellular model were studied by high-performance liquid chromatography coupled to an electrochemical detector (ECD-HPLC). With this approach, a common effect on dopamine metabolism has been observed. These findings lead to a whole new academic project in which the effect of the different mechanisms that have been involved in the pathogenesis of PD is studied in order to understand the disease. If the common effect is confirmed in other cellular and animal models, these findings could lead to the involvement of pharmaceutical companies to develop a new therapy for the PD patients.

Table of Contents

CHAPTER 2

CHAPTER 6

MONOAMINE METABOLISM IN ANIMAL AND CELLULAR PARKINSONISM MODELS 153

CHAPTER 7

List of Figures

List of Tables

Abbreviations

3-MT	3-methoxytyramine
3-OMD	3-*O*-methyldopa
5-HIAA	5-hydroxyindoleacetic acid
5-HTP	5-hydroxytryptophan
AADC	aromatic L-amino acid decarboxylase
ALDH	aldehyde dehydrogenase
APTS	9-aminopyrene-1,4,6-trisulfonic acid
BDNF	brain-derived neurotrophic factor
BH2	7,8-dihydrobiopterin
BH4	tetrahydrobiopterin
CBE	conduritol B epoxide
CNS	central nervous system
COMT	catechol-*O*-methyl transferase
CSF	cerebrospinal fluid
CYP	cytochrome P450
DA	Dopamine
DAT	dopamine transporter

DBH	dopamine β-hydroxylase
DE	detector electrode
DHPR	dihydropteridine reductase
DMEM/F-12	Dulbecco's modified Eagle's medium/Ham's F-12 nutrient mixture
DOPAC	3,4-dihydroxyphenylacetic acid
DTDS	dopamine transporter deficiency syndrome
DTT	dithiothreitol
ECD	electrochemical detection
EDTA	ethylenediaminetetraacetic acid
eNOS	endothelial nitric oxide synthase
ETC	electron transport chain
FBS	foetal bovine serum
GAPDH	glyceraldehyde 3-phosphate dehydrogenase
GBA1	lysosomal glucocerebrosidase
GBA2	beta-glucosidase 2
GCH1	GTP cyclohydrolase 1
GD	Gaucher disease
GFRP	GTPCH feedback regulatory protein

GlcSph	Glucosylsphingosine
GSH	reduced glutathione
GSSG	oxidised glutathione
GSH	reduced glutathione
GTP	guanosine triphosphate
GTPCH	GTP cyclohydrolase 1
H_2O_2	hydrogen peroxide
HPLC	high-performance liquid chromatography
HRP	horseradish peroxidase
HVA	homovanillic acid
iGBA1	silenced lysosomal glucocerebrosidase
iNOS	inducible nitric oxide synthase
iPS cells	induced pluripotent stem cells
JNK	c-Jun N-terminal protein kinase
L-DOPA	L-3,4-dihydroxyphenylalanine
LRRK2	leucine-rich repeat kinase gene
MAO	monoamine oxidase
M-COMT	membrane-bound isomer of catechol *O*-methyl transferase

MPP+	1-methyl-4-phenylpyridinium
MPPP	1-methyl-4-phenyl-4-propionoxypiperidine
MPTP	1-methyl-4-phenyl-1,2,3,6-tetrahydropyridine
mRNA	messenger RNA
$NADP^+$	oxidised form of NADPH
NADPH	nicotinamide adenine dinucleotide phosphate
nNOS	neural nitric oxide synthase
NO	nitric oxide
NOS	nitric oxide synthase
NSD-1015	3-hydroxybenzylhydrazine
$O_2^{\cdot-}$	Superoxide
$OH^{\cdot}$	hydroxyl radical
$ONOO^-$	peroxynitrite
PARK2	parkin gene
PARK7	DJ-1 gene
PARK8	LRRK2 gene
PARK9	mutation of the transmembrane lysosomal P-type ATPase gene
PBS	Dulbecco's phosphate buffered saline

PCD	pterin-4-carbinolamine dehydratase
PINK1	PTEN-induced putative kinase 1
PD	Parkinson's disease
PLP	pyridoxal phosphate
PNK	pyridoxine kinase
PNMT	phenylethanolamine N-methyltransferase
PNO	pyridoxine oxidase
PNP	pyridoxine phosphate
PTEN	phosphatase and tensin homologue
PTPS	6-pyruvoyltetrahydropterin synthase
qBH2	7,8-dihydrobiopterin
qRT-PCR	quantitative reverse transcription polymerase chain reaction
RA	retinoic acid
RNA	ribonucleic acid
RNS	reactive nitrogen species
ROS	reactive oxygen species
SAH	S-adenosyl-L-homocysteine
SAM	S-adenosylmethionine

S-COMT	soluble isomer of catechol *O*-methyl transferase
SE	screening electrode
SEM	standard error of the mean
SNCA	α-synuclein gene
SR	sepiapterin reductase
TH	tyrosine hydroxylase
TINTIN project	Training in Neurodegeneration, Therapeutics Intervention and Neurorepair project
TPH	tryptophan hydroxylase
V-ATPase	vacuolar-type H^+-ATPase
VMAT2	vesicular monoamine transporter 2

Declaration of collaboration

I, Carmen de la Fuente Barrigon, carried out monoamine measurement and interpreted data. I also prepared samples, unless stated otherwise in the sample preparation of that model (section 6.2). The following groups provided the models:

- Zebrafish with mutated GTPCH by Dr Marcus Keatinge from Prof. Oliver Bandmann's group (University of Sheffield, Sheffield, UK).
- Media of DAT deficiency syndrome iPS cells by Dr Serena Barral from Dr Manju Kurian's group (UCL GOS Institute of Child Health, London, UK).
- DAT deficiency syndrome mice by Dr Joanne Ng from Dr Manju Kurian's group (UCL GOS Institute of Child Health, London, UK).
- DAT deficiency syndrome zebrafish by Dr Kimberley Reid from Prof Robert Harvey's group (UCL School of Pharmacy, London, UK).
- hDAT HEK-293 cell line by Dr Yasmina Marti from Prof. Patrick Schloos's group (Universität Mannheim, Mannheim, Germany).
- Media of shGBA1 SH-SY5Y cell line by Dr Maria Garcia-Gomez from Prof. Simon Heales' group (UCL GOS Institute of Child Health, London, UK).
- GD mice by Dr Giulia Massaro from Dr Ahad Rahim's group (UCL School of Pharmacy, London, UK).
- Media of differentiated SH-SY5Y cell line by Dr Maria Garcia-Gomez from Prof Simon Heales' group (UCL GOS Institute of Child Health, London, UK).

Finally, I should like to acknowledge Dr Csaba Varadi for his help and guidance in the analysis of CSF during my two weeks secondment in the National Institute for Bioprocessing Research and Training (NIBRT, Dublin, Ireland).

Acknowledgments

Starting a PhD in a strange city in a foreign country was one of the toughest choices I have ever made. I expected it to be life-changing. However, I did not anticipate that it would be the most satisfying and memorable experience of my life, both professionally and personally.

First of all, I would like to thank my supervisors Prof. Simon Heales and Dr Simon Eaton. Thank you to Simon Heales for giving me this opportunity. His scientific and clinical knowledge, as well as his capacity to balance all the projects he is involved in, have been an inspiration for learning and maturing as a researcher. From him I have learnt that being energetic, passionate and committed to our work is key to developing ideas and theories. Thank you to Simon Eaton for his patience when explaining theoretical aspects of different techniques and for his knowledge of HPLC troubleshooting that saved me so many times. From him I have developed curiosity and a desire to work in a lab that will never leave me. Personally, I could not be more grateful for having both as mentors. I would not have achieved this without their guidance, support and advice.

I would also like to thank colleagues who have been with me on this PhD journey, Aziza (already Dr Khabbush) and Mesfer (soon-to-be Dr Al Shahrani); and of course, the past and present post-docs, Dr Maria Garcia-Gomez and Dr Michael Orford. Thanks to Aziza, my tissue culture and desk companion, for listening to all my crazy ideas while tasting different cuisines as true foodies. To Mesfer for his chats and showing me a different way of seeing life. Thanks to Maria, my Spaniard sister, for her endless support and initial guidance through the culture of this at-that-time unknown country. And thanks to Michael, my 149 colleague, for his generosity and kindness, for always listening, advising and helping me in every way he could.

I would also like to thank Dr Simon Pope from the National Hospital for his patience in teaching and helping me with HPLC. Also, thanks to Dr Derek Burke for sharing with me all his knowledge and experience working with Gaucher disease. Many thanks also to all my collaborators: it has been a pleasure to have the opportunity to discuss results and theories with you all. Special thanks to Dr Manju Kurian and Dr Serena Barral for allowing me to use their western blotting and qRT-PCR facilities, as well as helping me with the immunostaining.

I would also like to thank all the people who, despite not sharing my lab-life, have been with me throughout, sharing laughter and tears. Especially my parents, Tomás and Marisa, for skyping with me, even when I was not in the best of moods, to cheer me up. Also, thanks to my sister, Paloma, for being as amazing as a person can be. Thanks for the year spent here in London, sharing lots of Sunday brunches, making 2017 the most special year of all. Finally, thanks to my love, Francesco, for his extraordinary capacity to calm me down and make me feel at home.

Last, but not least, I want to thank the Marie Curie Actions and European Union Seventh Framework Programme for funding this PhD within the Training in Neurodegeneration, Therapeutics Intervention and Neurorepair (TINTIN) project, and enabling me to meet wonderful members of the TINTIN family.

CHAPTER 1

Introduction

1.3.6. Dopamine Homeostasis

Dopamine acts as an extracellular signal in several tissues; for example, the brain and adrenal medulla, and is highly regulated both upstream and downstream. There are several diseases related to this pathway, either inherited or acquired, known collectively as parkinsonism. When first discovered at the beginning of the 20th century, dopamine was thought to be a precursor for noradrenaline (Iversen and Iversen, 2007). It was not until the 1960s that Dr Arvin Carlsson demonstrated that dopamine was not just a precursor but itself a neurotransmitter and won the Nobel Prize in Physiology and Medicine 2000 for this discovery. Today, it is known that dopamine is related to voluntary movement, reward-motivated behaviour and cognitive functions (Meiser et al., 2013). All these functions are deteriorated in PD patients due to degeneration of dopaminergic neurons.

1.3.7. Dopamine synthesis

Neuronal dopamine biosynthesis takes place in the substantia nigra pars compacta and ventral tegmental area. The classical biosynthesis pathway starts in the cytosol of dopaminergic neurons, where L-tyrosine is hydroxylated by tyrosine hydroxylase (TH) to produce L-3,4-dihydroxyphenylalanine (L-DOPA). TH has a requirement for tetrahydrobiopterin (BH4) as a cofactor. This first step is described as the rate-limiting reaction of dopamine synthesis. Subsequently, L-DOPA is decarboxylated by aromatic L-amino acid decarboxylase (AADC) to produce dopamine. AADC uses pyridoxal phosphate (PLP) as a cofactor ***(Figure 1.1)***. An alternative route can metabolise L-DOPA by catechol-*O*-methyl transferase (COMT), generating 3-*O*-methyldopa (3-OMD).

Several publications have proposed an alternative route for dopamine synthesis involving cytochrome P450 (CYP) (reviewed by Meiser et al., 2013). CYP is a multi-gene

family of monooxygenases known for their role in detoxifying natural toxins and pharmacological drugs (reviewed by Gopisankar, 2017). Via this parallel pathway, dopamine is synthesised from tyramine in the presence of nicotinamide adenine dinucleotide phosphate (NADPH) (Hiroi et al., 1998). Tyramine can be either endogenous, via tyrosine decarboxylation by AADC, or exogenous, from fermented food such as cheese and wine (Hiroi et al., 1998). Although this route was first described in hepatic microsomes of rat, it became a topic of interest in neurodegenerative diseases once its expression in non-hepatic tissues was established (reviewed by Gopisankar, 2017). Among all the isoforms, CYP2D6 has been reported to be the predominant isoform in the brain and to show the highest ability to synthesise dopamine (Hiroi et al., 1998; Wang et al., 2014). CYP2D6 messenger ribonucleic acid (mRNA) and protein have been reported to be expressed in several brain regions, and this enzyme would be more abundant in the cerebellum than in the substantia nigra (Miksys et al., 2002; Siegle et al., 2001). However, Siegle et al. (2001) reported that while CYP2D6 mRNA is expressed in both glial and neuronal cells, its protein was only detected in neurons. Differences in the glia:neuron ratio of these regions (Azevedo et al., 2009) could explain why CYP2D6 expression seemed lower in the substantia nigra (ratio glia/neurons = 11.35) compared to the cerebellum (ratio glia/neurons = 0.23). Nonetheless, CYP2D6 activity in the substantia nigra was reported as significantly higher than in other brain regions (Bromek et al., 2011). Although this pathway should be taken into consideration for further work, this thesis focuses on the classical pathway.

After its synthesis, dopamine is stored within pre-synaptic vesicles for release. Alternatively, noradrenergic neurons metabolise dopamine to noradrenaline by dopamine β-hydroxylase (DBH) ***(Figure 1.1)***. This enzyme requires the presence of ascorbate and O_2 to catalyse the hydroxylation. In adrenergic neurons, noradrenaline is methylated to produce adrenaline by phenylethanolamine *N*-methyltransferase (PNMT) ***(Figure 1.1)***,

which uses *S*-adenosylmethionine (SAM) as a methyl donor (reviewed by Meiser et al., 2013).

1.3.8. Dopamine neurotransmission

Due to dopamine instability at physiological pH, this neurotransmitter is internalised into synaptic vesicles by the vesicular monoamine transporter 2 (VMAT2) (Chaudhry et al., 2008). VMAT2 uses a proton gradient generated by the proton pump vacuolar-type H^+-ATPase (V-ATPase). Within these vesicles, the pH is two units lower than in the cytosol, so dopamine does not spontaneously oxidise (Guillot and Miller, 2009). VMAT2 exchanges two H^+ ions for one positively charged monoamine, reducing the neurotransmitter concentration and preventing oxidative stress in the cytosol (Alter et al., 2013). It has been reported that VMAT2 couples to AADC and TH, forming a complex (Cartier et al., 2010) that increases the efficiency of transport from the cytosol to the vesicles ***(Figure 1.2)***.

Once loaded, full vesicles move within the cell towards the pre-synaptic membrane ready for the signal to release dopamine. The synaptic vesicles are attached to the membrane by the soluble N-ethylmaleimide-sensitive factor (NSF) attachment protein receptor (SNARE) proteins, which are present in both vesicular and cellular membranes. These proteins form a complex that lead to a fast membrane fusion to efficiently release the neurotransmitter (reviewed by Chen and Scheller, 2001). Membrane depolarisation opens the voltage-gated Ca^{2+} channels and the resulting Ca^{2+} influx causes the membranes to approach one another, releasing dopamine. Once in the synaptic cleft, dopamine binds to receptors located on the post-synaptic membrane and triggers post-synaptic neuron depolarisation. It also binds to pre-synaptic receptors responsible for termination of the neurotransmitter signal, by both reuptake and degradation of dopamine.

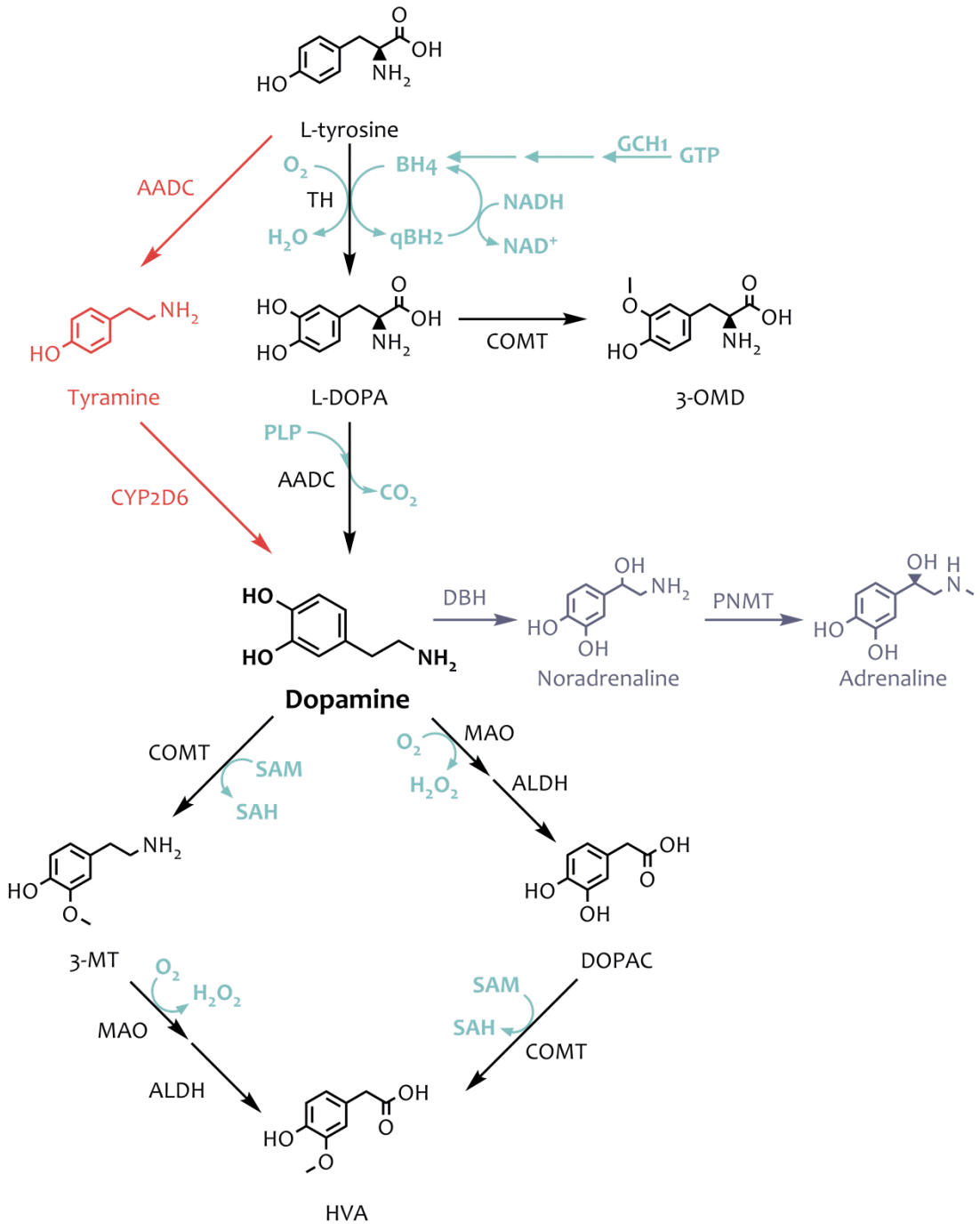

Figure 1.1 Dopamine pathway.
The classical pathway is shown in black and the alternative cytochrome-mediated pathway is shown in red. Pathway cofactors and the biosynthesis of those relevant for this project are shown in blue. Finally, the classical synthesis pathway of the other catecholaminergic neurotransmitters is shown in grey. 3-MT (3-methoxytyramine), 3-OMD (3-O-methyldopa), AADC (aromatic L-amino acid decarboxylase), ALDH (aldehyde dehydrogenase), BH4 (tetrahydrobiopterin), COMT (catechol-O-methyl transferase), CYP2D6 (cytochrome P450 2D6), DBH (dopamine β-hydroxylase), DOPAC (3,4-dihydroxyphenylacetic acid), GCH1 (GTP cyclohydrolase 1), HVA (homovanillic acid), L-DOPA (L-3,4-dihydroxyphenylalanine) MAO (monoamine oxidase), PLP (pyridoxal phosphate), PNMT (phenylethanolamine N-methyltransferase), qBH2 (7,8-dihydrobiopterin), SAH (S-adenosyl-L-homocysteine), SAM (S-adenosylmethionine), TH (tyrosine hydroxylase).

1.3.9. Dopamine recycling and degradation

Dopamine must be removed from the synaptic cleft before the arrival of the next nerve impulse. For that purpose, the pre-synaptic neuron captures the released dopamine ***(Figure 1.2)***. This reuptake is driven by the dopamine transporter (DAT) (Nishida et al., 2008; reviewed by Eriksen et al., 2010). It has been described that DAT is not present within the synaptic cleft, so the dopamine must diffuse from the synapse to the transporter before being sequestered (Nirenberg et al., 1996). As in the synaptic vesicles, endocytosis of dopamine depends on an electrochemical gradient generated by the plasma membrane Na^+/K^+ ATPase (Torres et al., 2003). The transport of dopamine from the synaptic cleft to the cytosol co-transports two Na^+ ions and one Cl^- ion. A two-step process then takes place to recycle the dopamine: firstly, dopamine is stored in synaptic vesicles by VMAT2; and, secondly, the vesicles approach the neuron's pre-synaptic end.

Although in physiological conditions, dopamine reuptake is the mechanism by which the neurotransmitter is cleared from the synaptic cleft (Espinoza et al., 2012), the non-recycled neurotransmitter can be degraded by both neurons and glial cells ***(Figure 1.2)***. Dopamine is metabolised on two parallel pathways (reviewed by Meiser et al., 2013). On the first pathway, monoamine oxidase (MAO) and aldehyde dehydrogenase (ALDH) metabolise dopamine to 3,4-dihydroxyphenylacetic acid (DOPAC). Then, COMT metabolises DOPAC to homovanillic acid (HVA). On the second pathway, COMT metabolises dopamine to 3-methoxytyramine (3-MT), which is then metabolised to HVA by consecutive action of MAO and ALDH ***(Figure 1.1 and Figure 1.2)***.

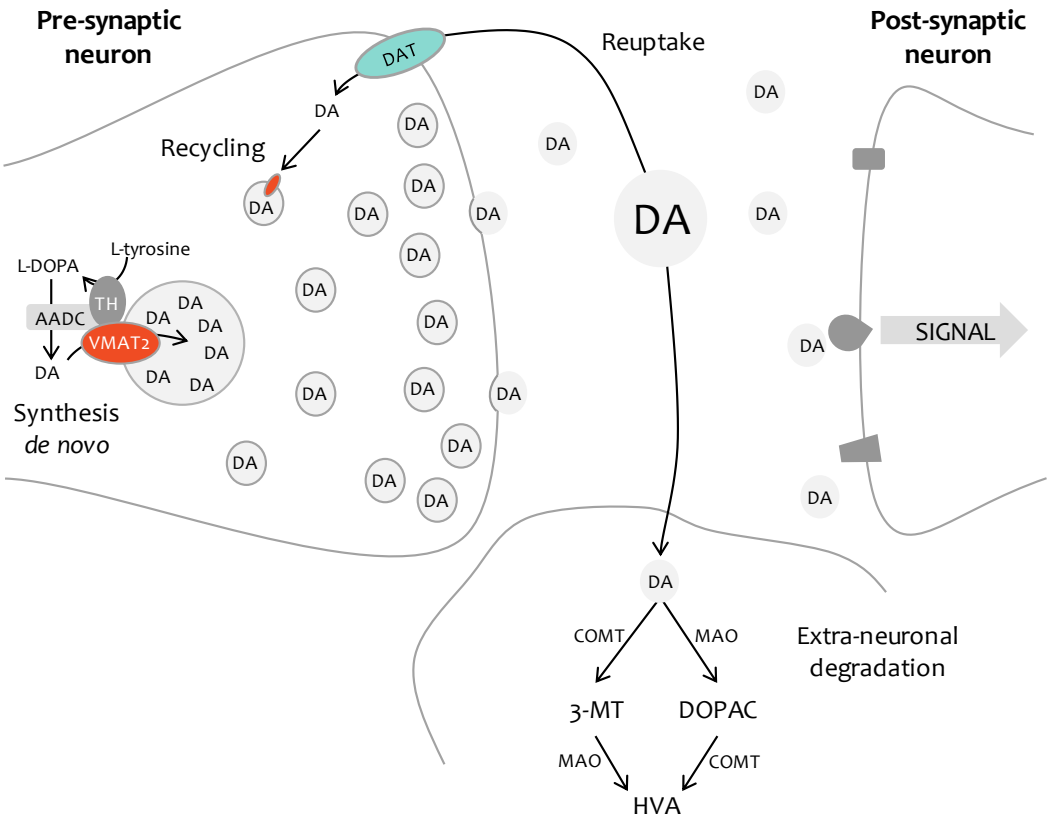

Figure 1.2 Dopamine recycling and degradation.
Dopamine is synthesised in the pre-synaptic terminal, where the enzymes TH and AADC are coupled to the vesicular transporter VMAT2. The full vesicles move towards the pre-synaptic membrane ready for the signal to release dopamine. After the signal, dopamine has to be removed from the synaptic cleft. It can either undergo reuptake by the DAT and be recycled, or it is degraded by the consecutive action of MAO and COMT by both neurons and glial cells.

The degradation enzymes are essential for the regulation of dopamine neurotransmission. Two of the three enzymes involved in this degradation, MAO and COMT, are notable for their importance in regulation of neurotransmitter turnover. Initially, MAO oxidises dopamine and 3-MT to aldehydes. This reaction requires flavin adenine dinucleotide as a cofactor and produces hydrogen peroxide (H_2O_2). The corresponding aldehydes are rapidly oxidised to DOPAC and HVA respectively. MAO exists in two isoforms, MAO-A and MAO-B, which are encoded by two different genes. Although structurally diverse, both are mainly located in the outer mitochondrial membrane and catalyse the same reaction. While MAO-A principally catalyses

noradrenaline and serotonin, MAO-B principally has dopamine and 3-MT as substrates, producing DOPAC and HVA respectively (reviewed by Ng et al., 2014). COMT, with Mg^{2+} as a cofactor, catalyses the transfer of a methyl group from SAM to the hydroxyl groups of dopamine and DOPAC. This reaction generates 3-MT and HVA respectively. COMT can also be found in two isoforms but, in this case, both are encoded by the same gene. One isoform is soluble and can be found in the cytoplasm of glial and peripheral cells. The second isoform is membrane bound and is predominantly present in neurons, attached to the rough endoplasmic reticulum. This second isoform shows more affinity for catecholamines but lower capacity (Mannisto and Kaakkola, 1999).

1.3.10. Toxicity derived from dopamine metabolism

Despite dopamine being rapidly sequestered into vesicles after its synthesis or its reuptake, some leakage from vesicles can occur (Meiser et al., 2013). If dopamine accumulates in the cytosol, it can either be degraded or autooxidise (reviewed by Munoz et al., 2012). As described in section 1.3.9, dopamine degradation is an oxidative process as MAO produces H_2O_2 as a by-product. H_2O_2 is a reactive oxygen species (ROS) that is detoxified by antioxidant enzymes known as peroxidases to produce water. Although it is widely accepted that ROS have a signalling role, some of them; for example, hydroxyl radicals, are more likely to react with and oxidise other cellular components (Schieber and Chandel, 2014). While H_2O_2 is only a weak pro-oxidant, it can produce more reactive ROS by Fenton reactions (***Figure 1.3***). Therefore, dopamine metabolism is a natural source of ROS that could be enhanced in pathological conditions in which dopamine turnover is altered.

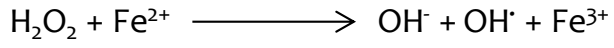

Figure 1.3 Fenton reaction.
H_2O_2 in the presence of a ferrous ion (Fe^{2+}) results in a hydroxyl radical and a hydroxide ion (OH^- and $OH^\bullet$) in conjunction with a ferric ion (Fe^{3+}).

Cytosolic dopamine and some of its metabolites can also produce highly oxidative molecules (reviewed by Munoz et al., 2012). Dopamine and DOPAC can be spontaneously oxidised at cytosolic pH to dopamine-quinones and semi-quinones by metal-catalysis. This pathway comprises three main steps (***Figure 1.4***): (I) dopamine is oxidised by metals, ROS and oxygen, producing semi-*o*-quinones and *o*-quinones; (II) physiological pH leads to the cyclisation of these dopamine *o*-quinones into aminochrome; and (III) two molecules of aminochrome combine to form neuromelanin (Graumann et al., 2002). The first step, i.e. dopamine-*o*-quinone formation, can be achieved in three ways. The first comprises two consecutive single e^- oxidations (***Figure 1.4***, steps (1) and (3)), forming an intermediate molecule, the dopamine-*o*-semiquinone radical. The second involves this intermediate. The combination of two *o*-semiquinone radicals (***Figure 1.4***, step (2)) produces one molecule of dopamine and one of dopamine-*o*-quinone. The third is a two e^- oxidation of dopamine, which produces dopamine-o-quinone in one step (***Figure 1.4***, step (4)).

Dopamine-quinones are the precursors of aminochrome (Munoz et al., 2012), a potentially harmful molecule that can interact with several essential proteins and organelles altering correct cellular function ***(Figure 1.4)***. Some examples are mitochondrial complexes I and III of the electron transport chain (ETC), α-synuclein and α/β-tubulin (reviewed by Munoz et al., 2012). This suggests that aminochrome could induce mitochondrial dysfunction, oxidative stress and, consequently, neurotoxicity.

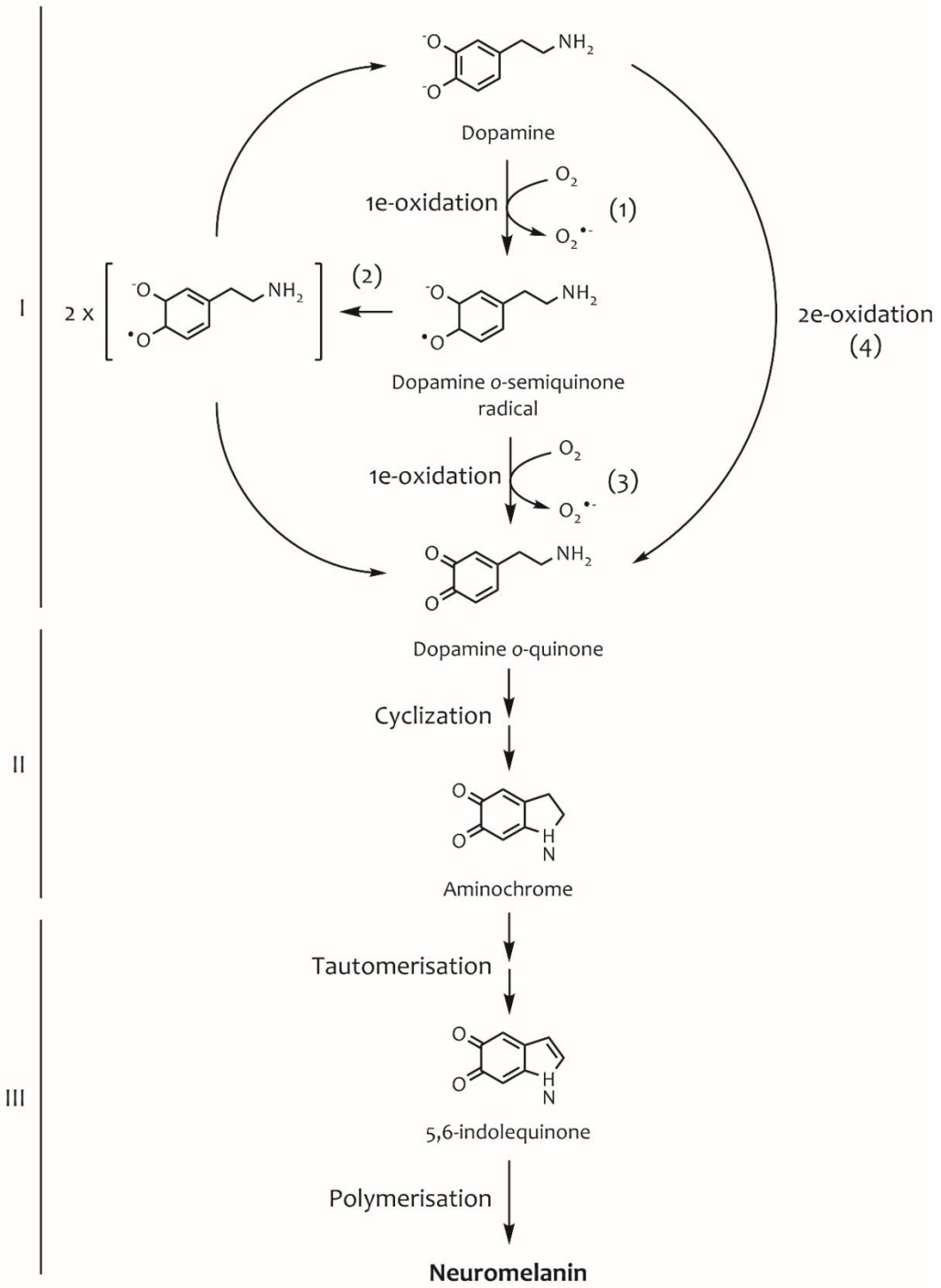

Figure 1.4 Dopamine oxidation.
Dopamine at cytosolic pH can undergo oxidation via a three-step pathway: (I) formation of dopamine-o-quinone, (II) cyclization to aminochrome, and (III) formation of neuromelanin. Dopamine oxidation to quinone can be achieved in three ways: a two-step one e^- oxidation (1 and 3), a one-step two e^- oxidation (4) and a two-dopamine-o-semiquinone association (2).

Aminochrome can form aggregates with different proteins or be phagocytised and stored in vacuoles as neuromelanin. The physiological role of neuromelanin is still unclear. However, some theories propose a neuroprotective physiological role that can become neurodegenerative in a pathological environment (Gerlach et al., 2003). The neuroprotective function could be via action as an iron chelator reducing the progress of Fenton reaction; but when there is an excessive accumulation, neuromelanin deposits would be degraded resulting in the sudden release of the stored iron (Gerlach et al., 2003). It has also been proposed that neuromelanin production could be a consequence of cytosolic dopamine accumulation, in order to sequester free dopamine and decrease its presence in the cytosol (Sulzer et al., 2000).

1.3.11. Dopamine-related pathways

Dopamine metabolism is closely related to serotonin synthesis and degradation, as the pathways share some enzymes ***(Figure 1.5)***. Serotonin synthesis starts with the hydroxylation of L-tryptophan by tryptophan hydroxylase (TPH) and the cofactor BH4. This reaction is the rate-limiting step in this pathway and produces 5-hydroxytryptophan (5-HTP), which is serotonin's immediate precursor. 5-HTP is decarboxylated by AADC with PLP as cofactor, synthesising serotonin. As with dopamine, serotonin needs to be quickly degraded after its action. To accomplish this, MAO oxidises serotonin to 5-hydroxyindoleacetic acid (5-HIAA), its final degradation metabolite.

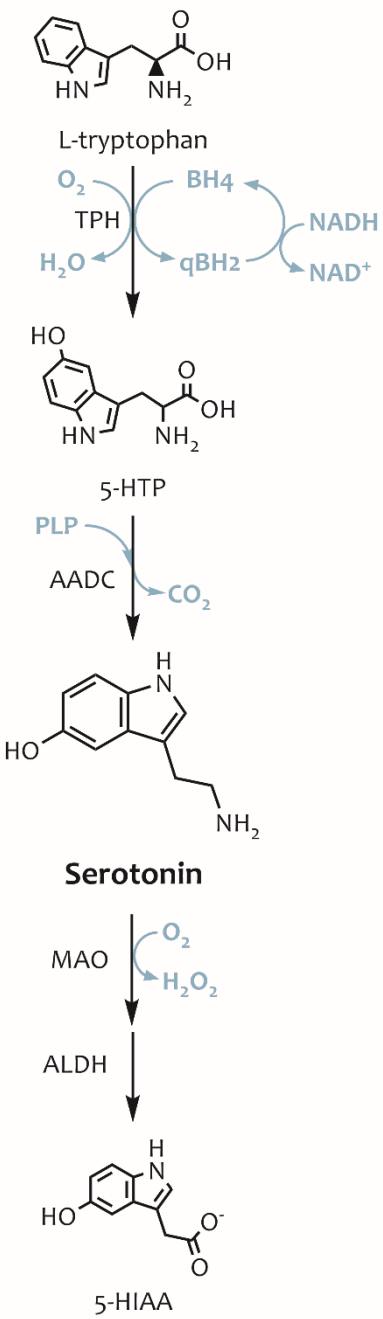

Figure 1.5 Serotonin pathway.
The serotonin synthesis pathway (black) shares most of the enzymes with the dopamine pathway. Pathway cofactors and the biosynthesis of those relevant for this project are shown in blue. 5-HIAA (5-hydroxyindoleacetic acid), 5-HTP (5-hydroxytryptophan), AADC (aromatic L-amino acid decarboxylase), ALDH (aldehyde dehydrogenase), BH4 (tetrahydrobiopterin), MAO (monoamine oxidase), PLP (pyridoxal phosphate), qBH2 (7,8-dihydrobiopterin), TPH (tryptophan hydroxylase).

While most of the enzymes involved in this pathway are also present in the dopamine pathway, TPH is distinct from TH. TPH, TH and phenylalanine hydroxylase all belong to the biopterin-dependent aromatic amino acid hydroxylase family. The three enzymes are structurally and functionally related, as they drive the same reaction using the same cofactor, BH4. As TH and TPH are tetramers, Mockus et al. (1997) proposed a possible heterotetramerisation including TH and TPH subunits. However, later studies reported that these enzymes do not form heterotetramers (Mockus et al., 1998). More than a decade later, Albizu et al. (2011) proposed a possible crosstalk between dopamine and serotonin pathways through the heteromerisation of dopamine and serotonin receptors. Due to limited knowledge and potential new therapeutic approaches, this possible crosstalk has been attracting increasing attention in recent years.

1.2. Enzymes and Cofactors of the Dopamine Pathway

Dysregulation of the dopamine pathway enzymes could be a cause or a consequence of the events described in PD. Indeed, several studies have focused on studying the structure of these enzymes and the regulatory mechanisms that could affect their expression or activity (Hadjiconstantinou and Neff, 2008; Mannisto and Kaakkola, 1999; Daubner et al., 2011; Youdim and Bakhle, 2006). In addition, knowing how cells react to changes in L-DOPA and dopamine concentration in physiological and pathological conditions could be fundamental for a better understanding of PD and its treatment. A brief summary of what is known about the enzymes of the dopamine pathway relevant for this thesis is described below.

Tyrosine hydroxylase (TH)

TH comprises four identical and catalytically active subunits coded by a single gene (reviewed by Daubner et al., 2011; Meiser et al., 2013). Each contains an N-terminal regulatory domain, a catalytic site and a C-terminal leucine zipper domain, and there are four isomers due to alternative splicing of the first domain. The leucine zipper domain is essential for tetramer assembling and it has been reported that the enzymatic activity decreases by 70% when it is not formed (Vrana et al., 1994). As described above, TH catalyses the first and rate-limiting step of dopamine synthesis ***(Figure 1.1)***. TH activity is highly regulated (reviewed by Daubner et al., 2011). Each subunit requires BH4, Fe^{2+} and O_2 to convert L-tyrosine into L-DOPA. In addition, TH can be phosphorylated and dephosphorylated in various positions, changing its activity rates and affinity for the substrates and cofactors (Daubner et al., 2011). For instance, phosphorylation of its serine in position 40 increases TH enzymatic activity 20-fold. Some studies report that TH can be inactivated by dephosphorylation through the action of nitric oxide synthase (NOS) and *S*-thiolation (Daubner et al., 2011). This is of special interest, as in PD the levels of oxidative species are increased in the brain (Dias et al., 2013). It has been proposed that TH stability could also be controlled by protein–protein interactions: the TH N-terminal regulatory domain forming complexes such as the TH, AADC and VMAT2 association (Cartier et al., 2010). This increase in stability could be due to decreased degradation via the ubiquitin-proteasome system, as the lysine target might be in the N-terminus. Catecholamines compete with BH4 for the Fe^{2+} in the active site of TH, negatively regulating its enzymatic activity (Meiser et al., 2013); this negative feedback is functional even when TH forms complexes.

1.2.12. Aromatic L-amino acid decarboxylase (AADC)

The regulation of catecholamine synthesis at the level of AADC is not completely understood (Berry et al., 1996). A number of theories have been proposed, but no consensus has been reached. It is thought that long-term regulation could occur via transcriptional changes, and that short term regulation occurs as a result of post-translational changes in enzymatic activity (Meiser et al., 2013). The *AADC* gene can exhibit alternative promoter usage and splicing that is species- and tissue-specific (Zhu and Juorio, 1995). It has also been proposed that dopamine, its precursors and its receptors could have a regulatory function in AADC enzymatic activity (Hadjiconstantinou and Neff, 2008; Lovenberg et al., 1962).

1.2.13. Catechol *O*-methyl transferase (COMT)

COMT transfers activated methyl groups from SAM to catechol-hydroxyl groups. There are two isoforms coded by the same gene: soluble (S-COMT) and membrane-bound (M-COMT). While S-COMT is found in the cytosol of glial cells and periphery, M-COMT is found in the rough endoplasmic reticulum and is prevalent in neurons (Espinoza et al., 2012). Both isoenzymes are dependent on Mg^{2+}, and although it has been reported that there is no COMT activity in the dopaminergic neurons of the substantia nigra, M-COMT shows a high affinity for catecholamines and is mainly responsible for their metabolism originated by dopaminergic and adrenergic neurotransmission (reviewed by Mannisto and Kaakkola, 1999). Conversely, it has been described that S-COMT is responsible for metabolism of exogenous catecholamines. While some studies have described single-nucleotide polymorphisms related to a lower enzymatic activity in PD, others have linked these polymorphisms to the response to PD treatment (Chen et al. 2004; Hernan et al.; 2002; Tunbridge, 2010). However, most groups conclude that there is no relationship between COMT polymorphisms and PD (reviewed by Jimenez-Jimenez et al., 2014).

1.2.14. Monoamine oxidase (MAO)

MAO catalyses the oxidative deamination of catecholamines to aldehydes, generating H_2O_2. This enzyme is present in both the central nervous system (CNS) and peripheral tissues. Within the CNS, MAO can be found in neurons, microglia and astrocytes. MAO occurs in two isoforms: MAO-A and MAO-B, coded for by two different genes (Youdim and Bakhle, 2006). Both isoforms are located in the outer mitochondrial membrane. The different isoforms have different affinity to substrates, although both can catalyse dopamine (Youdim and Bakhle, 2006). Neurons in the substantia nigra show a decreased MAO presence compared to that in other neurons or glial cells. In PD, MAO-B inhibition has been reported to improve motor and non-motor symptoms. In fact, a wide range of MAO-B inhibitors is used clinically; for example, selegiline and rasagiline are both irreversible MAO-B inhibitors used to decrease motor fluctuations after L-DOPA treatment (Riederer and Laux, 2011). Conversely, MAO-A inhibitors were quickly excluded because of side effects, such as hypertensive interaction with dietary tyramine (Anderson et al., 1993).

1.2.15. Tetrahydrobiopterin (BH4)

BH4 is a cofactor for several enzymatic processes involving amino acids ***(Figure 1.1)***. This cofactor is synthesised both in the liver and in the brain by *de novo* and salvage pathways (Kapatos, 2013; Longo, 2009). BH4 *de novo* classical synthesis in the brain starts with the transformation of GTP to 7,8-dihydroneopterin triphosphate by GTP cyclohydrolase 1 (GTPCH), the rate-limiting enzyme of the pathway. Then, 7,8-dihydroneopterin triphosphate is converted to 6-pyruvoyltetrahydropterin by 6-pyruvoyltetrahydropterin synthase (PTPS). Lastly, 6-pyruvoyltetrahydropterin is reduced three consecutive times by the enzyme sepiapterin reductase (SR) to finally yield BH4. When BH4 acts as a cofactor, it loses electrons resulting in its oxidised derivative 7,8-

dihydrobiopterin (BH2) (Longo, 2009). BH2 can revert to BH4 via two consecutive steps catalysed by pterin-4-carbinolamine dehydratase (PCD) and dihydropteridine reductase (DHPR) with the consumption of NADH.

As BH4 synthesis is key to maintain monoamine neurotransmission, GTPCH activity could be essential for the activity of TH and the production of dopamine in nigrostriatal neurons (Kapatos, 2013; Kurian et al., 2011a). This enzyme is coded for by one gene, *GCH1*, with three splicing variants, although only one has been reported as catalytically active. GTPCH is expressed in a tissue-specific manner with increased mRNA expression in serotoninergic neurons (Kapatos, 2013; Kurian et al., 2011a). As for other enzymes, it is regulated by its own product: BH4 promotes the expression of GTPCH feedback regulatory protein (GFRP), which, in turn, inhibits GTPCH (Kapatos, 2013). This enzyme can also interact with other proteins as a regulatory mechanism; for example, it has been proposed that phosphorylated GTPCH can interact with activated TH, preventing BH4-mediated GTPCH inhibition (Kapatos, 2013). Previous studies have proposed that carriers of rare *GCH1* variants show a higher risk of developing PD as a result of dopamine depletion and increased predisposition to cell loss (Mencacci et al., 2014). BH4 deficiency can also result from impairment of other enzymes on the biopterin pathway (Longo, 2009). While mutations affecting PTPS are the most frequent of the pterin metabolism disorders, mutations affecting DHPR cause the most severe phenotypes with lower success in treatment (Longo, 2009). In all cases, early diagnosis of mutations by analysis of neurotransmitters and/or biopterins in the urine and cerebrospinal fluid (CSF) of patients is key before starting treatment and to avoid phenotypical consequences of BH4 deficiency; for example, mental retardation (Longo, 2009; Ormazabal et al., 2006).

1.2.16. Pyridoxal phosphate (PLP)

PLP is the active form of vitamin B_6 and acts as a cofactor in several cytosolic processes; for example, AADC activity (Percudani and Peracchi, 2003). As a vitamin, B_6 levels in humans are dependent upon dietary absorption. Two B_6 transport systems have been described, requiring absorption of unphosphorylated B_6 vitamers or directly as PLP (Whittaker, 2016). Therefore, another event key in the utilisation of exogenous B_6 vitamers is cellular ability to convert the vitamin into PLP. Vitamers must first be phosphorylated by pyridoxine kinase (PNK) to pyridoxine phosphate (PNP). PNP is membrane-impermeable and is therefore trapped in the cytosol. PNP is then oxidised by pyridoxine oxidase (PNO) to form PLP.

Vitamin B_6 deficiency can be caused by poor dietary absorption, limited cellular internalisation, impaired conversion to PLP and/or limited intracellular PLP trafficking (Percudani and Peracchi, 2003). A wide range of enzymes require PLP as a cofactor; for example, AADC in cytosol and in heme biosynthesis in mitochondria. Consequently, deficiency in vitamin B_6 or PLP has been associated with several disorders, including epilepsy and neurodegenerative diseases (Whittaker, 2016).

1.3. Parkinson's Disease

PD is the second most common neurodegenerative disease and mainly affects the motor system. This disease is a chronic and progressive disorder characterised by the following four symptoms: tremor, rigidity, bradykinesia and postural instability. Despite the great amount of research in the field, the initial cause is unknown. Currently, PD therapies provide temporary relief of motor symptoms, but none stops the progression of neurodegeneration. Therapies comprise administration of dopamine precursors; for

example, L-DOPA, or inhibitors of dopamine-degradation enzymes; for example, MAO inhibitors. It is widely accepted that PD patients present loss of dopaminergic neurons in the substantia nigra (Dauer and Przedborski, 2003), loss of mitochondrial complex I activity (Betarbet et al., 2000), autophagy dysfunction (Lynch-Day et al., 2012) and impaired protein degradation and abnormal protein deposits (Beyer, 2007). Altogether, these result in dopamine deficiency, increased oxidative stress and α-synuclein accumulation forming Lewy bodies (Beyer, 2007). These events have been extensively studied in both cellular and animal models, including analysis of their role in neurodegeneration (Hauser and Hastings, 2013; Fujita et al., 2014). Several gene mutations have been identified in familial PD patients, some have also been found in spontaneous PD patients with no familial history of parkinsonism; for example, mutation in the *parkin* gene (Dauer and Przedborski, 2003). It is of note that historically, in the search for the initial cause of PD, most of these events have been studied individually. Recently, a multi-causal theory has been proposed to explain the triggering of PD (Fujita et al., 2014). Prior to this, very little has been reported that relates these episodes to dopamine or its metabolism (Burbulla et al., 2017). This is surprising given that absence of dopamine is the cause of PD symptoms and is the deficiency being treated. None of the studies published have answered the question that always arises: what do dopaminergic neurons have that makes them vulnerable to the development of selective neurodegeneration characteristics of PD?

1.2.1. PD and dopamine

Increasing the dopamine levels in the brains of PD patients can ameliorate the symptoms. Because dopamine is unable to cross the blood–brain barrier, L-DOPA is used as symptomatic treatment in PD and L-DOPA-responsive dystonia. L-DOPA is the immediate dopamine precursor and can cross the blood–brain barrier. To avoid peripheral

metabolism of L-DOPA decreasing the concentration that reaches the brain, and to prevent the peripheral action of dopamine, treatment with L-DOPA is combined with AADC inhibitors such as carbidopa. Rasagiline (*N*-propargyl-1 R-aminoindan), an irreversible MAO-B inhibitor, is used as a monotherapy in early stages of PD to increase the half-life of dopamine; and in combined therapy along with L-DOPA in more advanced cases (Mandel et al., 2005). In addition, and as a side effect, it has been reported that rasagiline has a neuroprotective role in both cellular and animal PD models (Youdim et al., 2004), suppressing the mitochondrial apoptosis cascade (Youdim and Weinstock, 2001) and increasing the expression of anti-apoptotic genes (Akao et al., 2002).

The use of MAO inhibitors was first thought to increase the half-life of dopamine in the brains of those PD patients with a decreased number of dopaminergic neurons. However, this treatment could have more relevance than initially anticipated as subsequent studies have reported increased enzymatic activity of this enzyme in the substantia nigra of post-mortem PD brains (Birkmayer et al., 1975; Sai et al., 2008). Inhibiting the activity of this enzyme would also result in lower H_2O_2 production and decreased dopamine-metabolism-derived oxidative stress. The inhibition of COMT has been used to increase L-DOPA and dopamine half-life (Ruottinen and Rinne, 1998). COMT inhibitors are specific and reversible and can target the enzyme both peripherally and/or centrally, depending on their ability to cross the blood–brain barrier.

Paradoxically, increasing dopamine availability could be detrimental for the neurons. Either dopamine degradation or accumulation could increase the stress levels of the cells: dopamine degradation produces H_2O_2 and its accumulation in cytosol could lead to dopamine oxidation as described in section 1.3.10. Indeed, one possible explanation for the high levels of oxidative stress in dopaminergic neurons could be dopamine itself as it is potentially oxidant in several ways. Also, neurons are post-mitotic cells with an

increased oxidative environment and limited antioxidant availability, which make them more vulnerable to oxidative stress (Heales and Bolanos, 2001; Sian et al.; 1994; Heales et al., 1997). Recent publications on the use of dopaminergic neurons derived from induced pluripotent stem (iPS) cells of PD patients report that dopamine oxidation could be an early event in disease development leading to the dysfunction of mitochondrial complex I and lysosomal glucocerebrosidase (GBA1) (Burbulla et al., 2017). Oxidised dopamine could directly inhibit mitochondrial complex I activity as proposed by Aguirre et al. (2012). This study also reported changes in the expression of iron transporters after exposure to aminochrome, leading to increased iron uptake. Altogether, this would enhance ROS production and hydroxyl radical synthesis by Fenton reaction, both events characteristic of PD. Although it is thought that neuromelanin might be initially protective (see section 1.3.10), it can interact with lipids, proteins and Fe^{2+} (Double et al., 2002), which could be detrimental if the aggregate accumulates.

Lastly, monoamine neurotransmitter disorders are rare inherited neurometabolic syndromes characterised by dysfunction or absence of any of the proteins involved in dopamine synthesis and homeostasis. Deficiency of either the enzymes TH or AADC, or the cofactors BH4 or PLP, results in dopamine deficiency. Transporter deficiency produces changes in dopamine homeostasis. VMAT2 deficiency affects dopamine packaging for synaptic transmission, while DAT deficiency depletes dopamine recycling (Kurian et al., 2011b). The diagnosis of most of these disorders takes place during childhood, as these syndromes lead to neurological, developmental and motor disorders (reviewed by Ng et al., 2014).

1.2.2. PD and mitochondria

Mitochondria are both the source and target of ROS. The ETC transfers electrons to create a proton gradient, which is used to synthesise ATP. A small percentage of those

electrons are captured by O_2 to produce superoxide ions. Of the ETC complexes, complex I has been the most extensively studied since identification of the link between mitochondria and PD (Schapira et al., 1990). This relationship was first described after some drug users presented with parkinsonian symptoms after 1-methyl-4-phenyl-1,2,3,6-tetrahydropyridine (MPTP) exposure (Davis et al., 1979). MPTP is a side-product in the synthesis of 1-methyl-4-phenyl-4-propionoxypiperidine (MPPP), a synthetic opioid drug with similar effects to those of morphine. MPTP can cross the brain–blood barrier and it is transformed to 1-methyl-4-phenylpyridinium (MPP+) via MAO-B within the glial cells. MPP+ is then released and specifically internalised in the dopaminergic neurons by DAT, where it inhibits mitochondrial complex I activity and initiates a degeneration cascade.

As a result of this discovery, it has been shown that exogenous and endogenous toxins, such as rotenone and nitric oxide (NO) respectively, can produce mitochondrial dysfunction leading to early onset PD (Heales et al., 1999). For instance, several publications have reported that NO can inhibit the ETC complexes; and the degree of that inhibition, i.e. reversible or irreversible, is dependent upon the efficiency of the antioxidant system (reviewed by Heales et al., 1999). Various processes have been proposed to explain the consequences of the loss of complex I activity. The most characterised are higher ROS production, increased oxidative stress and impairment of ATP synthesis (Abou-Sleiman et al., 2006). Some studies have proposed that ETC dysfunction first increases ROS levels and then leads to impairment of the energy metabolism (Jacobson et al., 2005). Indeed, (Davey et al., 1998) proved that the reduction in activity of complex I needed to decrease ATP synthesis was lower in the presence of oxidative stress. Nonetheless, the impairment of mitochondrial complex I activity has been described as a contributing factor in dopaminergic neuron death in PD (Abou-Sleiman et al., 2006; Choi et al., 2011).

Rotenone, a naturally occurring pesticide, has often been used to study the relationship between mitochondrial impairment and PD. This compound impairs electron transfer from the iron–sulphur clusters of complex I to ubiquinone, boosting the transport of electrons from the intermembrane space to the mitochondrial matrix and increasing the production of reactive oxygen species (Hirst and Roessler, 2016). It has been proposed that rotenone-induced cell death is caused by ROS production, which triggers apoptosis and cytoskeleton destabilisation (Choi et al., 2011). Furthermore, it has been shown that rotenone also inhibits the dopamine transporter VMAT2 (Chaudhry et al., 2008; Choi et al., 2015; Watabe and Nakaki, 2008). Some authors have suggested that this inhibition could be due to reduced ATP production after rotenone treatment, as ATP is necessary to create the H^+ gradient that VMAT2 uses to endocytose dopamine into vesicles (Chaudhry et al., 2008). In addition, it has been proposed that rotenone could directly inhibit VMAT2 function (Choi et al., 2015; Watabe and Nakaki, 2008). All these factors would result in dopamine accumulation in cytosol, possibly preceding its oxidation to form aminochrome and neuromelanin (see section 1.3.10). It has been described that aminochrome can directly inhibit complex I, leading to an energy-deficiency state in dopaminergic-like SH-SY5Y cells (Aguirre et al., 2012), although this effect could be partially prevented by reduced glutathione (GSH) (Munoz et al., 2012). In summary, all mechanisms support the theory that if cytosolic dopamine accumulates, it would increase neurotoxicity, leading to apoptosis of dopaminergic neurons (Choi et al., 2015; Chaudhry et al., 2008; Watabe and Nakaki, 2008).

The role of mitochondria in producing energy and the consequences of a dysfunctional ETC is one of the most studied events in PD. Although oxidative damage and mitochondrial dysfunction have been proposed to be key to the triggering of neurodegeneration, as both events are present in several neurodegenerative diseases (Dias et al., 2013), it is accepted that the mechanisms that cause dopaminergic

neurodegeneration are complex and not completely understood. Other mitochondrial functions should also be taken into consideration, as this organelle has other roles as relevant for PD as the ETC and ATP synthesis, such as calcium homeostasis (see section 1.2.3) or maintenance of mitochondrial dynamics. In fact, several of the genes causing familial PD are related to some of these mitochondrial functions; for example, *phosphatase and tensin homologue (PTEN)-induced putative kinase 1* (*PINK1*). More about the role of mitochondrial-related proteins affected in PD is described below in section 1.2.6.

1.2.3. PD and oxidative stress

Oxidative stress is the result of the interruption of the balance between the oxidant molecules produced by biological processes and the antioxidant molecules, such as alpha-tocopherol, ascorbate and GSH, that detoxify them (Bolanos et al., 1995; Barker et al., 1996; Riederer et al., 1989). This balance is known as redox potential and, in physiological conditions, acts as a regulator of several biological processes. There are different sources for ROS production but dopaminergic neurons of the substantia nigra are the ones affected in PD. In these dopaminergic neurons, some of the biological processes that contribute to the formation of ROS are dopamine metabolism (section 1.3.10), mitochondrial dysfunction, iron and/or calcium dyshomeostasis, and lipid peroxidation (reviewed by Dias et al., 2013).

In addition to ROS, there are also reactive nitrogen species (RNS) producing nitrosative stress (Heales and Bolanos, 2001). RNS are formed by the combination of NO with the superoxide anion ($O_2^{\cdot-}$). This extremely favourable reaction produces peroxynitrite ($ONOO^-$), which is highly cytotoxic due to its capacity to oxidise different cellular components. NO is a soluble gas, which acts as a messenger molecule, and has a short half-life due to its high reactivity with oxidative molecules. Indeed, NO competes with the antioxidant enzyme superoxide dismutase for $O_2^{\cdot-}$ (Heales et al., 1999). NO is

synthesised by NO synthases (NOS). There are three types of NOS; inducible (iNOS), endothelial (eNOS) and neural (nNOS). While iNOS is expressed transiently and is very important in the immune response, eNOS and nNOS are constitutively expressed and calcium-dependent. It has also been reported that nNOS can be induced after neural damage (Heales et al., 1995), suggesting a possible link with microglial activation. While neurons express only nNOS, astrocytes also express iNOS, converting them to a major source of NO (Heales et al., 1999; Bolanos et al., 1994), however, this observation could be due to microglia being present in the primary cell culture. This contrasts with their high resistance to RNS and the higher sensitivity of neurons (Bolanos et al., 1995). This difference can be explained by the fact that both NO and $ONOO^-$ can diffuse through membranes, raising the possibility of trans-toxicity between different cell types (Heales et al., 1997).

Hydroxyl radicals ($OH^\cdot$) and $ONOO^-$ are the most potent oxidising agents amongst ROS and RNS, respectively (Dias et al., 2013). Amongst their main targets are complexes I and IV of the mitochondrial ETC. The inhibition of the ETC by ROS and RNS might lead to an energy-deficiency state resulting in increased cell death (Bolanos and Heales, 2010). However, it has been observed that, while neurons die after this toxic exposure, astrocytes are resistant (Heales et al., 1997). This increased resistance could be due to a compensatory increase in glycolysis and anaerobic metabolism in the latter (Bolanos et al., 1997). Therefore, the higher vulnerability of neurons to oxidant molecules could be due to the inability of neurons to maintain the cellular energy demands and an inferior capacity to handle oxidising species, as it has been reported that astrocytes contain double the concentration of GSH found in neurons (Heales et al., 1997).

Glutathione is a potent antioxidant in its reduced form (GSH). This tripeptide can be synthesised *de novo* in an ATP-dependent pathway starting with the conjugation of

cysteine and glutamate by the γ-glutamyl cysteine ligase. This reaction forms γ-glutamyl cysteine, which becomes GSH when a glycine is added by glutathione synthetase (***Figure 1.6***). GSH can also be formed by recycling its oxidised form (GSSG) through the action of the glutathione reductase and the oxidation of NADPH (***Figure 1.6***). GSH can detoxify ROS and RNS (Smeyne and Smeyne, 2013). For instance, to detoxify one molecule of H_2O_2, the enzyme glutathione peroxidase oxidises two molecules of GSH and produces two molecules of water (***Figure 1.6***). However, under conditions of intense stress, the use of GSH through GSH peroxidase means an irreversible loss of intracellular antioxidant power (Sian et al., 1994). Indeed, a 40% decrease in GSH levels has been reported in the substantia nigra of PD patients and not in other brain regions (Smeyne and Smeyne, 2013), probably due to the oxidative environment within dopaminergic neurons. This was also observed in pre-symptomatic patients (Smeyne and Smeyne, 2013). Nonetheless, whilst GSH levels are decreased in both groups, complex I activity was reported to be decreased only in the symptomatic group (Sian et al., 1994). This therefore raises the possibility that GSH loss precedes and contributes to the loss of complex I, a hypothesis that is supported by a number of observations in cellular and animal models (Heales and Bolanos, 2001; Bolanos et al., 1994; Heales et al., 1994). In turn, mitochondrial damage could affect GSH synthesis, as it is an energy-dependent pathway (Heales et al., 1994; Heales et al., 1999). Additionally, *in vivo* and *in vitro* studies concluded that chemical GSH depletion could increase NOS activity, further enhancing cytotoxicity (Heales and Bolanos, 2001; Heales et al., 1995).

Regarding iron dysregulation, post-mortem tissue studies have revealed higher levels of iron in the substantia nigra of PD patients than in controls (Riederer et al., 1989). In physiological conditions, iron is a cofactor for several enzymes, for example TH, and Fe^{2+} and Fe^{3+} ion levels are similar in the substantia nigra (Smeyne and Smeyne, 2013). However, under stress conditions, accumulation of Fe^{2+} and dopamine oxidation have

been proposed as key events in increasing neurotoxicity (Dias et al., 2013). It is not known whether Fe^{2+} accumulation is a cause or a consequence of neuronal death (Dias et al., 2013). While pre-symptomatic PD patients show no changes in iron levels (Sian et al., 1994), in symptomatic patients increased iron levels could lead to increased neuronal degeneration through oxidative stress. This could form a vicious cycle since superoxide anions could cause release of iron from ferritin (Dias et al., 2013). In addition, dopamine oxidation could increase iron levels by modifying expression of transporters regulating the uptake of iron (Aguirre et al., 2012).

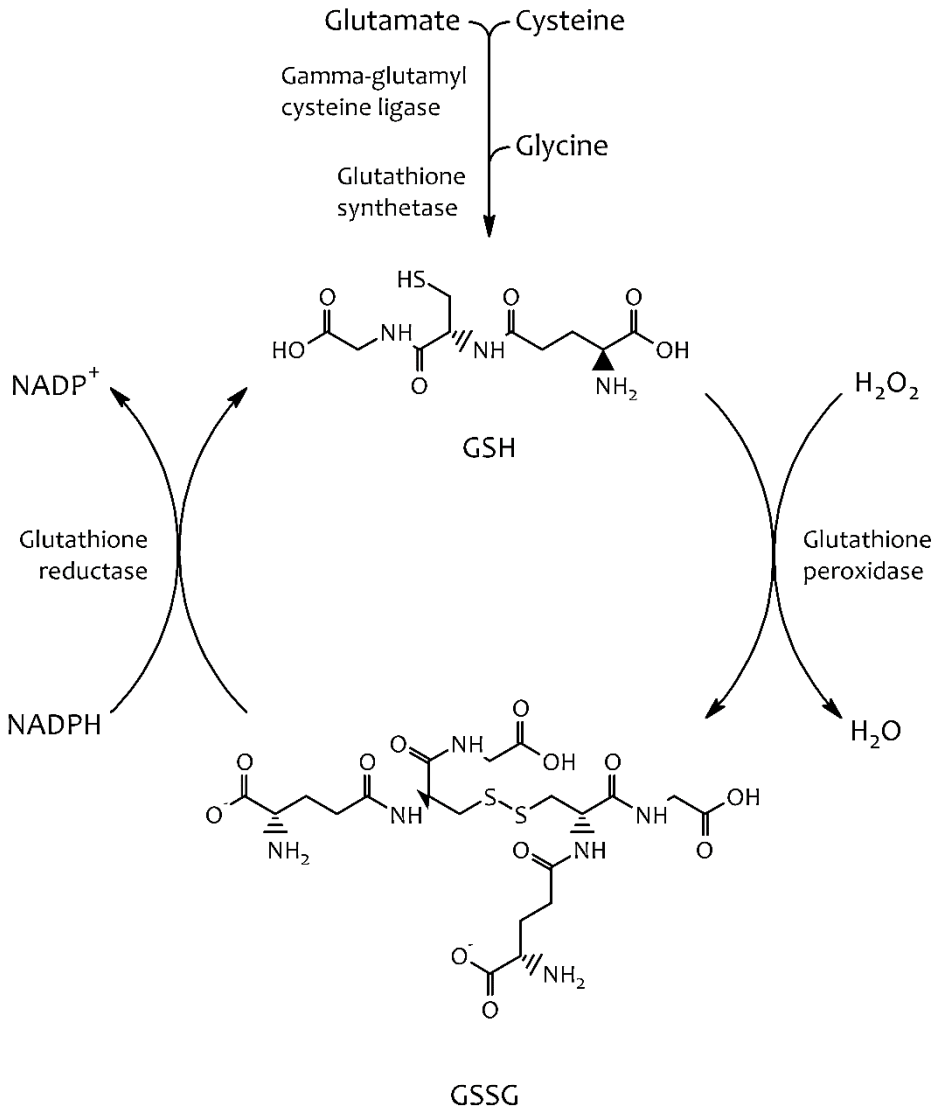

Figure 1.6 GSH synthesis pathway.
Reduced glutathione (GSH) can be synthesised de novo *by a two-step pathway or recycled from oxidized glutathione (GSSG).*

Calcium homeostasis is highly energy-dependent (Gleichmann and Mattson, 2011). Even under physiological conditions, regulation of calcium intracellular levels would increase mitochondrial activity with a consequent increase in ROS formation. In addition, nNOS is calcium-dependent; therefore, increased levels of calcium in the cytosol could also increase oxidative stress by enhancing nNOS activity and result in higher RNS formation (Gleichmann and Mattson, 2011). Burbulla et al. (2017) also proposed that calcium could regulate mitochondrial oxidative stress and dopamine synthesis and oxidation in PD patients and carriers of mutant *DJ-1* (see section 1.2.6).

1.2.4. PD and lysosomes

Lysosomal impairment has also been related to PD since a proportion of Gaucher disease (GD) patients also show parkinsonian features (Migdalska-Richards and Schapira, 2016; Lynch-Day et al., 2012). GD is a rare lysosomal storage disorder caused by GBA1 deficiency. GBA1 hydrolyses glucosylceramide into glucose and ceramide. When GBA1 is absent, glucosylceramide accumulates in the spleen, liver, bone marrow and other tissues. Two of the three types of GD exhibit a neuropathic phenotype. The difference between these types is that GD type 2 is acute and type 3 is chronic. Current pharmacological therapies are not effective with these GD types, as the drugs cannot cross the blood–brain barrier (reviewed by Migdalska-Richards and Schapira, 2016). Patients with all three types of GD, and carriers of the GBA1 mutation, show a 5-fold greater risk of developing PD, hence GBA1 mutations are the most common risk factor for PD (Neumann et al., 2009). Indeed, PD patients who have the GBA1 mutation and those who have the idiopathic form cannot be distinguished clinically (Migdalska-Richards and Schapira, 2016). Moreover, Gegg et al. (2012) found that PD patients with no modifications in the GBA1 gene showed a decreased GBA1 activity. Several theories have been considered to explain the association of a higher risk of developing PD and lysosomal dysfunction seen in GD. Some studies

have proposed a bidirectional feedback between α-synuclein and GBA1, as the absence of GBA1 could enhance α-synuclein accumulation and, α-synuclein in turn could directly bind GBA1, decreasing its activity (Sidransky and Lopez, 2012; Mazzulli et al., 2011; Gegg et al., 2012; Bae et al., 2015). Other theories involve autophagy dysfunction, oxidative stress, mitochondrial impairment and lower ETC activity (reviewed by Migdalska-Richards and Schapira, 2016), all of which have been associated with the pathology of PD.

Although the possible link between lysosomal *GBA1* mutation and PD pathogenesis has been extensively studied, there are other mutations of lysosomal enzymes that can lead to parkinsonism. For instance, the mutation of the transmembrane lysosomal P-type ATPase called ATP13A2 (*PARK9*) causes a recessive autosomal form of early-onset PD (Dehay et al., 2012). Although its physiological role has not been yet elucidated, it appears to involve impairment of autophagy processes, possibly as a consequence of increased lysosomal pH (Dehay et al., 2012). Another example is mutations in the sphingomyelin phosphodiesterase 1 gene, which cause Niemann–Pick disease. This enzyme produces ceramide from sphingomyelin, and its mutation has also been reported to increase the risk of developing PD (Moors et al., 2016). One common feature of these mutations is that a substrate accumulates and the lysosomal degradation mechanisms are impaired, leading to cellular death.

1.2.5. PD, protein degradation and dysfunction in autophagy

Another key mechanism implicated in PD pathogenesis is failure of autophagy, which leads to impaired protein degradation and abnormal protein deposits forming Lewy bodies (Lynch-Day et al., 2012; Beyer, 2007). The main degradation pathway for oxidised and misfolded proteins is the ubiquitin-proteasome system. Proteins to be degraded are tagged with poly-ubiquitin chains on an ATP-dependent three-step pathway. Enzyme 1 (E1) activates the ubiquitin and transfers it to E2, which binds to E3. E3 then recognises

the target and mediates the transfer of ubiquitin from E2 to the damaged protein. It has been hypothesised that enzymes 2 and 3 form a complex to increase the target specificity. This pathway is considered neuroprotective during oxidative stress conditions, as it prevents aggregation of oxidised proteins. Therefore, a loss of function would result in increased oxidative stress within the cells (Dias et al., 2013). Betarbet et al. (2005) reported that oxidative stress inhibits the proteasome pathway, suggesting that these events form a vicious cycle sentencing the cell to apoptosis.

Additionally, degradation by autophagosomes could be affected. Autophagy is important for degrading and recycling several cytoplasmic proteins and organelles that cannot be degraded by the proteasome (reviewed by Glick et al., 2010). Three types of autophagy have been described in the literature based on the size and the mechanisms of transportation of the cargo: macro-, micro- and chaperone-mediated autophagy (Glick et al., 2010). In all three, molecules and organelles are accumulated in vacuoles before the subsequent transport into lysosomes for degradation (Munoz et al., 2012). Consequently, in post-mitotic neurons, autophagy dysfunction results in the accumulation of aberrant proteins and organelles, such as defective mitochondria (Lynch-Day et al., 2012; Beyer, 2007).

In both sporadic and familial PD, misfolded proteins aggregate forming Lewy bodies. The main component of these Lewy bodies is insoluble α-synuclein (Beyer, 2007). This protein is conserved and abundant in the CNS but, despite its redundancy and the high number of groups working on this model, the function of α-synuclein is still unclear. It has been proposed that α-synuclein is related to synaptic vesicles in the pre-synaptic terminals and regulates the cycle of the vesicles ready to be released (Bendor et al., 2013). It has also been suggested that this protein might play an important role in cellular membrane dynamics and the correct localisation of membrane proteins such as DAT (Butler et al.,

2015). Beyer (2007) proposed that α-synuclein can be both neurotoxic and neuroprotective depending on its secondary structure. Nonetheless, the cause of this accumulation is not clear, as some PD patients show a point mutation in the α-synuclein (*SNCA*) gene (see section 1.2.6). The accumulation of α-synuclein could also be partially enhanced by the loss of dopamine as Mazzulli et al. (2006) reported that the neurotransmitter inhibited α-synuclein aggregation and promoted the production of soluble intermediates. However, the interaction between α-synuclein and dopamine is not clear. Conway et al. (2001) found that *in vitro* aminochrome, the toxic product of dopamine metabolism, could stabilise α-synuclein protofibrils.

1.2.6. Inherited mutations in PD

Several inherited mutations have been related to PD and other parkinsonisms. Most are due to mutations in proteins that have been related to the pathogenesis of PD described above or are monoamine disorders that are directly related to dopamine synthesis and homeostasis.

The α-synuclein depositions found in PD brains result from repetitions of the *SNCA* gene. The most common *SNCA* mutation in PD is A53T, a missense mutation that results in an autosomal dominant form of PD (Stefanis, 2012). The conformation of α-synuclein fibrils is most commonly present in Lewy bodies, causing oxidative and nitrosative stress (see section 1.2.5).

Parkin is a cytoplasmic and nuclear protein that belongs to the ubiquitin-proteasome system, acting as an E3 ubiquitin ligase (reviewed by Dawson and Dawson, 2010). This protein has been described as crucial for survival of dopaminergic neurons as it plays a neuroprotective role against α-synuclein toxicity and oxidative stress (Dias et al., 2013). Parkin gene (*PARK2*) mutation leads to autosomal recessive early-onset PD. *PARK2*

mutation decreases the expression of Parkin, leading to a dysfunctional proteasome protein degradation pathway. Mutation of PTEN-induced putative kinase 1 (PINK1) also causes an autosomal recessive form of PD (Dawson and Dawson, 2010). It is a mitochondrial targeted kinase, deficiency of which results in abnormal mitochondria and loss of complex I activity. A PINK1/Parkin pathway has been hypothesised to be responsible for the clearance of damaged mitochondria (Abou-Sleiman et al., 2006). PINK1 is thought to be involved in recruiting Parkin into damaged mitochondria, where it ubiquitinates proteins involved in mitochondrial fusion to start ubiquitin-proteasome system degradation and mitophagy.

Another mutation leading to autosomal recessive early-onset PD is the mutation of the DJ-1 gene (*PARK7*) (Dawson and Dawson, 2010). DJ-1 is a highly conserved neuroprotective protein that is involved in the regulation of anti-oxidant, anti-apoptotic and anti-inflammatory mechanisms (Dias et al., 2013). For instance, it has been reported that DJ-1 acts as a transcriptional cofactor of glutamate cysteine ligase and VMAT2, involved in GSH synthesis and dopamine storage respectively (Dias et al., 2013). Burbulla et al. (2017) reported that induced pluripotent stem (iPS) cells from *PARK7* mutation homozygotes and heterozygotes showed increased mitochondrial oxidative stress and loss of GBA1 function due to oxidised dopamine compared to healthy controls.

Mutation in the leucine-rich repeat kinase (LRRK2) gene (*PARK8*) results in an enzymatic gain of function that is responsible for an autosomal dominant form of PD (Dawson and Dawson, 2010). LRRK2 is located in autophagic vesicles and its malfunction leads to autophagy impairment and accumulation of autophagy vesicles.

A summary of the processes relevant for this project are presented in ***Figure 1.7***.

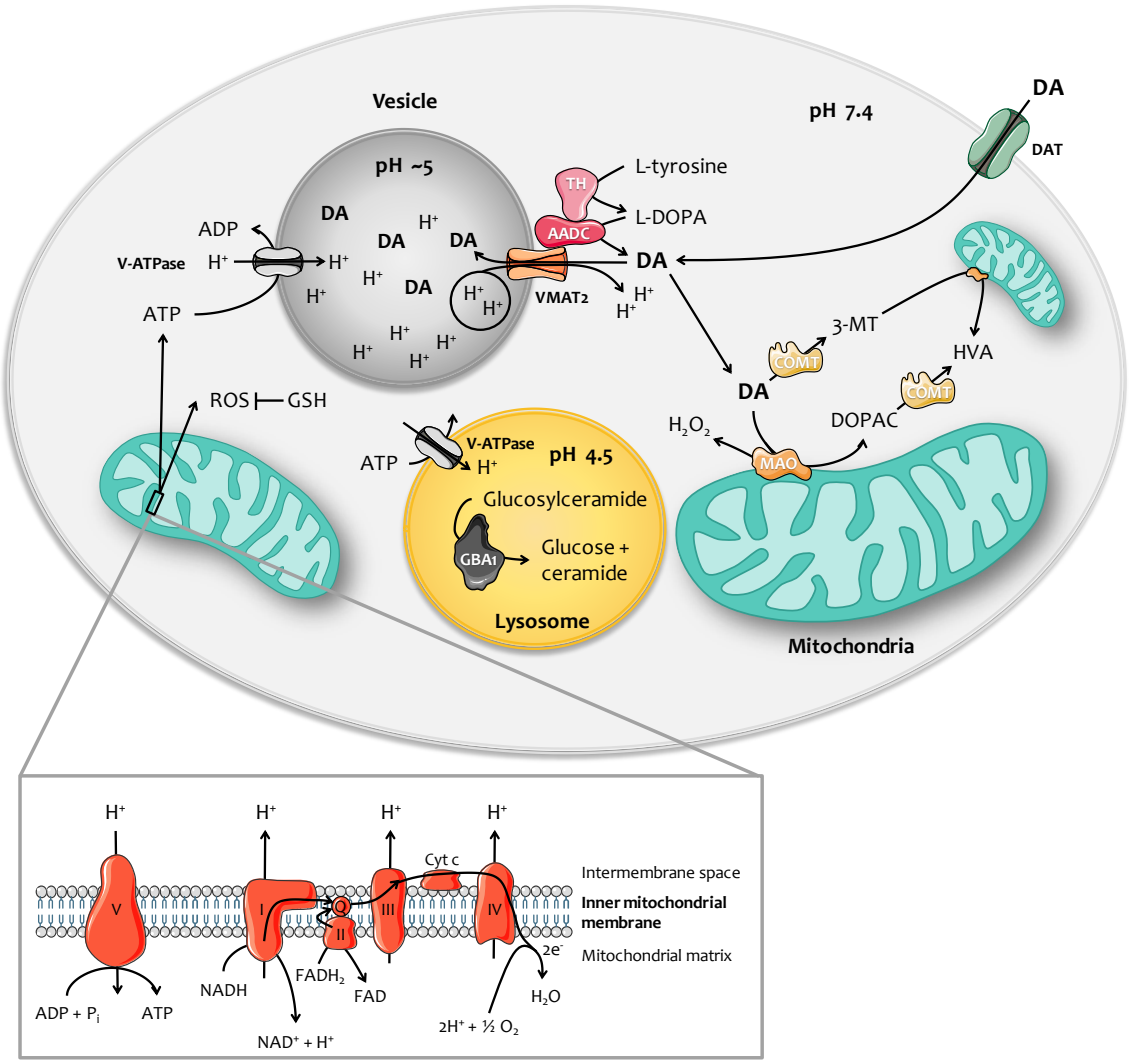

Figure 1.7 Dopamine metabolism, mitochondrial and lysosomal function in physiological cell conditions.

The electron transport chain (ETC) creates a proton gradient that is used by complex V (ATP synthase) to join ADP and inorganic phosphate (Pi) to produce ATP. The vacuolar type H^+ ATPase (V-ATPase) uses the energy released from the hydrolysis of ATP to internalise H^+ ions into vesicles against gradient. These H^+ ions are then used by the vesicular monoamine transporter 2 (VMAT2) to antiport dopamine (DA) into those vesicles, where it is stored. In parallel, dopamine transporter (DAT) is responsible for reuptake of dopamine from the synaptic cleft to cytosol for recycling. If dopamine is not stored – or recycled – in the vesicles, it is catabolised by the degradation enzymes COMT and MAO, preventing oxidative stress. However, MAO generates H_2O_2 as a side-product that, along with other ROS, is detoxified by antioxidant molecules like reduced glutathione (GSH). Lysosomes are essential to maintain correct cellular function and eliminate damaged organelles. They contain several important degradation enzymes; for example GBA1, which hydrolyses glucosylceramide to glucose and ceramide.

1.4. Aims

In this work, it is hypothesised that changes in dopamine metabolism could be a key factor triggering neurodegeneration in PD and other neurometabolic disorders. Under stress conditions or age-related deterioration, the turnover would be compromised, causing cytosolic dopamine accumulation and generating neurotoxicity. The aim of this project was to investigate dopamine metabolism in cellular PD models using the neuroblastoma cell line SH-SY5Y, using inhibitors to impair mitochondrial and lysosomal function. The overall purpose of this study was to examine links between mitochondrial and/or lysosomal impairment and dopamine metabolism in PD. This could be useful to provide a better understanding of PD and eventually propose a new therapeutic target for PD. To assess this, the objectives planned were to:

- Evaluate dopamine and serotonin metabolism in a cell model by measuring the extracellular levels of neurotransmitters and/or their metabolites in control and L-DOPA treated cells, as well as the effect of the inhibition of mitochondrial complex I or lysosomal GBA1. In order to do so, a high-performance liquid chromatography (HPLC) method was developed to measure and quantify these monoamines by electrochemical detection (ECD).

- Study the expression and activity of the enzymes involved in the dopamine pathway by quantitative reverse transcription polymerase chain reaction (qRT-PCR), western blot and enzymatic activity assays in all the cell models before and after L-DOPA treatment. In addition, intracellular levels of GSH were also quantified in these cell models by HPLC.

- Measure monamines in several models of PD and related disorders by the ECD-HPLC method developed to assess their dopamine and serotonin metabolism. Some of the models included iPS cells, mice or zebrafish with mutations in *GCH1*, *DAT* or *GBA1* among others.

- Analyse the glycoprofile in the CSF of patients with low HVA levels and compare it to the profile of non-parkinsonian patients (control). This analysis took place during my secondment in the National Institute for Bioprocessing Research & Training (NIBRT, Dublin, Ireland).

CHAPTER 2

Materials and Methods

2.1. Materials

The following were purchased from Sigma Aldrich (Poole, UK): 3,4-dihydroxyphenylacetic acid (DOPAC); 5-hydroxyindole acetic acid (5-HIAA); homovanillic acid (HVA); dopamine hydrochloride; L-3,4-dihydroxyphenylalanine methoxy-L-tyrosine monohydrate (3-OMD); L-3,4-dihydroxyphenylalanine (L-DOPA); reduced glutathione (GSH); 3-hydroxybenzylhydrazine (NSD-1015); 1-octanesulfonic acid sodium salt; ethylenediaminetetraacetic acid (EDTA) disodium; trizma base; rotenone; conduritol B epoxide (CBE); monoamine oxidase activity assay kit (MAK136); L-glutamine solution; Dulbecco's phosphate buffered saline (PBS) modified without calcium chloride and magnesium chloride; Bradford reagent.

The following were purchased from Thermo Fisher Scientific UK Ltd (Loughborough, UK): Dulbecco's modified Eagle's medium/Ham's F-12 nutrient mixture (DMEM/F-12); DMEM/F-12 phenol red free; foetal bovine serum (FBS), heat inactivated; 0.25% trypsin-EDTA; methanol HiPerSolv for HPLC; 85% orthophosphoric acid for HPLC; oligo (dT) primer; superscript III reverse transcriptase; DNAse I; nuclease-free H_2O; restore Western Blot stripping buffer.

The following were purchased from Bio Rad Laboratories Ltd (Hemel Hempstead, UK): TC10 counting kit and trypan blue; mini-protean TGX stain-free gels 4%-20% polyacrylamide; trans-blot turbo transfer pack (PVDF, 7 x 8.5 cm); clarity Western ECL substrate.

Sodium acetate trihydrate and citric acid monohydrate were purchased from VWR International Ltd (Lutterworth, UK). C18HS column, 250 mm × 4.6 mm with a pore size of 100 Å and a particle size of 5 µm, was purchased from Kromatek (Dunmow, UK). 0.3 ml clear vials with screw caps were purchased from Chromacol (Welwyn Garden City, UK).

RNeasy Mini Kit was purchased from Quiagen (Manchester, UK). Mesa blue qPCR MasterMix for SYBR® was purchased from Eurogentec (Seraing, Belgium).

The human neuroblastoma cell line SH-SY5Y was purchased from the European Collection of Cell Cultures (Public Health England, Salisbury, UK). Antibodies were purchased from Abcam (Cambridge, UK) and from New England Biolabs (Hitchin, UK): rabbit monoclonal to monoamine oxidase A (HRP conjugate, EPR7101); rabbit monoclonal to monoamine oxidase B (EPR7102); rabbit monoclonal to catechol *O*-methyltransferase (EPR6490); rabbit monoclonal to glyceraldehyde 3-phosphate dehydrogenase (GAPDH) (HRP conjugate, 14C10); anti-rabbit IgG (HRP conjugate).

2.2. Tissue Culture: SH-SY5Y Cell Line

2.2.1. Passaging and seeding

SH-SY5Y cells were seeded in a 75 cm^2 tissue culture flask with DMEM/F-12 supplemented with 10% FBS and 1% L-glutamine. Cells were grown at 37 °C in a 5% CO_2 incubator. The medium was changed once every other day. When 80–90% confluent, cells were washed with PBS and lifted from the flask with 1 ml/flask 0.25% trypsin at 37 °C for 3 min. Then 4 ml of complete medium were added to inactivate the trypsin, before cells were recovered by centrifugation at 500 ×*g* for 5 min at room temperature. After that, the supernatant was removed, and the cells were washed by re-suspension in PBS. Cells were collected by centrifugation at 500 ×*g* for 5 min at room temperature. Finally, the supernatant was removed, and the cells re-suspended in supplemented DMEM/F-12. An aliquot of the cell suspension was mixed 1:1 with trypan blue and counted using a Bio-Rad TC20™ automated cell counter before seeding at a density of 6×10^4 cells/cm^2 in 25 cm^2 flasks for the experiments. The medium was changed on even days, taking as day 0 the

day the cells were seeded. All cells used for the experiments were between passages 21 and 24.

2.2.2. Treatments

2.2.2.1. L-DOPA

To study the release of dopamine and its metabolites from cells to the medium, SH-SY5Y cells were treated with 100 µM L-DOPA (Woodard et al., 2014). On day 7 after seeding, 100 µM L-DOPA solution was freshly made in DMEM/F-12 phenol-red-free medium supplemented with 10% of FBS. For each experiment, cells were seeded in four 25 cm^2 flasks as described in section 2.2.1. 5 ml of the 100 µM L-DOPA solution were added to three flasks, and 5 ml of supplemented DMEM/F-12 phenol-red-free medium were added to the remaining flask, used as a control. The media samples were collected as described in section 2.2.3.1 at different time points: 30 min, 1 and 3 h. Samples from the control flask were collected together with the 3 h treatment to quantify the basal release of the neurotransmitters.

2.2.2.2. NSD-1015

To confirm L-DOPA was being metabolised through the dopamine pathway, proliferative SH-SY5Y cells were pre-treated with the AADC inhibitor, NSD-1015. Stock aliquots of 2 mM NSD-1015 were made in ultrapure H_2O, filtered and stored at –20 °C. Cells were seeded in two 25 cm^2 flasks per experiment as previously described in section 2.2.1. On day 6 after seeding, one flask was treated with 10 µM NSD-1015 and the other one was not treated and used as a control (Allen et al., 2013). 24 h later, the medium was removed and cells were treated with 100 µM L-DOPA for 1 h as described in section 2.2.2.1. Finally, the media samples were collected as described in section 2.2.3.1.

2.2.2.3. Rotenone

1 mM rotenone stock was made in ethanol, warmed to dissolve, filtered and aliquoted in a diluted concentration of 100 µM for further use. SH-SY5Y cells were seeded in three flasks for the rotenone treatment: one for the cell line control, another for the vehicle control and another for the rotenone treatment. On day 6 after seeding, cells were treated with 100 nM rotenone (Aylett et al., 2013). Simultaneously, the same amount of ethanol (0.01 v/v %) was added to the ethanol control. 24 h later, the flasks were removed treated with 100 µM L-DOPA for 1 h or 3 h as described in section 2.2.2.1. Media samples were collected as described in section 2.2.3.1 at the required time points: 1 or 3 h.

2.2.2.4. Conduritol B epoxide

Stock aliquots of 20 mM conduritol B epoxide (CBE) were made in DMEM/F-12 supplemented with 10% FBS, filtered and stored at –20 °C. SH-SY5Y cells were seeded in two 25 cm^2 flasks per experiment, as described in section 2.2.1, with the only difference that, in this case, the supplemented DMEM/F-12 medium in one of the flasks contained 100 µM CBE. The medium with CBE was changed on even days, taking day 0 as the day when the cells were seeded. On day 7, the cells were treated with 100 µM L-DOPA for 1 or 3 h as described in section 2.2.2.1. Media samples were collected as described in section 2.2.3.1 at the appropriate time: 1 or 3 h. This concentration of CBE has been proved to inhibit GBA1 but not beta-glucosidase 2 (GBA2). Treatment concentration and times were optimised by Dr Derek Burke (personal communication, UCL, London).

2.2.3. Sample collection

At least three flasks were seeded for each treatment and replicate. At the same time, each treatment was incubated with L-DOPA 100 μM for 1 and 3 h. The remaining flask of each treatment was kept as a control, i.e. was not treated with L-DOPA. From each flask the media and the cells were used in different experiments ***(Figure 2.1)***. Samples were always collected for the catecholamine measurement by HPLC and cells could be processed in two ways depending on the experiment. First, cells could be lysed (see 2.8) to measure protein content, expression and enzymatic activity. Alternatively, cells could be stored as a pellet to analyse mRNA expression by qRT-PCR or for GSH quantification by HPLC. A summary of the treatments and objective of the samples is shown in ***Figure 2.1***.

2.2.3.1. Culture medium: measurement of catecholamine release by HPLC

Samples were collected from the flask at the specified times and quickly mixed 1:1 with 0.8 M perchloric acid. Samples were placed in dry ice until all had been collected. After thawing, samples were incubated for 10 min at 4 °C in the dark and centrifuged at 12000 ×*g* for 5 min at 4 °C. The supernatant was collected and analysed by HPLC.

2.2.3.2. Cell pellets: quantification of intracellular GSH and RNA

Cells were lifted following the protocol described in section 2.2.1. Then, cells were washed with PBS and centrifuged at 500 ×*g* for 5 min at room temperature. Finally, PBS supernatant was removed, and the cell pellet stored at –80 °C until analysis.

2.2.3.3. Protein extraction: protein quantification, enzymatic activity and western blot

After sample collection, cells were lifted following the protocol described in the section 2.2.1. This was followed by washing the cells with PBS, centrifugation and

removing the supernatant. Then cells were re-suspended in 1 ml of cold isolation buffer: 10 mM trizma base (pH 7.4), 1 mM EDTA and 320 mM sucrose in ultrapure H_2O. To lyse the cells, samples were thawed at 37 °C and frozen in a dry ice/methanol bath three times. Samples were maintained at –80 °C.

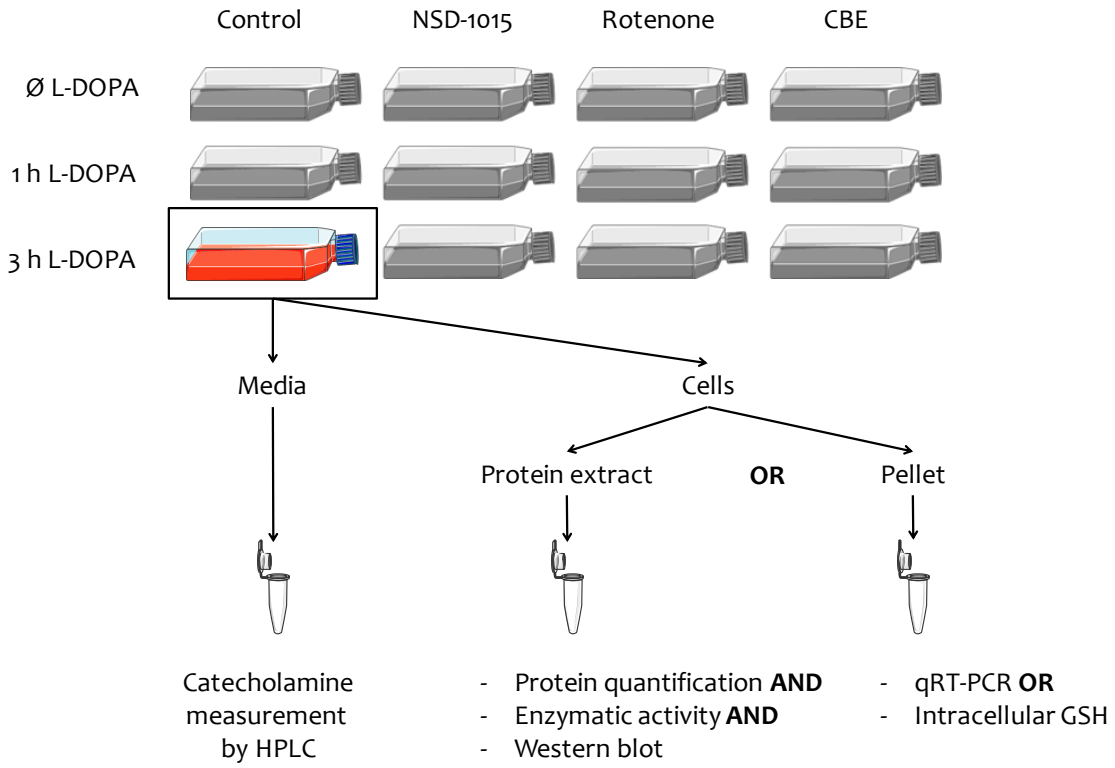

Figure 2.1 Summary of the SH-SY5Y treatments.
Each flask was used for two or more experiments: catecholamine measurement, protein and mRNA expression, enzymatic activity and GSH quantification.

2.3. Immunofluorescence

SH-SY5Y cells were seeded on a 24-well plate at a density of 6×10^3 cells/cm^2 and grown until 80% confluence. Then cells were washed with PBS, fixed with 4% paraformaldehyde for 10 min and washed four times with PBS. To eliminate unspecific binding, a blocking solution (PBS, 0.1% Triton X-100 and foetal calf serum) was added to the cells followed by incubation for 30 min at room temperature. After that, the solution

was removed, and cells incubated overnight at 4 °C with anti-TH chicken antibody diluted 1:500 in blocking solution. The next day, cells were washed three times with PBS before being incubated with fluorescence-conjugated secondary antibodies. Anti-chicken antibody Alexa Fluoro 594 was diluted 1:400 in blocking solution and incubated for 45 min in the dark at room temperature. The solution was removed, and cells were washed once with PBS. Finally, cells were incubated with 4',6-diamidino-2-phenylindole 1:1000 solution for 5 min at room temperature. Cells were washed and maintained in PBS at 4 °C in dark conditions until further analysis by fluorescence microscopy. Images were taken on an Olympus IX71 inverted scope with Hamamatsu Orca R2 monochrome camera. This method was fulfilled following a protocol optimised by Dr Kurian's lab.

2.4. MAO Enzymatic Activity Assay

2.4.1. Principle

The activity of MAO was determined by H_2O_2 production in the presence of excess substrate, *p*-tyramine. H_2O_2 is used by horseradish peroxidase (HRP) to oxidise the dye reagent, which is determined by a fluorimetric method at λ_{ex} = 530/λ_{em} = 585 nm. Then, each sample is measured under three conditions: basal conditions and then following incubation with clorgyline or pargyline to a final concentration of 1 µM, inhibitors of the two isoenzymes MAO-A and –B, respectively. The difference between H_2O_2 production by control and inhibited samples was considered MAO-A or –B activity. Under the assay conditions, one unit of MAO produced 1 µmole of H_2O_2 per minute.

2.4.2. Protocol

The MAO activity assay kit was purchased from Sigma, and the experiments were carried out in a black 96-well plate with flat-transparent bottom following manufacturer's instructions. Cell lysates were diluted in the assay buffer in order to add a final concentration of 50 µg of total protein to each well (see 2.8). Then, a final concentration of 1 µM of clorgyline or pargyline was added to MAO-A or MAO-B inhibited wells, respectively. Ultrapure H_2O was added to the control wells. Subsequently, samples were incubated for 10 min at room temperature. While incubating, the master mix and calibration curve were prepared. The master mix for each well comprised 50 µl of assay buffer, 1 µl of *p*-tyramine, 1 µl of HRP and 1 µl of dye reagent. A 7-point calibration curve was then made from 0 to 20 µM H_2O_2. Finally, the master mix was added to every well and fluorescence measured with an Infinite f200 plate reader (Tecan, Reading, UK) at 37 °C every minute for 20 min at λ_{ex} = 530/λ_{em} = 585 nm. Standards and samples were all measured in triplicate. Activity was calculated from linear regression of sample fluorescence units against the H_2O_2 calibration curve applying the equation below ***(Equation 2.1)***.

$$\text{pmols } H_2O_2/\text{min/mg of protein} = \frac{\overline{X_{rep}}(Flu_{t20} - Flu_{t0})_T - \overline{X_{rep}}(Flu_{t20} - Flu_{t0})_I}{Slope_{CC} \times t \times [prots]}$$

Equation 2.1 Formula used to calculate MAO-A and –B activity.

$\overline{X_{rep}}$: *average of the triplicates (repetitions);* Flu_{t20}*: fluorescence measured after 20 min;* Flu_{t0}*: fluorescence measured at time 0;* T*: total* H_2O_2 *production;* I*:* H_2O_2 *production after MAO-A or –B inhibition;* $Slope_{CC}$*: slope of the calibration curve; t: time = 20 min;* [prots]*: concentration of proteins per well = 50* µg*.*

2.4.3. Validation

Some experiments were carried out to determine the optimum parameters for the cell type used in this study, as the MAO kit is intended for use with purified proteins. The linearity of the calibration curve over time was first assessed. The calibration curve was prepared and measured for 20 min as described in section 2.4.2. All the points remained stable for the length of the experiment and its linearity was confirmed (r^2 = 0.995, ***Figure 2.2***). Next, two concentrations of proteins were studied. Control SH-SY5Y cells not treated with L-DOPA were diluted to 25 and 50 µg of protein per well. Both dilutions were above the detection limit, but 50 µg was chosen as the best concentration for further MAO activity experiments due to the higher signal ***(Figure 2.3)***.

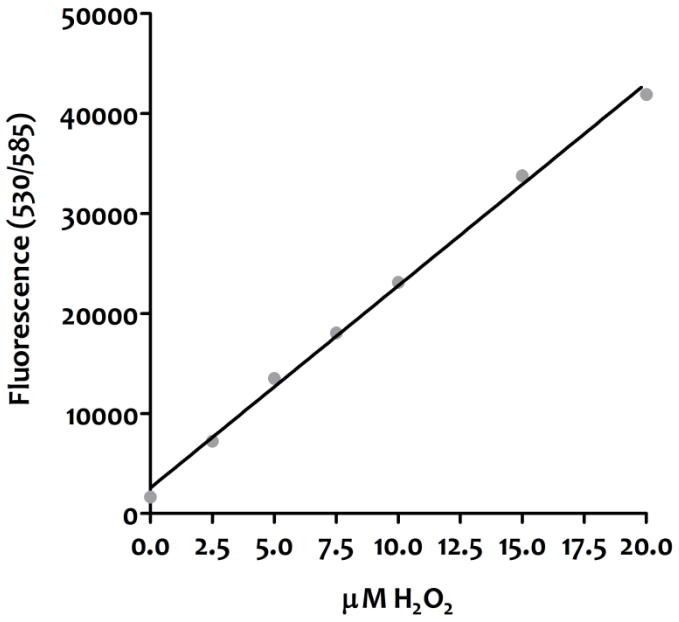

Figure 2.2 MAO kit H_2O_2 calibration curve.
The relationship between H_2O_2 concentration and fluorescence at λex = 530/λem = 585 nm was linear between 0 and 20 µM. Time: 20 min.

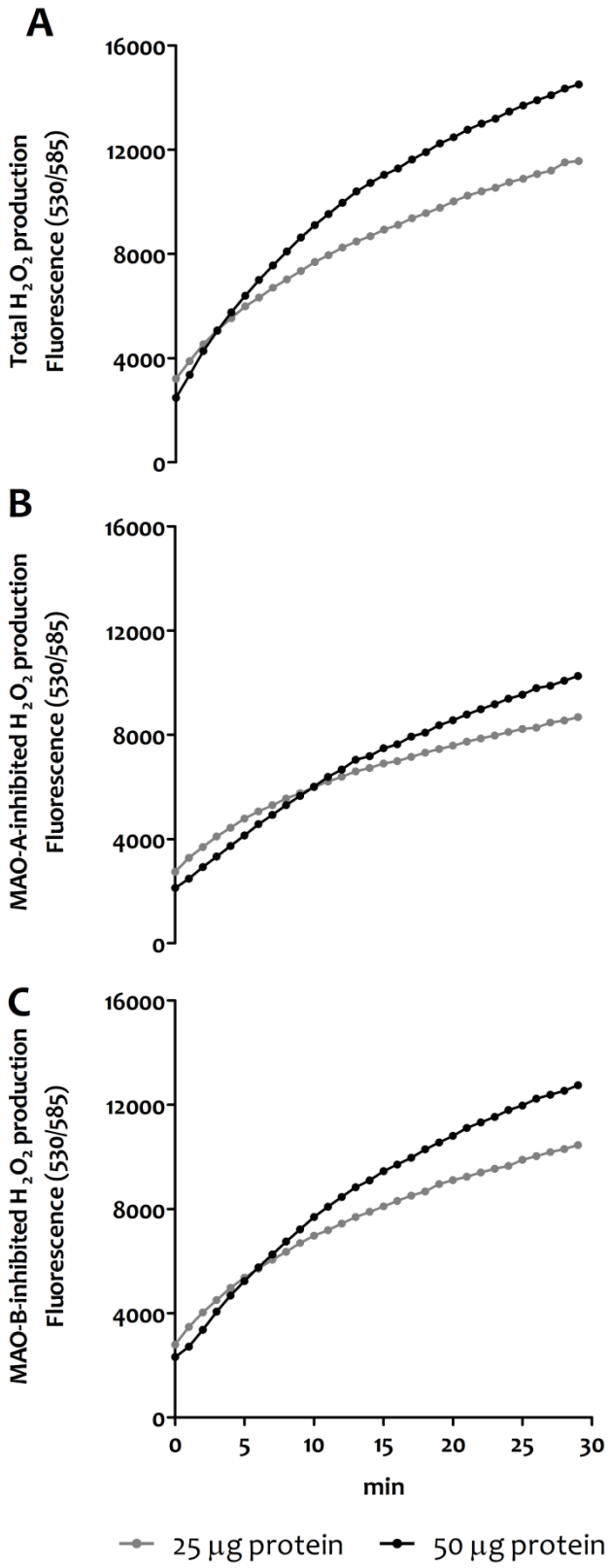

Figure 2.3 Optimisation of the protein concentration per well for the MAO activity assay. *Changes in the fluorescence of A: total; B: MAO-A-inhibited; and C: MAO-B-inhibited wells were compared at two protein concentrations (25 and 50 µg).*

The manufacturer's protocol specified a single measurement of the fluorescence 20 min after adding the master mix. However, the experiment time was increased to 30 min in all the assays. Rates obtained at 20 and 30 min were compared and no statistical differences were found, confirming the linearity of the assay ***(Figure 2.4)***. Finally, the specificity of the substrate and inhibitors was evaluated. Changes in H_2O_2 production were studied in four different scenarios: the absence of the substrate (*p*-tyramine), in the presence of just one MAO inhibitor (clorgyline or pargyline) and in the presence of both inhibitors. As shown in ***Figure 2.5***, H_2O_2 production was similar when the substrate was absent to that seen when the two isoenzymes were individually inhibited. Also, the specificity of the inhibitors was confirmed, as combining the results for H_2O_2 production in the presence of individual inhibitors totalled that seen for concurrent dual inhibition ***(Figure 2.5)***.

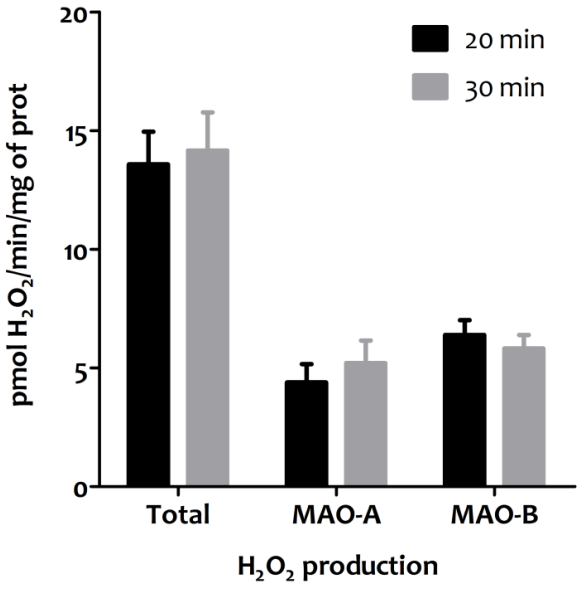

Figure 2.4 Comparison of H_2O_2 production after 20 and 30 min.
No statistical differences were detected in the rate of H_2O_2 production between 20 and 30 min groups. Paired Student's t-test was used to compare the H_2O_2 production of both groups (n = 3 experimental replicates). Data are presented as mean ± SEM.

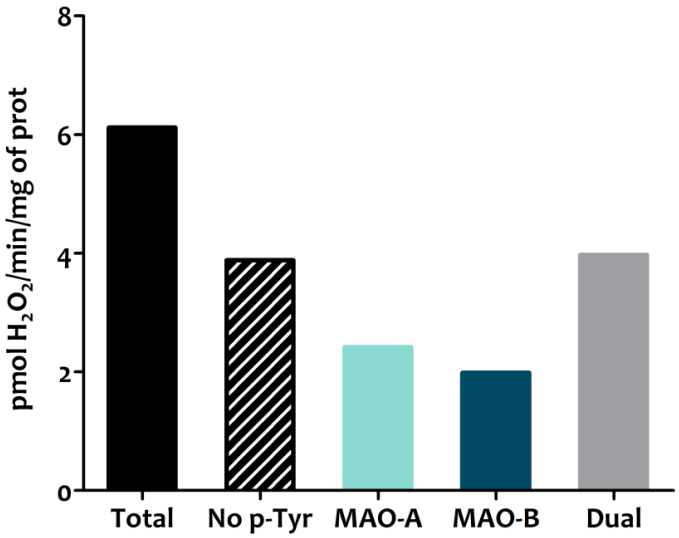

Figure 2.5 Validation of H_2O_2 production dependent on MAO activity.
The production of H_2O_2 by 50 µg of protein was first studied in basal conditions (total). The same sample was analysed in parallel with a master mix without substrate, p-tyramine (No p-Tyr). Finally, the sample was incubated in the presence of 1 µM clorgyline (MAO-A inhibitor), 1 µM pargyline (MAO-B inhibitor) or a 1 µM mix of both (Dual). H_2O_2 production in the presence of MAO isoforms is about 66% of the total as deduced from the measurements without the substrate p-tyramine or with dual inhibition (n = 1 experimental replicate).

2.5. Western Blot

After quantifying the total protein amount (see 2.8), the expression of dopamine catabolic enzymes was assessed. Each sample contained 25 µg of protein, 2.5 µl of Leammli 4x buffer, 2 µl of 0.1 M dithiothreitol (DTT) in ultrapure H_2O up to 10 µl. The samples were denatured by heating at 100 °C for 5 min. The 4–20% polyacrylamide gels were placed in the Bio Rad Mini-PROTEAN® tetra system along with TGS 1x running buffer. 5 µl of dual-colour ladder and 10 µl of the samples were loaded in the gel and the Bio Rad PowerPac basic electrodes were set at 300 V for 17 min. For the transfer, a Bio Rad Trans-Blot turbo transfer pack was prepared as shown in ***Figure 2.6***. The Bio Rad Trans-Blot TURBO™ transfer system was used and set at 21 V for 7 min.

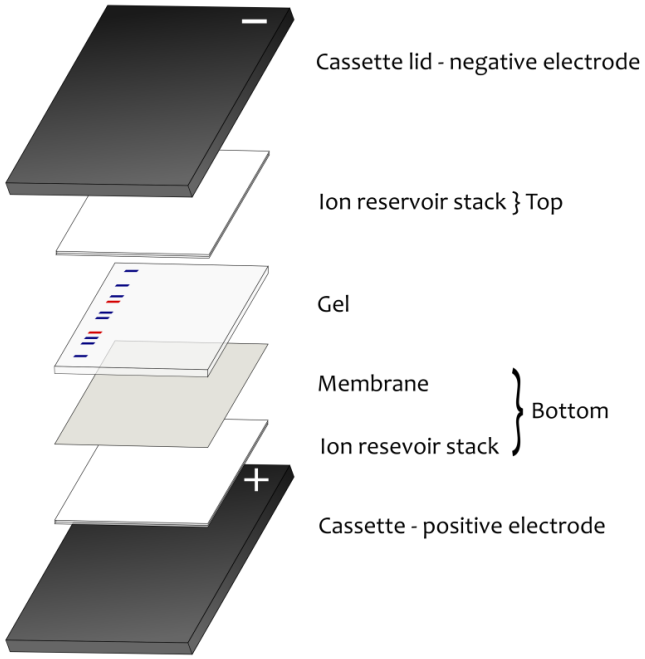

Figure 2.6 Assembly of the transfer sandwich for western blot.
The blotting was prepared as described by the manufacturer. The bottom stack was placed on top of the positive electrode. This stack contained the membrane onto which the proteins would be transferred. The gel was placed above the membrane and the top stack positioned beneath the negative electrode.

To prevent the unspecific binding of antibodies, membranes were incubated with a blocking solution: 5% milk with 0.5% Tween detergent for COMT and MAO-A and 5% milk with 0.1% Tween for MAO-B. Afterwards, membranes were incubated overnight at 4 °C in 1% milk as follows:

- Rabbit monoclonal anti-MAO-A, HRP conjugate (EPR7101, Abcam): dilution 1:5000 in 1% milk 0.5% Tween.
- Rabbit monoclonal anti-MAO-B (EPR7102, Abcam): dilution 1:1000 in 1% milk 0.1% Tween.
- Rabbit monoclonal anti-COMT (EPR6490, Abcam): dilution 1:2000 in 1% milk 0.5% Tween.

Membranes were washed three times with PBS Tween in the rotor at room temperature for 10 min. MAO-B and COMT were incubated with the secondary antibody. The anti-rabbit IgG antibody was diluted 1:3000 in 1% milk and the membranes incubated for 1 h at room temperature in the rotor. The membrane with anti-MAO-A primary antibody was not incubated with the secondary antibody as the primary was already conjugated to HRP. The membranes were then washed three times with PBS Tween in the rotor at room temperature for 10 min. Bio Rad Clarity Western ECL substrate solution was used to resolve the bands. Then, a Bio Rad ChemiDOC^{TM} MP imaging system was utilised in automatic exposure mode to detect the bands' intensity.

The membranes were washed with PBS Tween and stripped with the restore western blot stripping buffer at 37 °C for 15 min. 5% milk 0.5% Tween was used to block the membranes before incubating with rabbit monoclonal anti-GAPDH, HRP-conjugated (14C10, New England Biolabs), for 1 h at room temperature (dilution 1:3000). Resolution was carried out in the same way for all antibodies. Ultimately, Image J was used to quantify band intensity. Molecular weights were always confirmed by comparison with the ladder ***(Figure 2.7)***. Protein expression was normalised against the housekeeper protein, GAPDH.

2.5.1. Optimisation of antibody dilution

Anti-MAO-A, MAO-B and COMT antibodies were optimised for the SH-SY5Y cell line. In order to do so, control untreated and 3 h L-DOPA treated cells were used and processed as described in section 2.2.3.3. Two membranes were incubated with anti-MAO-A at two different concentrations: 1:5000 and 1:1000 in 1% milk 0.5% Tween ***(Figure 2.8 A)***.

A further two membranes were incubated with anti-MAO-B also at 1:5000 and 1:1000 dilutions in 1% milk 0.5% Tween ***(Figure 2.8 B, left and centre)***. One membrane was incubated with 1:2000 anti-COMT in 1% milk 0.5% Tween, the concentration optimised for SH-SY5Y cell line as stated by the manufacturer ***(Figure 2.8 C, left)***.

Finally, one membrane was incubated with 1:3000 dilution of the anti-rabbit only to exclude any unspecific interaction ***(Figure 2.8 C, right)***. Due to the long exposure time required to develop the MAO-B band, 1:1000 dilution in 1% milk 0.1% Tween was tested ***(Figure 2.8 B, right)***. After these experiments, membranes were stripped and incubated with anti-GAPDH 1:3000 as described in section 2.5. Finally, the dilutions specified in section 2.5 were chosen.

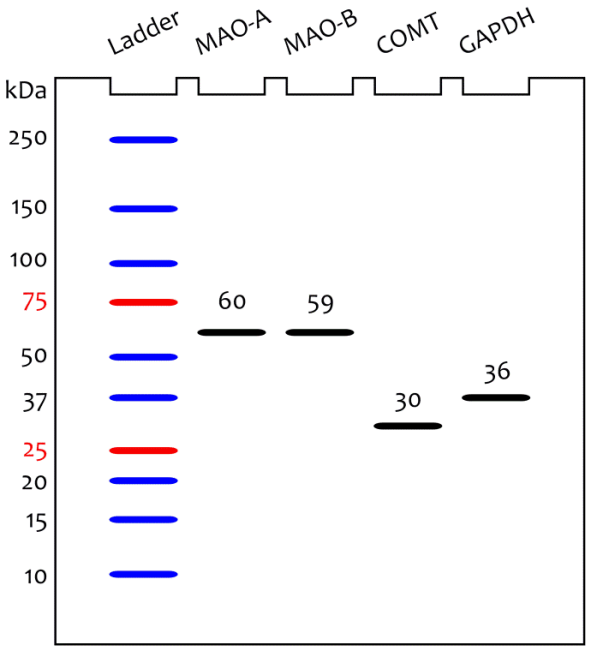

Figure 2.7 Molecular weights of the proteins analysed by western blot.
Monoclonal rabbit antibodies were used to detect MAO-A (60 kDa), MAO-B (59 kDa), COMT (30 kDa) and, as a housekeeper, GAPDH (36 kDa). A secondary anti-rabbit IgG HRP-linked was used to detect MAO-B and COMT. MAO-A and GAPDH primary antibodies were HRP conjugated.

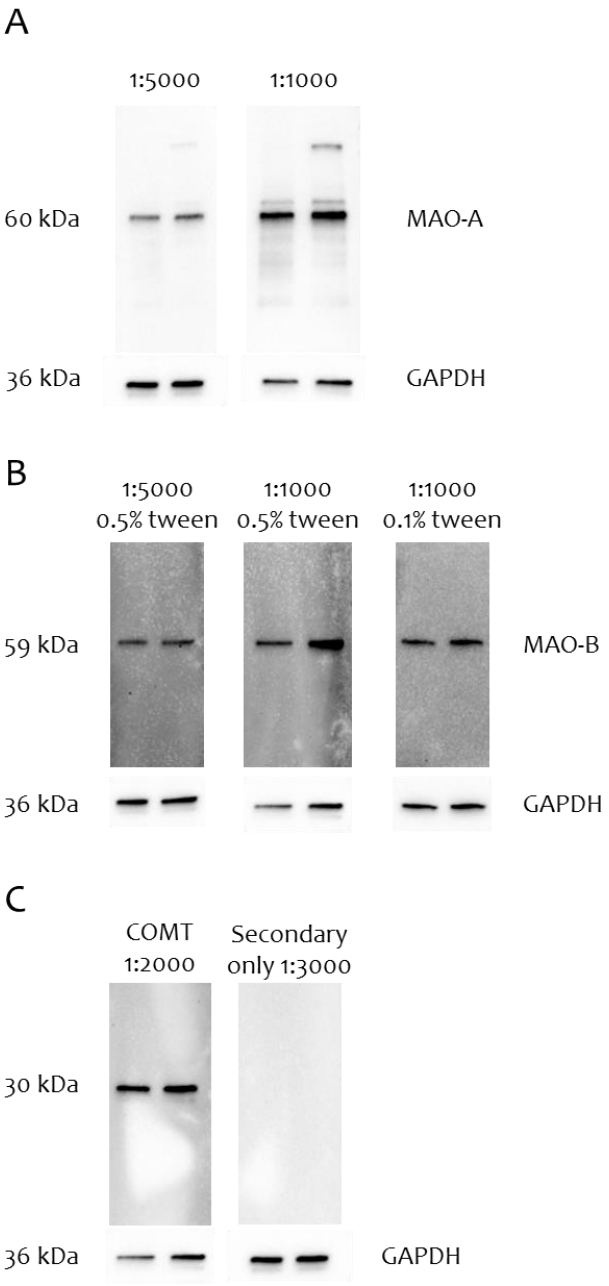

Figure 2.8 Optimisation of antibody dilution.
All the antibodies were tested to confirm their specificity and to optimise the dilution for the SH-SY5Y cell line under the current conditions. The samples tested were SH-SY5Y cells in basal conditions (first lane) and treated for 3 h with 100 μM L-DOPA (second lane). Both anti-MAO-A (A) and anti-MAO-B (B) were diluted 1:5000 and 1:1000 in 1% milk with 0.5% Tween. As anti-MAO-B dilutions needed long exposure times to detect the band, the antibody was diluted 1:1000 in 1% milk with 0.1% Tween. Anti-COMT (C) was only diluted 1:2000 in 1% milk with 0.5% Tween as the manufacturer stated that this was the optimum dilution for the SH-SY5Y cell line. Lastly, membranes were incubated with a dilution of 1:3000 of the anti-rabbit only (C) to confirm its specificity.

2.6. qRT-PCR

2.6.1. Total RNA extraction

Total RNA was extracted using the RNeasy Mini Kit following the manufacturer's instructions. Frozen pellets were lysed by adding 350 µl RLT lysis buffer containing 0.01% of β-mercaptoethanol. The mix was vortexed for 1 min and 350 µl of 70% ethanol were added. It was mixed thoroughly and transferred to an RNeasy spin column placed in a 2 ml collection tube, before centrifuging for 15 sec at 8000 ×*g*. Flow through was discarded and 700 µl of RW1 buffer were added to the column. It was centrifuged again for 15 sec at 8000 ×*g*. Flow through was again discarded and 500 µl of RPE buffer were added to the column. It was centrifuged once more for 15 sec at 8000 ×*g*. The flow through was discarded and this centrifugation step was repeated, but time for 2 min. After discarding the flow through, the column was placed empty in a collection tube and centrifuged once more for 1 min at 8000 ×*g* to eliminate any possible carry over. The column was then placed in a new 1.5 ml collection tube. 30 µl of nuclease-free H_2O were added to elute the RNA before centrifuging for 1 min at 8000 ×*g*. Finally, the total RNA concentration in the samples was determined with a NanoDrop 2000 spectrophotometer (Thermo Fisher Scientific) by measuring absorbance at 260 nm. The sample quality was confirmed by 260/280 and 260/230 ratios. Lastly, the RNA concentration of the sample was calculated using a modified Beer-Lambert equation. Both ratios and sample concertation were calculated using Thermo Scientific NanoDrop 2000 software.

2.6.2. RNA purification

To avoid DNA contamination, a DNase I kit was used following the manufacturer's protocol. The following mix was prepared for each sample: 1 µg of RNA, 1 µl of 10x DNase I reaction buffer, 1 µl of DNase I and 7 µl of nuclease-free H_2O. Samples were incubated

with this mix at room temperature for 15 min. Finally, DNase I was inactivated by the addition of 1 µl of EDTA and incubation at 65 °C for 10 min.

2.6.3. mRNA reverse transcription

For the reverse transcription of the mRNA, superscript III reverse transcriptase kit and oligo (dT) were used as specified by the manufacturer. Oligo (dT) selects mRNA over tRNA and rRNA to enable retro-transcription. This process comprised two reactions carried out in a PCR plate, using a Verity 96 well thermal cycler (Applied Biosystems). For the first reaction, 3 µl of master mix I were prepared per sample. This consisted of 1 µl of a mix 1:1 of forward and reverse oligo (dT), 1 µl of dNTP mix and 1 µl of nuclease-free H_2O. The master mix I was added to the PCR plate along with the purified RNA sample. The plate was then sealed and heated at 65 °C for 5 min. Once finished, the plate was placed on ice for 1 min before adding 7 µl of the master mix II. This second mix comprised 4 µl of 5x first strand buffer, 1 µl of 0.1 M DTT, 1 µl of SuperScript™ III RT and 1 µl of nuclease-free H_2O. The plate was sealed and placed in the thermal cycler again. The reaction was carried out for 1 h at 50 °C and inactivated at 70 °C for 15 min. Samples were then stored at 4 °C. Finally, samples were diluted 1:25 in nuclease-free H_2O before being stored at –20 °C until required for the qPCR.

2.6.4. qPCR: cDNA amplification and quantification

Lastly, cDNA of dopamine pathway enzymes was assessed with Mesa Blue qPCR MasterMix plus (Eurogentec, Seraing, Belgium) as described by the manufacturer. To do so, samples were further diluted 1:2 in nuclease-free H_2O and loaded in a qPCR plate. Then, 10 µl of 2x Mesa Blue qPCR MasterMix plus (Eurogentec) and 1 µl of the primer stock were prepared per well. The primer stock comprised a mix 1:1 of forward and reverse primers ***(see Table 2.1)***. The qPCR plate was sealed and centrifuged at 2,000 rpm for 2 min, before

being placed in the StepOne Plus Real-time PCR system (Applied Biosystems). The run comprised MeteorTaq activation at 95°C for 5 min followed by 40 cycles of 15 sec at 95 °C of denaturation and 1 min at 60 °C of annealing and elongation. Data acquisition was registered and analysed with StepOne™ software v2.3.

Table 2.1 Primers used in the qPCR.
The primer codes were obtained from the literature as reported.

TH	Forward	CGGGCTTCTCGGACCAGGTGTA
	Reverse	CTCCTCGGCGGTGTACTCCACA

(Kirkeby et al., 2012)

AADC	Forward	TGCGAGCAGAGAGGGAGTAG
	Reverse	TGAGTTCCATGAAGGCAGGATG

(Reinhardt et al., 2013)

MAO-A	Forward	CTGATCGACTTGCTAAGCTAC
	Reverse	ATGCACTGGATGTAAAGCTTC

(Jiang et al., 2012)

MAO-B	Forward	GCTCTCTGGTTCCTGTGGTATGTG
	Reverse	TCCGCTCACTCACTTGACCAGATC

(Jiang et al., 2012)

COMT	Forward	TGAACGTGGGCGACAAGAAAGGCAAGAT
	Reverse	TGACCTTGTCCTTCACGCCAGCGAAAT

(Nackley et al., 2009)

GAPDH	Forward	TTGAGGTCAATGAAGGGGTC
	Reverse	GAAGGTGAAGGTCGGAGTCA

(Kirkeby et al., 2012)

2.6.5. Analysis

The expression of dopamine pathway enzymes was calculated using the $\Delta\Delta C_T$ method (Schmittgen and Livak, 2008). A control sample was routinely analysed in every qPCR to compare different plates. This control sample was obtained from untreated no-L-DOPA SH-SY5Y cells. Data are shown as fold change in the expression of the target compared to GAPDH and to the control sample, as described in ***Equation 2.2***.

$$\Delta\Delta C_T = \Delta C_T\ sample\ (C_T\ target - C_T\ GAPDH) - \Delta C_T\ control\ (C_T\ target - C_T\ GAPDH)$$

$$\text{Fold change} = 2^{-\Delta\Delta C_T}$$

Equation 2.2 Formulas used to calculate the mRNA expression of dopamine pathway enzymes. *The expression of the enzymes studied was normalised against the housekeeper gene GAPDH and the control sample to obtain $\Delta\Delta C_T$.*

2.7. Reduced Glutathione Quantification by HPLC

2.7.1. Equipment

PU-980 Intelligent HPLC pump (JASCO UK Ltd., Great Dunmow, UK); Degasys Populaire HPLC degasser DP2010 (Kromatek, Dunmow, UK); AS-2055 Plus Intelligent sampler (JASCO); TS-130 column oven (Phenomenex, Torrance, CA, USA); Coulochem III electrochemical detector (ESA Analytical Ltd., Aylesbury, UK); 5010A standard analytical cell (Thermo Fisher); and C18HS column, 250 mm × 4.6 mm with a pore size of 100 Å and a particle size of 5 µm (Kromatek). The electrochemical detector was coupled to a

computer and data acquisition was registered and analysed using AZUR software (Kromatek).

2.7.2. Sample preparation

To assess the intracellular concentration of GSH by HPLC, cells were stored as a pellet at –80 °C and processed immediately before the analysis. In order to do so, the cell pellet was homogenised with the protein isolation buffer as described in section 2.2.3.3. One aliquot of this homogenate was kept to measure protein content as described in section 2.8. Then, the homogenate was quickly diluted 1:10 in 15 mM orthophosphoric acid. Cells were lysed by 3 repetitions of the freeze–thaw cycle described in section 2.2.3.3. Afterwards, samples were incubated at 4 °C for 10 min, and centrifuged at 13,000 ×*g* for 5 min at 4 °C. Finally, the supernatant was collected and injected into the HPLC system.

2.7.3. Procedure

Reverse-phase HPLC attached to an electrochemical detector was used to measure GSH following the Riederer et al. (1989) method with minor modifications. The mobile phase comprised 15 mM orthophosphoric acid in ultrapure H_2O and the flow rate was set at 0.5 ml/min. The steady phase was a C18HS 250 mm × 4.6 mm column (Kromatek, Dunmow, UK) was maintained at 35 °C. Prior to analysis, samples were prepared as described in section 2.7.2 and placed in vials in the autosampler at room temperature. 50 µl of each sample were injected into the HPLC system. The screening electrode (SE) was set to 50 mV to oxidise molecules of low oxidation potential. A voltammogram from 100 to 650 mV was performed to select the detector electrode's (DE) potential ***(Figure 2.9 A)***. Despite obtaining the highest response at 650 mV, the background current was very high and the signal unstable. Therefore, DE was maintained at 550 mV to measure GSH.

Samples' GSH concentration was determined by comparison of the peak area against an external standard of 5 µM GSH in 15 mM orthophosphoric acid. A calibration curve from 0.01 to 25 µM GSH was completed in order to confirm the linearity between the peak area and the standard concentration (r^2 = 0.997, ***Figure 2.9 B***). Finally, the recovery of the sample was assessed by spiking. To do this, a known amount of each individual standard was added to the sample and the peaks quantified as described in section 2.7.4. The expected concentration is then divided by the resulting spiked concentration to obtain the recovery of the sample. The percentage of recovery of the sample in the current study was 97.22 ± 0.02.

2.7.4. Analysis

The identification of GSH was performed by comparison of the retention time between the standard and the sample. The intracellular GSH content was expressed as nmol GSH per mg of protein and was calculated following ***Equation 2.3***.

$$\text{GSH concentration (pmol/mg protein)} = \frac{[GSH]_{standard} \times Peak\ area_{sample}}{Peak\ area_{standard} \times [prot]}$$

Equation 2.3 Formula used to calculate GSH concentration.
$[GSH]_{standard}$: *GSH concentration standard = 5 µM*; $Peak\ area_{sample}$: *area of the GSH peak in the chromatogram*; [prots]*: concentration of proteins.*

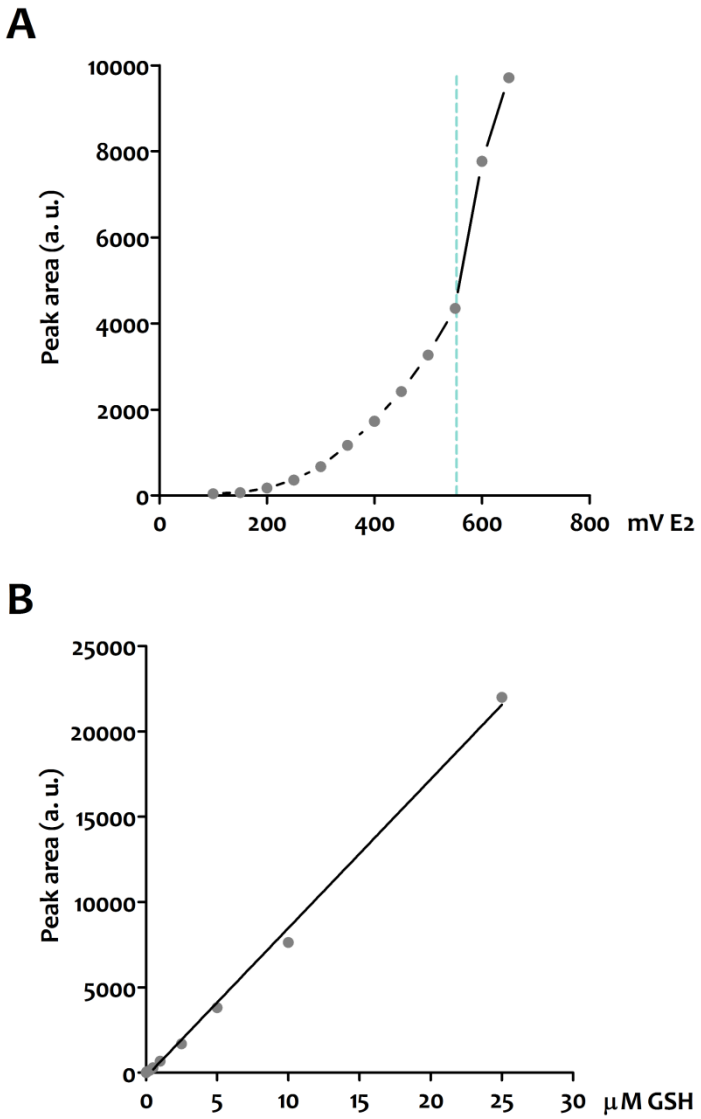

Figure 2.9 Voltammogram and calibration curve of GSH measurement.
(A) 5 µM GSH was injected into the system and quantified at different voltages of the detector electrode (E2) to select the optimum conditions. (B) A range of GSH concentrations were measured at 550 mV to confirm the linearity between GSH concentration and peak area.

2.8. Total Protein Quantification

2.8.1. Principle

Total protein concentration was determined using the Bradford assay (Bradford, 1976). When mixed, proteins bind to Coomassie blue dye turning the latter into a stable unprotonated blue mixture. Some studies have concluded that the dye binds to basic and

aromatic amino acid residues, such as arginine and tyrosine respectively (Compton and Jones, 1985). The absorbance of the samples is measured at λ = 595 nm and the protein concentration is calculated by linear regression against an external standard.

2.8.2. Method

The Bradford reagent was purchased from Sigma and assay run in a 96-well plate following manufacturer's instructions. SH-SY5Y cells were collected and processed as described in section 2.2.3.3. Then, samples were diluted 1:20 with ultrapure H_2O and 20 µl were added per well. Then, a 7-point calibration curve was prepared; dilutions from 0 to 200 µg/ml of bovine serum albumin were used as an external standard ***(Figure 2.10)***. Next, 180 µl of the Bradford reagent were added to each well. The plate was then placed in the Infinite f200 plate reader (Tecan, Männedorf, Switzerland), mixed by orbital shaking for 30 sec and incubated for 10 min at room temperature. Finally, absorbance was measured at 595 nm. All samples and standards were done in triplicate. Total protein concentration was calculated by linear regression comparing the sample's absorbance to the calibration curve.

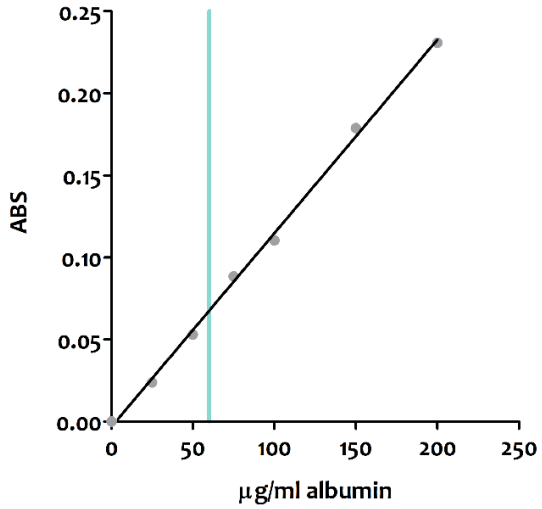

Figure 2.10 Bradford calibration curve.
A 7-point calibration curve (dilutions from 0 to 200 µg/ml) of bovine serum albumin was prepared and used as an external standard in every assay. This is a representative example where each point represents a n = 3 of technical replicates (R^2 = 0.9974). The blue line represents the average total protein concentration (60 µg/ml).

2.9. Statistical Analysis

Each experiment was repeated independently at least three times (n ≥ 3 experimental replicates). Results are expressed as mean ± standard error of the mean (SEM). In all models used in the present study, individual comparison of means was made using the Student's t-test by GraphPad Prism software (GraphPad Software INC. San Diego, CA, USA). For multiple comparisons, the one-way ANOVA test followed by the *post hoc* Tukey's test was performed. All ratios were transformed prior to statistical analysis by calculating the square root of the ratio. This calculation transforms the data to a normal distribution so that statistical analysis can be carried out (Gegg et al., 2004).

CHAPTER 3

Catecholamine Measurement by High Performance Liquid Chromatography Coupled to an Electrochemical Detector

3.1. History

In the 19th century, the botanist Mikhail Tsvet invented a technique to separate chlorophylls and carotenes in solution (Weil and Williams, 1951). He called this technique chromatography, as the coloured molecules travelled through an inert phase of cellulose. Initially, it was proposed that the components moved along the inert phase due to capillarity. It was later that terms such as affinity and adsorption were associated with this technique.

In the 1940s, Archer Martin and Richard Synge modified and applied this technique to biochemistry, winning the Nobel Prize in chemistry in 1952 (Martin and Synge, 1941). The new technique was called partition chromatography and consisted of the separation of compounds by two immiscible phases: one stationary and polar, and another liquid which would be non-polar. The revolutionary idea was using silica to retain water in the columns while the organic mobile phase circulates through, carrying the sample. This innovation led to the development of new chromatographic techniques, i.e. adsorption chromatography by Martin and others (Howard and Martin, 1950). However, the techniques used in the 1960s and the beginning of the 1970s for chemical separation were inadequate to quantify and separate similar molecules (chromatographic techniques summarised by Coskun, 2016).

Compound resolution by column chromatography was very slow as it depended on gravity. This, coupled with irregular flow rates, meant that it was not routinely used. However, during the 1970s, pressure to decrease the length of the process led to the development of high pressure liquid chromatography (HPLC) along with improved analytical equipment (Majors, 1994). Modification of the stationary phase led to new chromatographic properties; for example, chains of 18 carbons were attached to the silica matrix, changing the stationary phase from polar to non-polar. This is known as reverse-

phase HPLC, in contrast to the traditional normal-phase HPLC (naked silica). As these changes increased the reproducibility of the technique, the name was changed to high performance liquid chromatography, maintaining HPLC as the abbreviation (Horváth, 1988).

3.2. Principles

3.2.1. Separation

Compound separation by HPLC is highly dependent upon the conditions applied. Amongst these variables are pressure, composition and temperature of the mobile and stationary phase. The composition and temperature of the mobile phase are essential for the resolution of the compounds, as this determines the interactions between the compounds and the stationary phase. When the composition of the mobile phase remains constant throughout the experiment, the method is known as isocratic HPLC. On the contrary, if the composition of the mobile phase varies during the separation, it is called gradient elution HPLC. This method usually includes two mobile phases, one organic and one aqueous, that are pumped simultaneously at unequal proportions. The percentage of each mobile phase changes during the experiment, modifying the affinity between the stationary phase and the compounds. In isocratic HPLC, the pressure remains constant at a fixed solvent composition and directly depends on the flow rate.

In the present study, dopamine and its metabolites were quantified using reverse-phase isocratic HPLC. Using this technique, an analyte mixture in an aqueous solvent is pumped through the system. The compounds interact with the stationary phase inside the column, which comprises silica and chains of 18 carbons ***(Figure 3.1)***. The strength of this interaction can be modified by ion pairing, as these ionic molecules can modify the

retention and selectivity of ionic compounds like monoamines (Dolan, 2008). Thus, under these conditions hydrophobic molecules interact with the stationary phase for longer than hydrophilic molecules, which elute before.

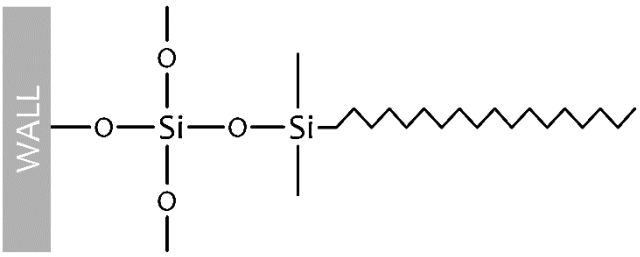

Figure 3.1 Chemical structure of the stationary phase.
While the silica interacts with the walls of the column, the chains of 18 carbons (C18) interact with the analytes. The affinity of that interaction depends on the composition of the mobile phase.

3.2.2. Detection

This selective detection method uses specific characteristics of the compounds to be measured, such as their fluorescence or their chemical properties. The method used in this study is electrochemical detection, which uses the inherent electrochemical properties of monoamine. An essential parameter for this detection is the applied voltage, which determines the number of electrons transferred from the electrode to the molecule or vice versa, directly influencing the electric current measured by the software (Kilpatrick et al., 1986). After being separated in the column, the compounds pass through the electrochemical detector, two electrodes that create an electrical potential to oxidise or reduce the molecules passing between them. The first electrode, the screening electrode (SE), is maintained at lower voltages to oxidise low-oxidation potential molecules. The second is the detector electrode (DE). The voltage applied by this second electrode oxidises or reduces the target analytes. To increase the selectivity, this voltage needs to be

the minimum possible to oxidise the target molecules only and not molecules with higher oxidation potential.

A positive voltage was used here; therefore, the oxidation of the molecules was quantified. Oxidation is proportional to the concentration of the molecule injected into the system, leading to changes in the input current. These changes were quantified with the EZChrom Elite™ chromatography data system, version 3.1.7 (JASCO UK Ltd., Great Dunmow, UK). Finally, the values analysed from the chromatograms were retention time and peak area. The retention time is the time that a certain compound takes to elute. The peak area is proportional to the concentration of the compound, although this needs to be validated with known standards. Both values depend on the technical properties of the HPLC and are exclusive for each compound.

3.3. Equipment

PU-1580 Intelligent HPLC pump (JASCO UK Ltd., Great Dunmow, UK); DG-980-50 3-Line Degasser (JASCO); AS-1555 Intelligent sampler (JASCO) with an injection loop of 100µl; CO1560 Intelligent Column Thermostat (JASCO); Coulochem II electrochemical detector and 5010 analytical cell (ESA Analytical Ltd., Aylesbury, UK) were arranged as in the ***Figure 3.2***. The electrochemical detector was coupled to a computer and data acquisition was registered using EZChrom Elite™.

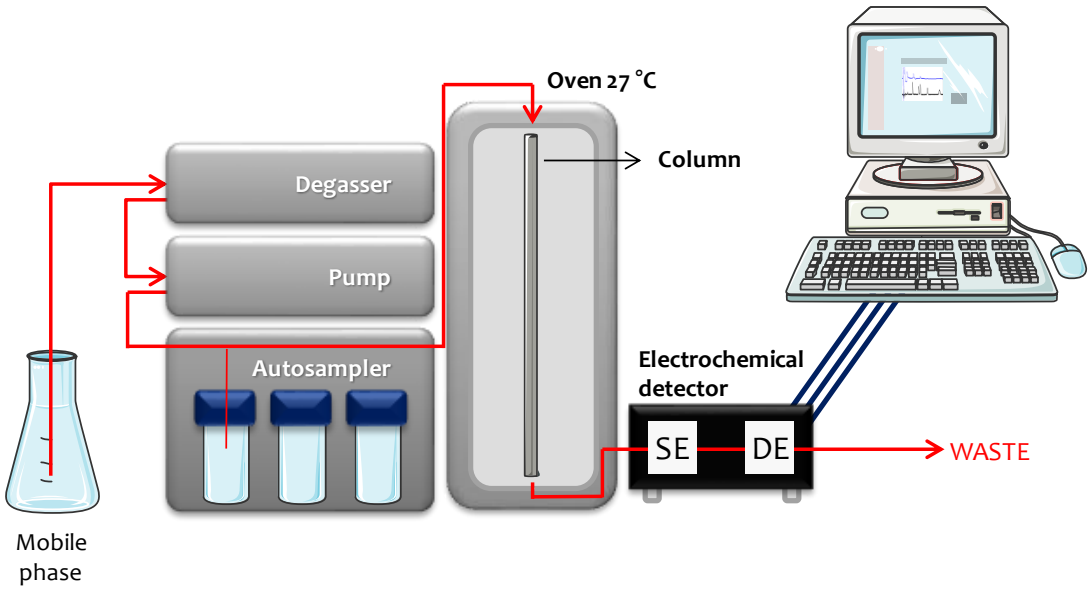

Figure 3.2 HPLC equipment.
Degassed mobile phase is pumped through the autosampler, in which samples are injected. It then crosses the column, which retains the molecules depending on its affinity with the molecule and the mobile phase characteristics. Finally, the electrochemical detector oxidises or reduces the compounds. The oxidation/reduction quantification is performed with EZChrom Elite™ software. SE: screening electrode; DE: detector electrode.

3.4. Development of the Method

The method is based on that of Allen et al. (2013), modified for the simultaneous detection of DOPAC, 3-OMD, 5-HIAA, HVA and dopamine, as previous studies used two different methods to measure dopamine and serotonin metabolites. The modifications included acidification of the pH; increased concentration of the ion pairing molecule, i.e. 1-octanesulfonic acid; and a decrease in the temperature at which the stationary phase was maintained. With these changes, all five compounds eluted in experiments under 40 min with an optimum resolution.

After optimisation, the mobile phase comprised 20 mM sodium acetate trihydrate (pH 3.45), 12.5 mM citric acid monohydrate, 0.1 mM EDTA sodium, 3.35 mM 1-octanesulfonic acid and 16% methanol in ultrapure water. Samples were prepared as described in section 2.2.3.1 and kept at –80 °C. Before the experiment, samples were

thawed at room temperature and transferred to vials before placing them in the autosampler, set up at 4 °C. The column used was a C18HS column, 250 mm × 4.6 mm with a pore size of 100Å and a particle size of 5 µm (Kromatek). The flow rate was set at 1.5 ml/min and the oven was maintained at 27 °C. Within the electrochemical detector, a voltage of 450 mV was selected for the detector electrode (DE), while the screening electrode (SE) was maintained at 20mV. Finally, 50 µl of each sample were injected into the system ***(Figure 3.3, blue line)***. Sample quantification was calculated against an external standard mixture of 500 nM 3-OMD, dopamine, DOPAC, HVA and 5-HIAA, made in ultrapure water with few drops of 12 M hydrochloric acid ***(Figure 3.3, black line)***. ***Equation 3.1*** was used for the quantification of each molecule.

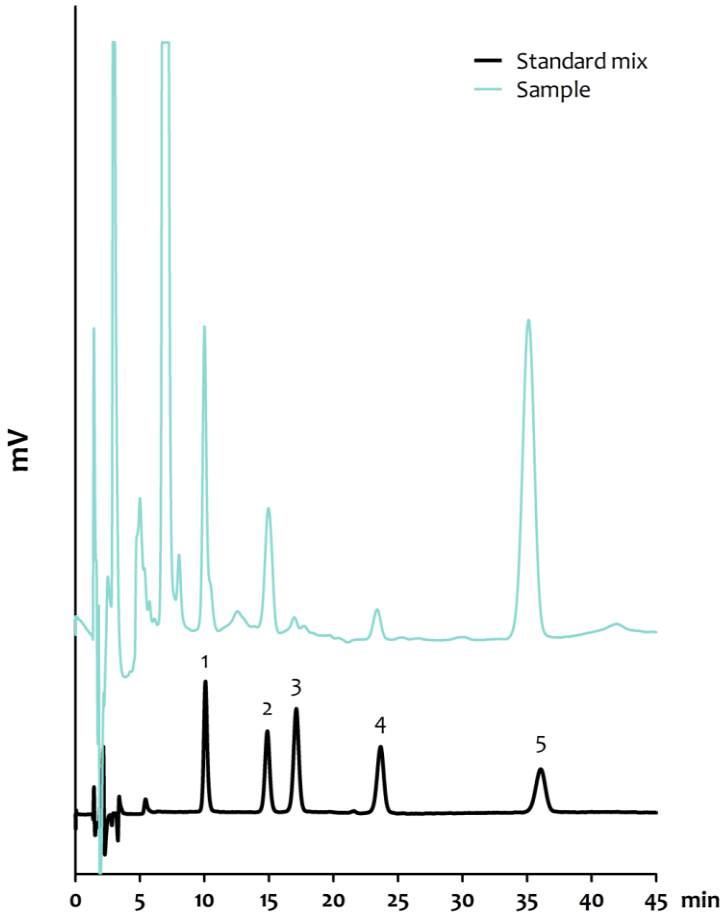

Figure 3.3 Sample and standard chromatograms.
Chromatogram of an SH-SY5Y sample after L-DOPA treatment is represented in blue and compared to a 500 nM standard mix (1, DOPAC; 2, 3-OMD; 3, 5-HIAA; 4, HVA; 5, dopamine).

$$[\text{Sample}] = \frac{Peak\ area\ (sample) \times [External\ standard]}{Peak\ area\ (external\ standard)}$$

Equation 3.1 Calculation of the catecholamine concentration.
[Sample]*: concentration of the molecule* $\boldsymbol{x}$ *in the sample;* [External standard]*: concentration of the molecule* $\boldsymbol{x}$ *in the external standard.*

3.4.1. Peak resolution and identification

Each compound was analysed separately to determine the individual retention times. A sample of 500 nM of each molecule was injected. The molecules always appeared in the following order: DOPAC, 3-OMD, 5-HIAA, HVA and dopamine ***(Figure 3.4, thin lines)***. To check that the mixture of all five compounds did not alter the retention time, a mixture of all five was also run ***(Figure 3.4, bold line)***. This confirmed that retention time is a good parameter for peak identification as it remains constant.

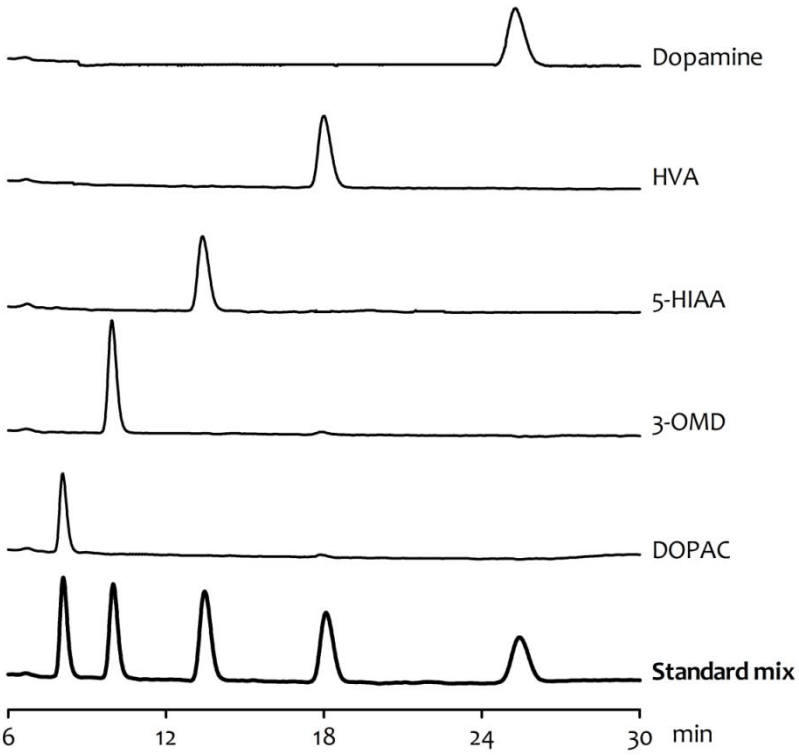

Figure 3.4 The retention time for peak identification.
The bold line shows a mixture of 500 nM of all five compounds, whereas the thin lines represent 500 nM of DOPAC, 3-OMD, 5-HIAA, HVA and dopamine, respectively from bottom to top. The retention time is a good parameter for peak identification as it remains constant and is specific for each compound.

3.4.2. Voltammograms

The standard mixture was analysed at different DE voltages to select the optimum value at which all the compounds were fully oxidised. These curves show a sigmoid shape due to the redox potential of the compounds, which is different for each one. The voltage needs to be higher than the redox potential of the compounds measured on the same sample. However, it needs to be the minimum value possible to obtain the maximum selectivity. This is because at higher voltages other compounds with higher redox potential could appear in the chromatogram, interfering with measurement of the molecules being studied. A 500 nM mixture of DOPAC, 3-OMD, 5-HIAA, HVA and dopamine was measured at DE voltages ranging from 30 mV to 500 mV. SE was maintained at 20 mV in all cases. Three separate measurements were taken for each voltage point. Finally, a voltage of 450 mV was selected to achieve the plateau phase when oxidation of all the molecules is at maximum level ***(Figure 3.5)***.

3.4.3. Calibration curves

Calibration curves were produced to determine the linear correlation between standard concentration and peak integration. A 2.5 mM DOPAC, 3-OMD, 5-HIAA, HVA and dopamine standard mixture was serially diluted and analysed by HPLC ***(Figure 3.6)***. The lower detection limit was found to be 12.5 nM; values under that concentration were classified as undetectable or zero. A linear correlation was confirmed for all five compounds between 12.5 nM and 2.5 mM ($r^2 > 0.99$).

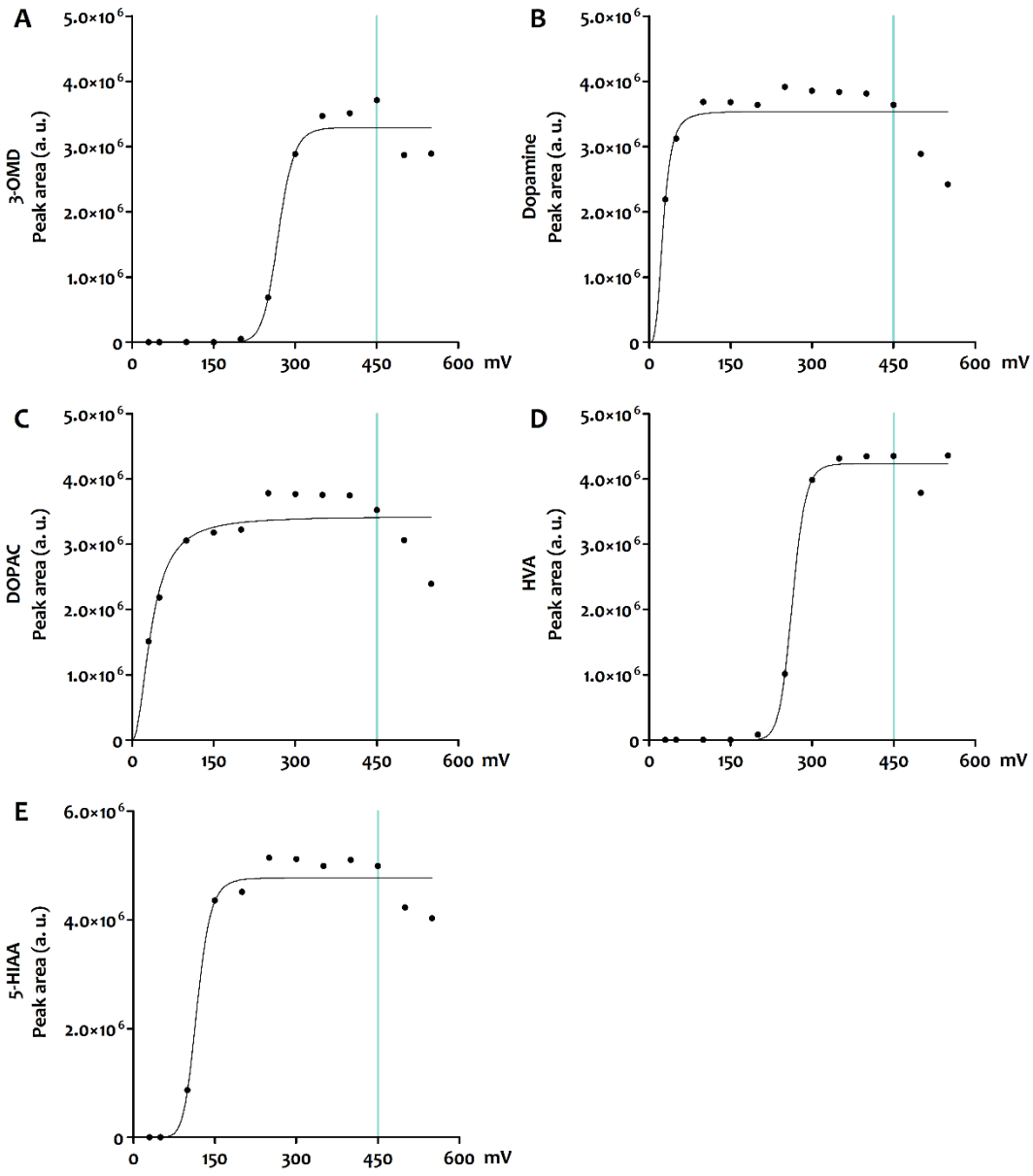

Figure 3.5 Voltammograms.
A 500 nM mixture of all five compounds (A, 3-OMD; B, dopamine; C, DOPAC; D, HVA; E, 5-HIAA) was run in a range of voltages from 30 mV to 550 mV. The area under the peak was integrated and plotted for each voltage. Finally, a voltage of 450 mV was selected as optimum (blue line), as all five compounds were on the plateau phase (n = 3 experimental replicates).

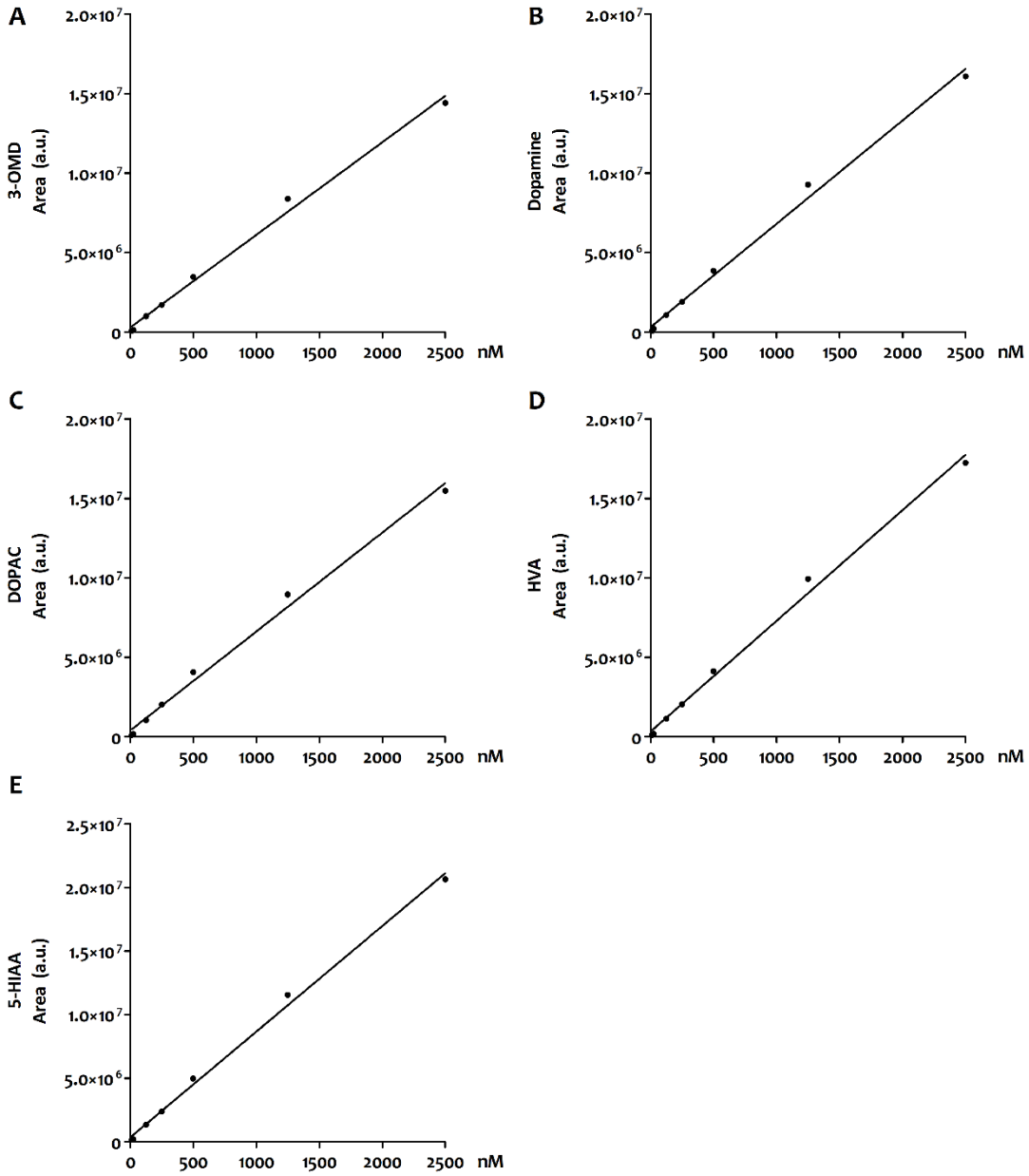

Figure 3.6 Calibration curves.
Serial dilutions from 2.5 mM to 7 nM of the standard mixture were run at 450 mV. The area under the peaks was integrated and plotted. Linear correlation was confirmed for 3-OMD (A, r^2 = 0.9937), dopamine (B, r^2 = 0.9944), DOPAC (C, r^2 = 0.9927), HVA (D, r^2 = 0.9944), and 5-HIAA (E, r^2 = 0.9962) between 12.5 nM and 2.5 mM (n = 3 experimental replicates).

3.4.4. Reproducibility

To study the variability of the technique, a fresh 500 nM standard mix was made every day for 5 days. The standards were kept at –80 °C and thawed prior to analysis. The results obtained with the fresh standard mix showed a variation of 5%. This variability is the average of all the compounds, some being more sensitive than others ***(Table 3.1)***. The signal to noise ratio was also analysed in the 500 nM standard mix and at 450 mV. The average of all the compounds was 3477 ***(Table 3.1)***. A decreased signal to noise ratio could explain the decline in the peak area at high voltages, see ***Figure 3.5***, as the input current increased markedly above 450 mV. Finally, the recovery of the samples was calculated. The remaining sample in the vial was combined with a known quantity of the standard mix and measured again. The expected and measured concentrations of the different molecules were then compared. The average recovery was 96% ***(Table 3.1)***, confirming that the peak specifically corresponded to one of the compounds.

Table 3.1 Reproducibility of the HPLC method.
The individual and average percentage of the coefficient of variation, recovery and signal to noise ratio are shown. % CV: percentage of the coefficient of variation.

	% CV	Signal to noise	% recovery
3-OMD	7%	3015	90%
Dopamine	4%	4570	97%
DOPAC	5%	2978	99%
HVA	7%	3518	96%
5-HIAA	4%	3306	97%
Average	5%	3477	96%

As all the compounds measured can oxidise, vials were kept at 4 °C in the autosampler to prevent/delay the oxidation of the molecules. A 500 nM standard mix was placed in the autosampler and measured every 2 h for 30 h. At the end of the experiment, the area under the peaks was integrated and plotted as percentage change in mV ***(Figure 3.7)***. It was noted that the concentration of DOPAC, HVA and 5-HIAA decreased over time, suggesting they were spontaneously oxidising despite being maintained at 4 °C.

Considering all the data, it was noted that 3-OMD had the highest coefficient of variation and the lowest recovery. However, when looking at its stability over time, integration at time 16 h is very similar to that at time 0. 3-OMD was also the most sensitive to change in pH and the composition of the mobile phase after several injections. Because of this variability, the 3-OMD peak could interfere with tailing of the neighbouring analytes. Therefore, 3-OMD identification was confirmed by recovery in every assay. DOPAC and HVA had the next-highest coefficients of variation. Although these molecules showed a better recovery, they also exhibited poorer performance over time, as did 5-HIAA. Although the increase in HVA levels over time could have been due to the enzymatic transformation from DOPAC, this is highly unlikely as pure compounds were used in these experiments.

In summary, external standards were run periodically in every experiment to control the oxidation of the molecules and to monitor possible changes in retention time due to changes in the pH of the mobile phase after several injections. Finally, to limit oxidation and avoid inaccurate quantification, each experiment had a maximum length of 16 h.

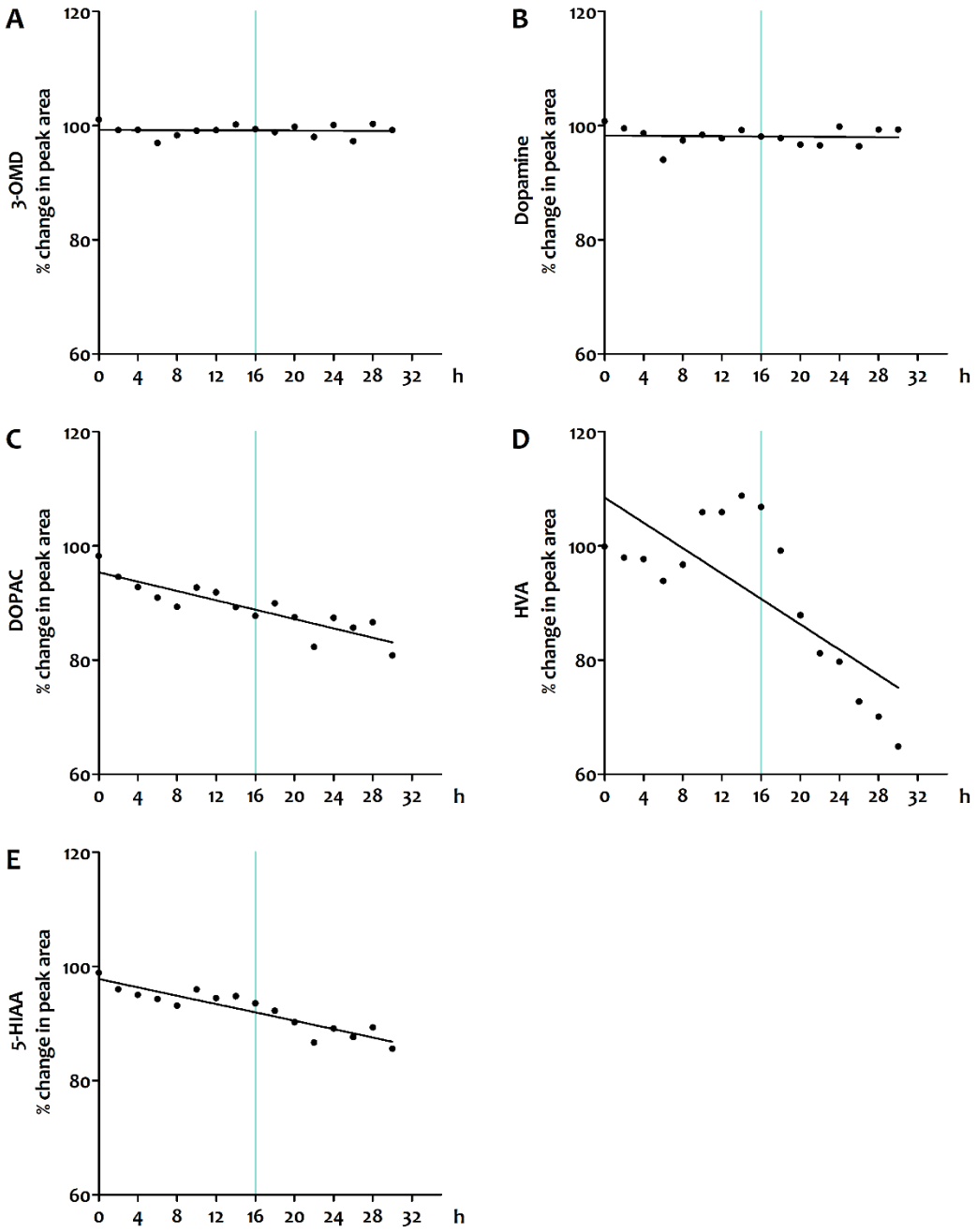

Figure 3.7 Stability of the standards over time.
A 500 nM standard mix was measured every two hours for 30 h. The area under the peaks was integrated and plotted as % change compared to time 0. DOPAC (C, $p<0.05$), HVA (D, $p<0.0001$) and 5-HIAA (E, $p<0.001$) signal significantly decreased after 30 h ($n = 3$ experimental replicates). The blue line represents the maximum length of time per experiment.

CHAPTER 4

Dopamine and Serotonin Metabolism in the SH-SY5Y Cell Line: Effects of Inhibition of Mitochondrial Complex I and Lysosomal Glucocerebrosidase

4.1. Introduction

Despite the considerable amount of research that has been carried out in PD, the primary cause is still unknown. Consequently, current therapies only provide temporary symptomatic relief by aiming to increase dopamine availability and/or signalling. This lack of knowledge is partially due to the nature of the disease and the difficulty of finding an accurate model. Historically, research into the pathogenesis of PD has been carried out in post-mortem brain tissue of PD patients or pharmacological animal models (summarised in Blesa and Przedborski, 2014). However, nowadays genetic animal models are quite often used (Blesa and Przedborski, 2014). More recently, iPS cells from affected patients are becoming a growing focus. iPS cells derive from fully mature cells, usually fibroblasts, which are reprogrammed to the pluripotent stage by treatment with transcription factors (Takahashi and Yamanaka, 2006). These iPS cells can then be differentiated to any cell type; for example, neurons. However, this is very arduous, time-consuming and not accurately reproducible.

Regarding basic research and generation of initial data that may provide insight into disease mechanisms, cell lines such as SH-SY5Y have been widely used in PD research. These cells are arrested in the G1 phase and show an adrenergic phenotype, expressing dopaminergic neuron-specific enzymes such as AADC, TH and transporters such as DAT (Khwanraj et al., 2015; Korecka et al., 2013). Initially, the SK-N-SH cell line was isolated from a bone-marrow biopsy of a four-year-old patient with neuroblastoma. This cell line was sub-cloned three times to generate the SH-SY5Y cell line. Like the original SK-N-SH cells, the SH-SY5Y cell line is composed of two different cell types: neuroblast- and epithelial-like cells. When treated with retinoic acid and brain-derived neurotrophic factor, SH-SY5Y neuroblast-like cells are selected and differentiate into a fully mature dopaminergic neuronal cell line (Nishida et al., 2008).

A number of putative pathogenic mechanisms have been considered in PD. These include oxidative stress, loss of mitochondrial function, particularly at the level of complex I, and reduced activity of GBA1 (Betarbet et al., 2000; Lynch-Day et al., 2012). Whilst such alterations in cellular metabolism can provide the basis for attractive hypotheses to explain dopaminergic neurodegeneration, little work has been done to study their effect on monoamine neurotransmitter metabolism. Furthermore, alterations in serotonin metabolism have been reported in PD (Stansley and Yamamoto, 2015). Consequently, the aims of this chapter are to:

- Characterise dopamine metabolism in SH-SY5Y cells. Additionally, due to a degree of overlap, serotonin metabolism was also documented.
- Document the effects of loss of mitochondrial complex I and/or lysosomal GBA1 activity on dopamine and serotonin metabolism.

4.2. Methods

4.2.1. Cell culture and sample preparation

SH-SY5Y cell line was grown as described in section 2.2.1. Cells were then pre-treated with AADC inhibitor (NSD-1015), rotenone and GBA1 inhibitor (CBE) as described in the sections 2.2.2.2–**Error! Reference source not found.**. Following the pre-treatment, SH-SY5Y cells were incubated with L-DOPA as described in section 2.2.2.1. Finally, samples were harvested and processed as detailed in section 2.2.3.1.

4.2.2. Monoamine measurement by HPLC

Monoamine concentration was quantified in the medium of pre-treated non-differentiated SH-SY5Y cells following the protocol described in Chapter 3.

4.2.3. Immunostaining

Proliferative SH-SY5Y cells were prepared for the immunostaining experiments as described in section 2.3. The cells used in these experiments were maintained in basal conditions, i.e. non-pre-treated and no L-DOPA incubation.

4.3. Results

4.3.1. SH-SY5Y cell line: dopamine metabolism in basal conditions

Dopamine and its metabolites were quantified in the culture medium of the SH-SY5Y cell line. After 3 h of incubation in the absence of L-DOPA no 3-OMD, dopamine, DOPAC or HVA were detectable in the medium collected ***(Figure 4.1 A)***. However, the serotonin metabolite (5-HIAA) was present. In view of these findings and the ongoing discussion as to whether SH-SY5Y cells consistently express TH (Lopes et al., 2010; Cui et al., 2015; McMillan et al., 2007), the expression of this enzyme was determined by immunostaining with previously validated antibodies by Kurian's lab. As shown in ***Figure 4.1 B***, TH immunostaining was negative, suggesting that the cells used here expressed little or no TH.

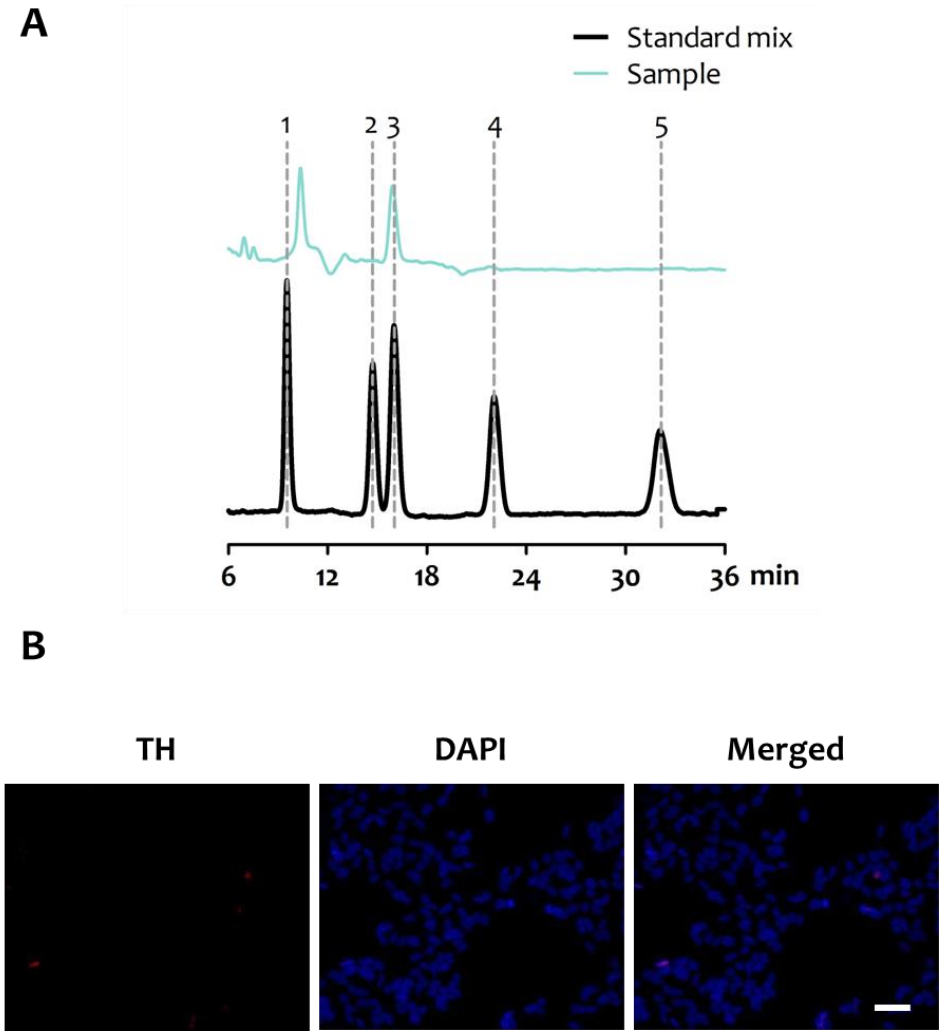

Figure 4.1 Dopamine secretion in undifferentiated SH-SY5Y cells.
(A) The identification of the peaks by the retention time showed SH-SY5Y cells did not secrete dopamine or dopamine metabolites to the medium in basal conditions (1, DOPAC; 2, 3-OMD; 3, 5-HIAA; 4, HVA; 5, dopamine). Blue line: chromatogram resulting from running a control medium sample. Black line: chromatogram of a 500 nM standard mixture. (B) Immunostaining of proliferative SH-SY5Y cells did not show any TH expression. Scale bar = 30 µm.

4.3.2. Dopamine metabolism after L-DOPA incubation

To study whether other enzymes of dopamine pathway beyond TH could synthesise dopamine, SH-SY5Y cells were incubated with 100 µM L-DOPA for 30 min, 1 and 3 h. After the L-DOPA incubation, cells were able to produce and release 3-OMD, dopamine, DOPAC and HVA into the medium ***(Figure 4.2)***. Additionally, the extracellular concentration of these compounds increased with longer treatment times.

To confirm whether L-DOPA was being metabolised via the dopamine pathway, AADC was inhibited before L-DOPA incubation. SH-SY5Y cells were treated with 10 µM NSD-1015 for 24 h (Allen et al., 2013), followed by 100 µM L-DOPA incubation for 1 h. While no effect was observed on 3-OMD release, NSD-1015 decreased the concentration of the molecules downstream in the pathway compared to the control ***(Figure 4.3)***. The release of dopamine, the direct AADC-metabolite, decreased by 80% after NSD-1015 treatment. However, the greatest decrease was in HVA, which decreased by 90%.

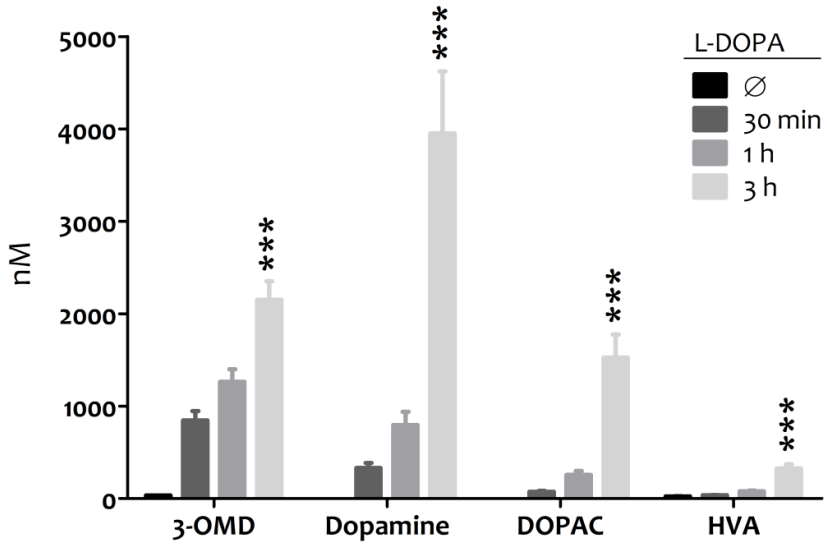

Figure 4.2 Time-dependent changes in the concentration of dopamine and its metabolites during incubation with L-DOPA.
*A higher extracellular concentration of 3-OMD (3-O-methyldopa), dopamine, DOPAC and HVA was observed after 3 h of L-DOPA incubation (n = 12 experimental replicates) when compared to all other three groups: no L-DOPA (ø, n = 14 experimental replicates), 30 min (n = 12 experimental replicates) and 1 h L-DOPA (n = 16 experimental replicates). Statistical analysis carried out by one-way ANOVA, followed by Tukey's post-test (***p < 0.0001). Data are presented as mean ± SEM.*

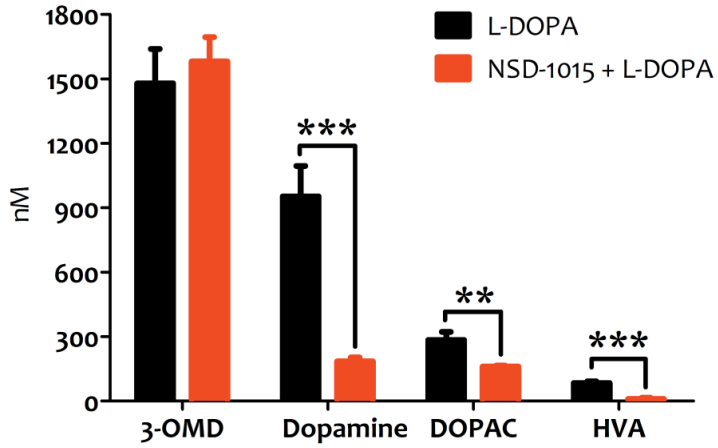

Figure 4.3 L-DOPA transformation via the dopamine pathway.
*Cells were treated with NSD-1015 for 24 h before L-DOPA incubation. NSD-1015 treatment (n = 12 experimental replicates) decreased the release of dopamine and its metabolites (L-DOPA, n = 16 experimental replicates). Statistical analysis carried out by unpaired Student's t-test (**p < 0.01; ***p < 0.0001). Data are presented as mean ± SEM.*

4.3.3. Extracellular 5-HIAA concentration after L-DOPA incubation

Serotonin turnover was also studied by quantifying 5-HIAA, its direct metabolite. These cells released 5-HIAA to the medium in basal conditions and that level of release remained constant and unaffected by L-DOPA incubation ***(Figure 4.4)***.

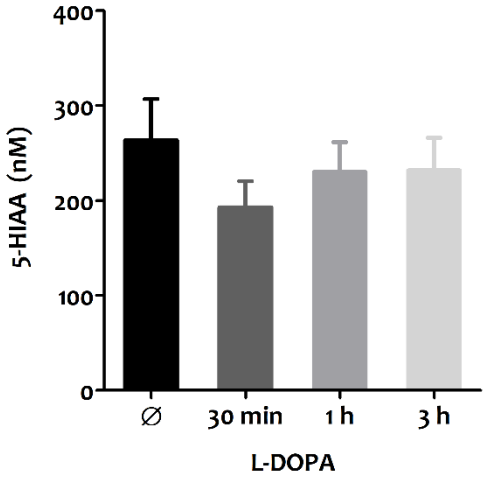

Figure 4.4 The effect of L-DOPA incubation on extracellular serotonin concentration.
Statistical analysis was carried out by one-way ANOVA, followed by Tukey's post-test. Data are presented as mean ± SEM. ø: no L-DOPA incubation.

4.3.4. Effect of L-DOPA incubation on overall dopamine metabolism

The relationship between neurotransmitters and their metabolites is a diagnostic tool. For example, the HVA to 5-HIAA ratio is calculated after measuring both molecules in the CSF of patients with neurotransmitter disorders (Burlina et al., 2017). With these ratios, not only can the absolute concentrations of dopamine and its metabolites be analysed, but also the turnover and homeostasis of the pathway.

In the current study, HVA to 5-HIAA and HVA to dopamine ratios were calculated. The HVA:5-HIAA ratio increased 6-fold after 3 h of L-DOPA incubation when compared to 30 min treatment ***(Figure 4.5)***. However, the HVA:dopamine ratio decreased 1.6 fold when the L-DOPA incubation was prolonged to 3 h ***(Figure 4.5)***. ***Equation 4.1*** was then applied to the data to calculate the turnover ratio. This third ratio allows a full comparison of dopamine with its degradation metabolites. It was observed that SH-SY5Y cells tended to degrade more dopamine during longer L-DOPA incubation times ***(Figure 4.5)***, but this increase was not significant ($p > 0.05$).

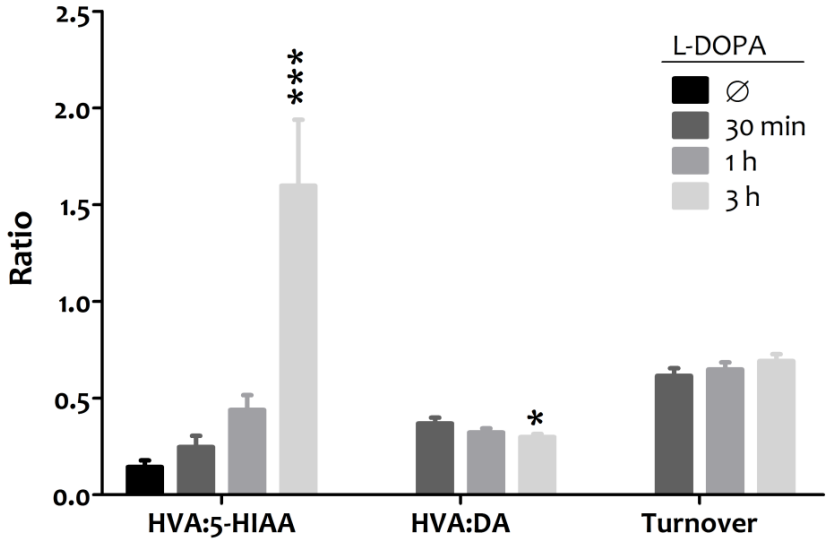

Figure 4.5 Changes in metabolite relationship after L-DOPA incubation.
*While the HVA:5-HIAA ratio increased after 3 h L-DOPA incubation, the HVA:DA ratio decreased with longer treatment times. Statistical analysis was carried out after square root transformation of the ratios and completed by one-way ANOVA, followed by Tukey's post-test (*p ≤ 0.05; ***p < 0.0001). Data are presented as mean ± SEM. ø: no L-DOPA incubation.*

$$\text{Turnover ratio} = \frac{[DOPAC] + [HVA]}{[Dopamine]}$$

Equation 4.1 Formula used to calculate the turnover ratio.
[DOPAC]*: DOPAC concentration;* [HVA]*: HVA concentration;* [Dopamine]*: dopamine concentration.*

4.3.5. Effect of rotenone and CBE treatments on monoamine levels

Rotenone is a mitochondrial complex I inhibitor that derives from a vegetable and acts as a natural insecticide, pesticide and piscicide. It impairs electron transfer from the iron–sulphur clusters of complex I to ubiquinone. SH-SY5Y cells were incubated with 100 nM rotenone for 24 h, which has been previously published to decrease complex I activity by 50% (Aylett et al., 2013), or with the vehicle (ethanol) before incubation with 100 µM L-DOPA for 1 h. No statistical differences were observed between control (untreated) and ethanol-treated cells ***(Table 4.1)***. Rotenone treatment had no effect on 3-OMD or dopamine release ***(Figure 4.6)***. However, cells incubated with rotenone released 2.2 times more DOPAC than control cells ***(Figure 4.6)***. Conversely, the release of HVA was 97% lower than in the control cells ***(Figure 4.6)***.

CBE is a selective and irreversible GBA1 inhibitor that has been used to model GD both *in vitro* and *in vivo* (Manning-Bog et al., 2009). In this study, the cells were treated with 100 µM CBE for one week. This treatment was followed by 1 h of 100 µM L-DOPA incubation before collecting the culture medium. CBE did not affect the release of 3-OMD or dopamine ***(Figure 4.6)***. However, the release of dopamine metabolites changed when GBA1 was inhibited. CBE increased the release of DOPAC 5.2 fold and decreased the release of HVA by 90% compared to the control ***(Figure 4.6)***.

Table 4.1 The effect of ethanol on monoamine release to the medium.
Ethanol pre-treatment was followed by 1 h of L-DOPA incubation (n = 3 experimental replicates), and no differences were observed compared to the cells incubated with L-DOPA only (control, n = 16 experimental replicates). Statistical analysis was carried out by unpaired Student t-test and data are presented as mean ± SEM. Units: nM.

	Control	Ethanol
3-OMD	1571 ± 168.4	1392 ± 444.9
Dopamine	1020 ± 148.3	968 ± 342.4
DOPAC	301 ± 41.2	257 ± 91.2
HVA	87 ± 7.7	58 ± 20.5
5-HIAA	313 ± 31.6	393 ± 9.1

Furthermore, cells pre-treated with rotenone and CBE were compared. It was noted that both treatments had the same effect on dopamine and HVA ***(Figure 4.6)***. That was not the case in the release of 3-OMD and DOPAC. SH-SY5Y cells treated with CBE showed decreased 3-OMD release compared to those treated with rotenone ***(Figure 4.6)***. Conversely, DOPAC release was significantly higher after CBE treatment compared to release after rotenone treatment ***(Figure 4.6)***.

4.3.6. 5-HIAA release after treatment with rotenone or CBE

Along with dopamine and its metabolites, 5-HIAA was also quantified after 1 h of L-DOPA incubation. Although incubation with L-DOPA had no effect on 5-HIAA release ***(Figure 4.4)***, incubation with rotenone or CBE together with L-DOPA significantly increased extracellular 5-HIAA concentration ***(Figure 4.6)***. 5-HIAA concentration was around 50% higher in the pre-treated cells than in the control.

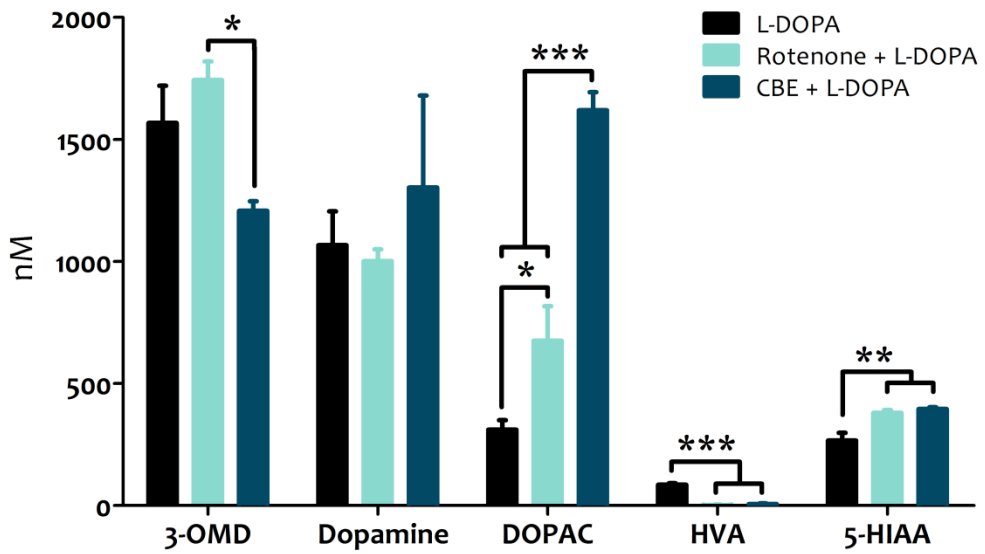

Figure 4.6 Release of dopamine and its metabolites after pre-treatment with rotenone or CBE. *Rotenone (n = 14 experimental replicates) or CBE (n = 9 experimental replicates) pre-treatments were followed by 1 h of L-DOPA. DOPAC and HVA release respectively increased and decreased in the pre-treated cells compared to those treated with L-DOPA only (n = 16 experimental replicates). 5-HIAA release also increased after both pre-treatments. Statistical analysis was carried out by one-way ANOVA, followed by Tukey's post-test (*p < 0.05; **p < 0.01: ***p < 0.0001). Data are presented as mean ± SEM.*

4.3.7. Monoamine turnover was altered after rotenone and CBE treatments

The results show that the relationship between metabolites changed after rotenone and CBE treatments. The HVA:5-HIAA ratio significantly decreased after rotenone or CBE treatment ***(Figure 4.7)***. This was a result of the decreased HVA and increased 5-HIAA release. The HVA:dopamine ratio also significantly decreased after both pre-treatments ***(Figure 4.7)***. In this case, the decrease was due to the lower release of HVA only, as dopamine release remained unaffected. Finally, while the turnover ratio tended to increase after both treatments, the increase was significant only after CBE ***(Figure 4.7)***.

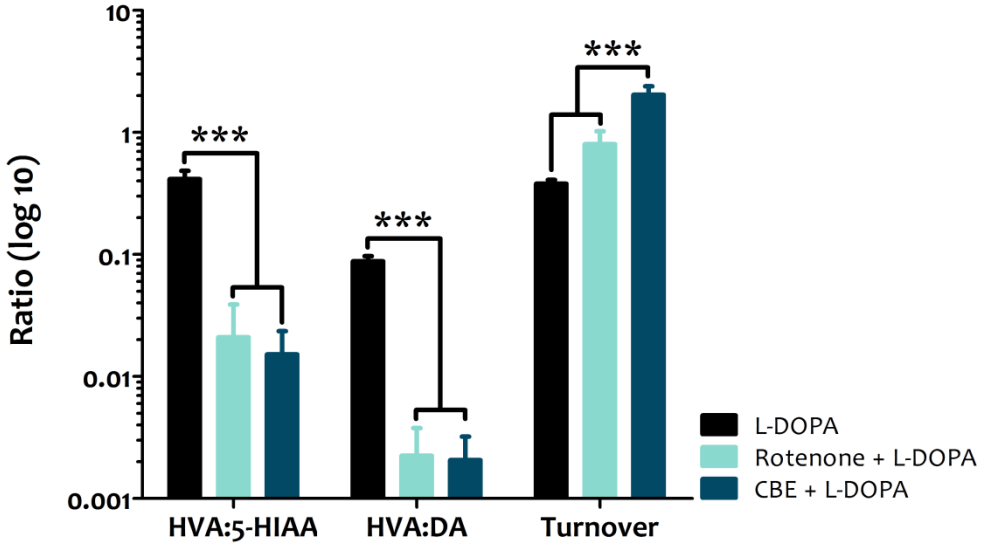

Figure 4.7 Changes in dopamine and serotonin homeostasis after pre-treatment with rotenone and CBE.
*Both HVA:5-HIAA and HVA:dopamine ratios decreased after both pre-treatments. The turnover ratio was higher in CBE cells only. Statistical analysis was carried out after square root transformation of the ratios. Then statistics were completed by one-way ANOVA, followed by Tukey's post-test (***p < 0.0001). Data are presented as mean ± SEM.*

4.3.8. Extracellular monoamine concentration after 3 h L-DOPA incubation

When both control and pre-treated cells were exposed to 100 µM L-DOPA for 3 h, the results observed differed from those described in the previous sections. The release of 3-OMD and dopamine were still unaffected by treatment with rotenone or CBE ***(Figure 4.8)***. Also, DOPAC and 5-HIAA concentration was higher after both pre-treatments ***(Figure 4.8)***. However, HVA release was comparable to control levels after the incubation with rotenone or CBE ***(Figure 4.8)***. While the HVA:5-HIAA ratio still decreased after both pre-treatments, the HVA:dopamine ratio remained unaffected due to the changes in HVA concentration ***(Figure 4.9)***. Finally, the turnover ratio was significantly higher after rotenone or CBE ***(Figure 4.9)***.

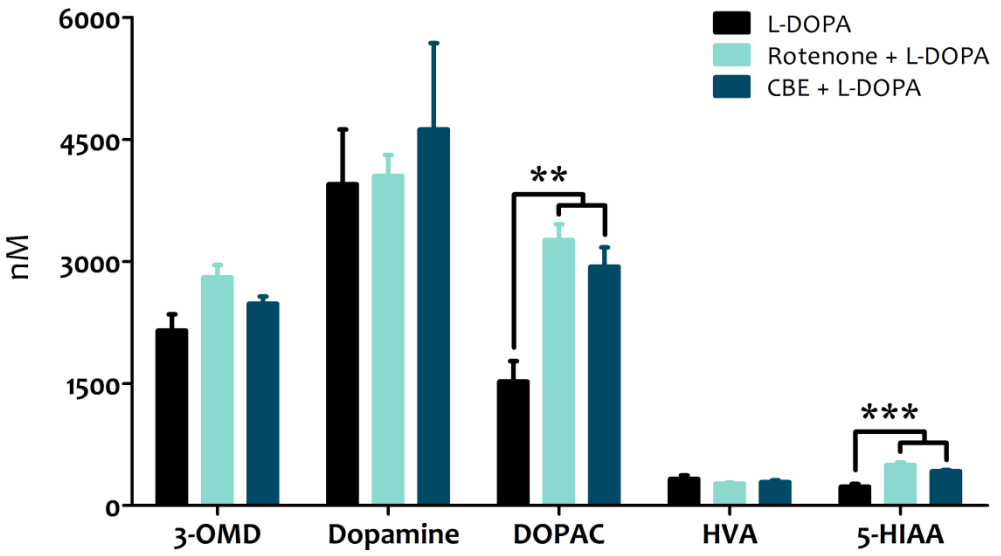

Figure 4.8 Changes in levels of MAO-dependent metabolites in rotenone or CBE cells after 3 h L-DOPA incubation.

*DOPAC and 5-HIAA release was still higher in cells treated with rotenone (n = 4 experimental replicates) or CBE (n = 9 experimental replicates) than in non-pre-treated cells (L-DOPA, n = 12 experimental replicates). Statistical analysis was carried out by one-way ANOVA, followed by Tukey's post-test (**p < 0.01; ***p < 0.005). Data are presented as mean ± SEM.*

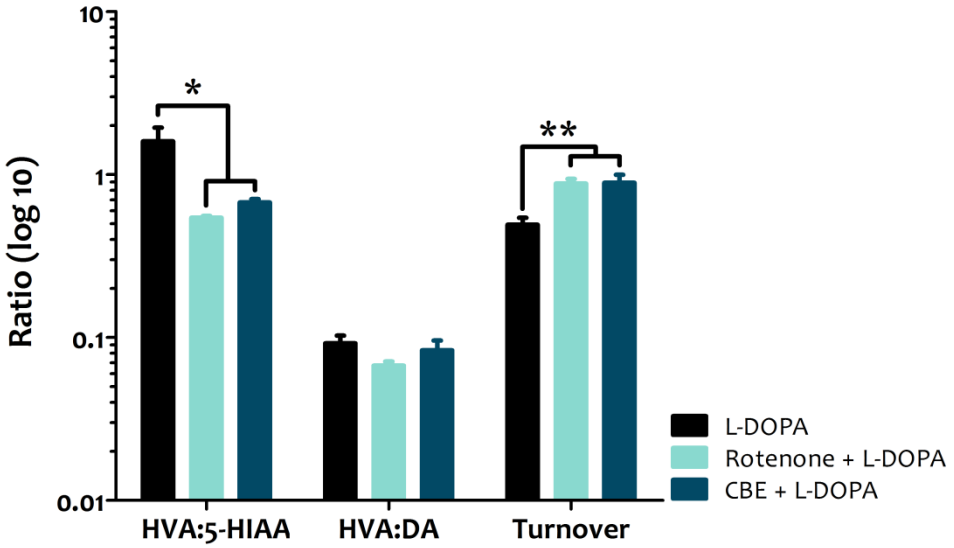

Figure 4.9 Changes in overall dopamine turnover in the pre-treated cells after 3 h L-DOPA incubation.

*The HVA:5-HIAA ratio was significantly lower after rotenone or CBE when L-DOPA incubation was extended up to 3 h. In contrast, the turnover ratio was significantly higher in pre-treated cells. Statistical analysis was carried out after square root transformation of the ratios and completed by one-way ANOVA, followed by Tukey's post-test (*p < 0.05; **p < 0.01). Data are presented as mean ± SEM.*

4.4. Discussion

4.4.1. Proliferative SH-SY5Y cells release dopamine but only after L-DOPA incubation

Although the SH-SY5Y cell line has been widely used in the study of PD, there is controversy about its phenotype. Due to the lack of consensus in the literature about this cell line as a PD cellular model (Xicoy et al., 2017), dopamine metabolism was assessed in the medium of proliferative SH-SY5Y cells in basal conditions. In the present study, extracellular medium was used as a relatively easy way to assess dopamine and serotonin metabolism in the current cell model without the need to harvest the cells. This is analogous to the use of CSF for assessing patient's monoamine metabolism (Burlina et al., 2017). Neither dopamine nor its metabolites were detectable in the extracellular medium under basal conditions, in agreement with what was described by Balasooriya and Wimalasena (2007). There could be at least two reasons for this: dopamine was synthesised but not released to the medium or, the cells did not express some of the enzymes of the dopaminergic biosynthesis pathway (Lopes et al., 2010).

Concerning the latter, TH expression was studied by immunofluorescence. It was found that the cells used here did not express TH protein ***(Figure 4.1 B)***, supporting the reports that these cells do not have an innate capacity to synthesise dopamine (Lopes et al., 2010; Cui et al., 2015; McMillan et al., 2007). To overcome this deficiency, the cells were incubated with 100 μM L-DOPA (Woodard et al., 2014). L-DOPA is a well-stablished treatment in PD, as this molecule is the direct precursor of dopamine and able to cross the blood–brain barrier. With this addition, the lack of cellular TH was bypassed, and the release of dopamine and its metabolites was quantified in the culture medium. As shown in ***Figure 4.2***, 3-OMD, dopamine and its metabolites were present in the culture medium after L-DOPA incubation, suggesting that the downstream enzymes are present. In

addition, the decreased release of the molecules after inhibiting AADC confirmed that the increase observed in the release of dopamine and its metabolites was due to L-DOPA metabolism catalysed by AADC.

4.4.2. Dopamine turnover could be altered by chronic L-DOPA incubation

Accumulation of dopamine in the cytosol may increase cellular oxidative stress as its spontaneous oxidation can produce molecules such as aminochrome and neuromelanin (Meiser et al., 2013). Therefore, dopamine turnover was studied in order to determine whether the changes observed in metabolite release could lead to accumulation of metabolites that possibly increase oxidative stress in the cells. Two ratios were calculated for that purpose: HVA:dopamine and turnover ***(Figure 4.5)***. The first ratio, that of dopamine to the final product of the pathway, HVA, decreased significantly after 3 h of L-DOPA incubation. This suggests that more dopamine was being synthesised than degraded after sustained L-DOPA incubation. The second ratio, that of both dopamine metabolites, DOPAC+HVA, to dopamine, tended to increase after sustained L-DOPA incubation. However, this increase was not significant. In this case, the results suggest higher dopamine degradation than synthesis. Looking at both ratios, data presented here raise the possibility that L-DOPA incubation could potentially lead to changes in dopamine metabolism, which could affect PD treatment as discussed later. The maintenance of the overall dopamine degradation would rely on a higher production of DOPAC by MAO, due to the diminution of further DOPAC catalysis to HVA by COMT in prolonged L-DOPA incubations.

4.4.3. Inhibition of mitochondrial complex I or lysosomal GBA1 is associated with increased dopamine turnover

Both mitochondrial and lysosomal integrity are essential for cellular viability. It is not surprising that those organelles are affected in several human diseases, including PD. Indeed, mitochondrial impairment has been proposed as one of the possible causes of cell death in PD (Hauser and Hastings, 2013). Additionally, GBA1 mutation is the most common genetic risk factor for PD, and idiopathic PD patients show a lower activity of this enzyme (Gegg et al., 2012). Furthermore, familial PD cases show mutations affecting mitochondrial proteins such as parkin, PINK1 and DJ1 (reviewed by Abou-Sleiman et al., 2006). While parkin and PINK1 are related to mitophagy and their mutation results in accumulation of damaged mitochondria, it has been proposed that DJ1 is a redox-responsive molecular chaperone that detects misfolded proteins. Loss of function of any of them contributes to an increase in cellular oxidative stress in PD (Hauser and Hastings, 2013). In the current study, the aim was examine the links between mitochondria, lysosomes and dopamine metabolism by analysing dopamine release to the culture medium. To model the impairment of these organelles, two well-established pharmacological treatments were used: rotenone and CBE.

The rotenone concentration used in this study was selected as Aylett et al. (2013) previously reported that it decreased complex I activity by 50%. The CBE concentration used in this study decreased GBA1 activity by 99.3% (Dr Derek Burke, oral communication, UCL, London); although it is known that CBE at higher doses can also inhibit the non-lysosomal GBA2 (Ridley et al., 2013). No differences were observed in 3-OMD or dopamine release when comparing rotenone or CBE pre-treated to non-pre-treated SH-SY5Y cells ***(Figure 4.6)***. These results were taken as a representation of cellular viability, i.e. the pre-treatments are not decreasing the cell density as the values are similar to those of the

control cells. Nonetheless, dopamine degradation was altered after the treatment with rotenone and CBE, as judged by the increased levels of DOPAC and decreased levels of HVA. This could be a result of decreased ETC activity that would lead to lower ATP production, followed by loss of vacuolar ATPase and, consequently, VMAT2 dysfunction (Chaudhry et al., 2008; Davey et al., 1998). If that is the case, dopamine would accumulate in the cytosol, increasing oxidative stress. However, if dopamine degradation were to increase, it would possibly maintain cytosolic dopamine levels within a physiologic and non-cytotoxic range. Intracellular monoamine concentration needs to be studied in order to explore this possibility.

4.4.4. Serotonin metabolism increased after complex I or lysosomal GBA1 impairment, but not after L-DOPA incubation

Because of parallels between the dopamine and serotonin pathways, serotonin metabolite 5-HIAA was also analysed along with dopamine and its metabolites. 5-HIAA was present in the samples, even in basal conditions ***(Figure 4.1)***. This indicates that SH-SY5Y cells were able to synthesise and degrade serotonin, suggesting they express all the enzymes of the serotonin pathway and all the substrates are available (Kollalpitiya and Wimalasena, 2008). When cells were incubated with L-DOPA for up to 3 h, 5-HIAA release remained unaffected ***(Figure 4.4)***. This result could indicate that the presence of dopamine precursor does not increase or restrain AADC activity, and serotonin synthesis would remain unaffected by L-DOPA incubation.

Studies in post-mortem brains of idiopathic PD patients show a depletion of serotoninergic terminals in the raphe nuclei and its target regions; for example, the hippocampus (Halliday et al., 1990). Although not as substantial as the dopaminergic loss, a correlation has been proposed between serotonin loss and motor and non-motor PD symptoms (Grosch et al., 2016). In the current study, the release of the serotonin

metabolite 5-HIAA increased after both rotenone and CBE treatments ***(Figure 4.6 and Figure 4.8)***. Although further work is needed, this result could be a side effect of increased dopamine degradation to maintain the cytosolic levels of the neurotransmitter.

4.4.5. Mitochondrial complex I and lysosomal GBA1 impairment reveal a common pattern in the effect on dopamine metabolism

Changes in the release of dopamine and serotonin metabolites by the cells with dysfunctional complex I or GBA1 followed the same pattern ***(Table 4.2)***, suggesting that mitochondrial and lysosomal impairment are affecting activity of degradation enzymes in the same way. This could explain how dysfunction of two independent organelles would result eventually in the same event: the dopaminergic loss characteristic of PD.

Table 4.2 Summary of how rotenone and CBE treatments affected monoamine release.
In this table, both pre-treatments are compared to control cells after 1 h of L-DOPA incubation. The statistically significant increased (↑) or decreased (↓) values are shown in red.

	3-OMD	Dopamine	DOPAC	HVA	5-HIAA
Inhibited complex I	↑	=	↑	↓	↑
Inhibited GBA1	↓	↑	↑	↓	↑

The enzymes responsible for dopamine degradation are COMT, MAO and ALDH. The latter is fairly promiscuous and, to date, nineteen genes have been described in the human genome (Vasiliou and Nebert, 2005). The activity of ALDH2, one of the isoforms present in the human brain, has recently been reported as increased in the putamen of sporadic PD patients (Michel et al., 2014). However, the role of this group of enzymes in the development and treatment of PD is not well characterised.

Due to their accepted involvement and inhibition during treatment of PD, this project focuses on MAO and COMT. COMT is responsible for transforming DOPAC into HVA. A decrease in its activity would explain the accumulation of its substrate DOPAC and the reduced release of its product HVA. COMT also metabolises L-DOPA to 3-OMD upstream in the dopamine pathway. Although SH-SY5Y cells with mitochondrial or lysosomal dysfunction showed a decrease in the release of HVA, the release of 3-OMD was not affected, suggesting that COMT activity would be unaffected. MAO metabolises dopamine into DOPAC and serotonin into 5-HIAA. The release of both molecules was significantly increased after mitochondrial and lysosomal dysfunction, indicating that both events could lead to increased MAO activity. Previous studies have described increased MAO activity in cellular models and post-mortem brains of PD patients (Birkmayer et al., 1975; Sai et al., 2008), suggesting that the activity of this enzyme could be another key factor in the development of dopamine deficiency.

4.5. Conclusion

In conclusion, it is hypothesised that MAO activity could be enhanced after mitochondrial and lysosomal dysfunction. Increased enzymatic activity would result in decreased dopamine availability, leading to a dopamine deficiency. At the same time, when MAO metabolises dopamine into DOPAC, H_2O_2 is produced as a side product of the catalysis. Also, COMT activity could be affected in these patients, as shown by the lower HVA production after mitochondrial and lysosomal impairment. To ascertain their role in PD pathogenesis, these enzymes were studied at functional, translational and transcriptional level in Chapter 5.

CHAPTER 5

Dopaminergic and Serotoninergic Enzymes and Glutathione Status in Cellular Models of Mitochondrial and Lysosomal Impairment

5.1. Introduction

In the Chapter 4, it was hypothesised that mitochondrial or lysosomal impairment would undermine dopamine homeostasis by enhancing MAO activity. COMT activity could also be compromised, as a loss of function of this enzyme could also be involved in the observed changes in DOPAC and HVA. In parallel, the serotonin pathway would also be affected by increased MAO activity. Additionally, it has been proposed that MAO would be mainly responsible for intraneuronal metabolism of dopamine and COMT for the extraneuronal (Espinoza et al., 2012). Therefore, changes in the expression or activity of these enzymes could result in altered dopamine concentration both inside and outside neurons.

It is not clear whether the reported increase in MAO-B activity in the substantia nigra of PD patients (Birkmayer et al., 1975) is due to transcriptional, translational or post-translational mechanisms. For example, some studies describe epigenetic regulation of *MAO* genes by smoking (Launay et al., 2009). Others describe a polymorphism in the intron 13 of the MAO-B gene (*MAOB*), which increases predisposition to develop PD in heterozygotes (Kurth et al., 1993). However, there is no consensus about which allele is responsible for that predisposition, whether there is a gender susceptibility or whether the carriers show a higher risk of developing the disease (Finch et al., 1995; Ho et al., 1995; Costa et al., 1997; Kang et al., 2006; Bialecka et al., 2007). Historically, the role of COMT in PD has been researched less than the role of MAO. However, the role and effect of COMT genetic variants have been studied in more detail recently (Klebe et al., 2013; Chen et al., 2004; Wu et al., 2001; Tunbridge et al., 2007; Schendzielorz et al., 2013; Espinoza et al., 2012). Several studies have focused on Val158Met polymorphism (Lotta et al., 1995), which causes a trimodal distribution, resulting in high, intermediate and low COMT activity (Hernan et al., 2002). Klebe et al. (2013) reported that Val/Val individuals showed

an earlier PD onset in a gender-dependent manner. Contrarily, other studies have concluded that there is no correlation between Val158Met polymorphism and PD (Wu et al., 2001; Bialecka et al., 2007). Despite the potential role of MAO and COMT in the development and evolution of PD, the function and consequences of these polymorphisms are still unclear. However, it is of interest that inhibitors of both enzymes have been used in the treatment of the disease for years with successful results, reducing motor fluctuations (Connolly and Lang, 2014).

Concerning dopamine biosynthesis, several studies have focused on the post-translational regulation of TH, GCH1 and AADC by phosphorylation, nitrosylation and *S*-thiolation, amongst others (Meiser et al., 2013). One of the most accepted theories is that phosphorylation in TH would facilitate interaction with other proteins, such as GCH1, AADC and VMAT2, and increase its activity (Daubner et al., 2011). Nowadays, gene therapies are being developed with the aim of increasing the efficacy of L-DOPA treatment. For this purpose, AADC is expressed in the putamen after adeno-associated virus (AAV) transduction. Other therapies aim for ectopic full dopamine synthesis by delivering TH, GCH1 and AADC genes via lentiviruses (reviewed by Muramatsu, 2010; Coune et al., 2012). However, this approach is still in the clinical trial phase.

Dopaminergic neurons are especially liable to increased oxidative stress. These cells are post-mitotic with great demand for energy and O_2, increased iron concentration, neuromelanin presence and high levels of dopamine, which make their environment highly oxidative and antioxidant mechanisms essential (Fujita et al., 2014; Munoz et al., 2012; Dauer and Przedborski, 2003). In physiological conditions, antioxidant molecules, enzymes and chaperones are able to control this oxidative stress. However, this frail balance between antioxidant and oxidant molecules is broken in PD (reviewed by Smeyne and Smeyne, 2013) probably as a result of increased H_2O_2 production due to higher MAO

activity and decreased GSH levels (Birkmayer et al., 1975; Sian et al., 1994). Additionally, it has been proposed that increased ROS production and iron accumulation in conjunction with decreased antioxidant response are some of the key events that can lead to neuronal death (Dauer and Przedborski, 2003).

In view of the data presented in Chapter 4 and the potential for oxidative stress to occur as a result of changes in MAO activity, the aims in this chapter are to examine:

- The effect of L-DOPA treatment, in the absence and presence of compromised mitochondrial complex I or lysosomal GBA, on the activity, transcription and translation of MAO isoenzymes (MAO-A and –B).
- The effect of L-DOPA treatment, mitochondrial and lysosomal impairment on the protein and mRNA expression of COMT.
- Whether L-DOPA or mitochondrial and lysosomal impairment have any effect on dopamine biosynthesis via AADC.
- Whether mitochondrial or lysosomal impaired cells display any evidence of oxidative stress, as reflected by changes in GSH availability.

5.2. Methods

5.2.1. Cell culture and treatment

SH-SY5Y cells were cultured and treated as described in sections 2.2.1 and 2.2.2 respectively.

5.2.2. MAO activity assay

MAO activity was studied as described in section 2.4 Samples were collected as explained in section 2.2.3.3.

5.2.3. Expression of dopaminergic enzymes

Protein expression was assessed by western blot as described in section 2.5. In parallel, mRNA expression was also quantified by qRT-PCR as described in section 2.6. For these assays, samples were collected as described in sections 2.2.3.2 and 2.2.3.3.

5.2.4. GSH quantification by HPLC

Intracellular GSH levels were quantified as described in section 2.7. Samples were collected as described in section 2.2.3.2, and prepared as described in section 2.7.2.

5.3. Results

5.3.1. Effects of L-DOPA treatment on MAO activity, protein, mRNA and GSH levels

Both MAO-A and MAO-B activities tended to increase after L-DOPA treatment ***(Table 5.1)***. While the effect on MAO-A activity was maintained after 3 h of treatment, MAO-B activity decreased by 50% at that time point compared to activity at shorter L-DOPA treatment times ***(Table 5.1)***. Surprisingly, after the incubation with L-DOPA no statistical differences were observed in protein and mRNA expression of any of the enzymes studied.

Table 5.1 L-DOPA effect on the enzymes of the dopamine pathway and GSH levels.
L-DOPA treatment had no significant effect on protein or mRNA of any of the enzymes or GSH levels. However, there were changes in MAO-B activity. Statistical analysis was carried out by one-way ANOVA, followed by Tukey's post-test. Statistics presented are untreated (ø) and 3 h L-DOPA against 1 h of treatment (ø vs 3 h not significant for any of the conditions). Data are presented as mean ± SEM (n = 3 experimental replicates). Units: mRNA, fold change to control (2^ΔΔCT), relative expression to GAPDH; activity, pmol H_2O_2/min/mg of protein; and protein, relative expression to GAPDH; GSH levels, nmol/mg of prot.

		L-DOPA			p-value	
		ø	1 h	3 h	1 h vs ø	1 h vs 3 h
TH	mRNA	0.43 ± 0.22	0.32 ± 0.14	0.31 ± 0.03	n.s.	n.s.
AADC	mRNA	0.79 ± 0.22	0.56 ± 0.14	0.75 ± 0.18	n.s.	n.s.
MAO-A	Activity	1.84 ± 0.51	4.39 ± 0.77	4.27 ± 0.89	n.s.	n.s.
	Protein	1.25 ± 0.05	2.02 ± 0.91	1.41 ± 0.22	n.s.	n.s.
	mRNA	1.04 ± 0.25	1.37 ± 0.20	1.52 ± 0.66	n.s.	n.s.
MAO-B	Activity	3.98 ± 0.45	6.39 ± 0.63	3.34 ± 0.70	0.0663	**0.0269**
	Protein	0.38 ± 0.09	0.47 ± 0.21	0.38 ± 0.19	n.s.	n.s.
	mRNA	0.43 ± 0.12	0.78 ± 0.31	0.68 ± 0.11	n.s.	n.s.
COMT	Protein	0.63 ± 0.18	0.64 ± 0.25	0.63 ± 0.17	n.s.	n.s.
	mRNA	1.03 ± 0.31	1.30 ± 0.46	0.97 ± 0.15	n.s.	n.s.
GSH levels		4.29 ± 0.49	4.89 ± 0.47	4.83 ± 0.60	n.s.	n.s.

5.3.2. Outcomes of ethanol treatment on enzymatic expression and activity

Ethanol was used as a vehicle for the rotenone treatment, in both cases at a concentration of 0.1% (v/v). Although the treatment with this vehicle had no effect on the release of dopamine metabolites, ethanol treatment increased MAO-B activity when compared with that in control cells ***(Table 5.2)***. No statistical differences were observed in the activity or protein/mRNA expression of any of the other enzymes studied or in the GSH levels when control and ethanol groups were compared ***(Table 5.2)***.

Table 5.2 The effect of ethanol on the enzymes of the dopamine pathway and GSH levels. *Ethanol had no effect on protein, mRNA or GSH levels of any of the enzymes compared to that in control cells. However, it is notable that the increase in MAO-B activity approached significance. Statistical analysis was carried out by unpaired Student t-test and data are presented as mean ± SEM (n = 3 experimental replicates). Units: mRNA, fold change to control (2^ΔΔCT) relative expression to GAPDH; activity, pmol H_2O_2/min/mg of protein; and protein expression relative to GAPDH; GSH levels, nmol/mg of prot.*

		Control	Ethanol	p-value
TH	mRNA	0.43 ± 0.22	0.38 ± 0.20	n.s.
AADC	mRNA	0.79 ± 0.22	0.71 ± 0.01	n.s.
MAO-A	Activity	1.84 ± 0.51	2.25 ± 0.82	n.s.
	Protein	1.25 ± 0.05	1.15 ± 0.06	n.s.
	mRNA	1.04 ± 0.25	1.10 ± 0.28	n.s.
MAO-B	Activity	3.98 ± 0.45	5.49 ± 0.35	0.0574
	Protein	0.38 ± 0.09	0.44 ± 0.15	n.s.
	mRNA	0.43 ± 0.12	0.40 ± 0.13	n.s.
COMT	Protein	0.63 ± 0.18	0.78 ± 0.28	n.s.
	mRNA	1.03 ± 0.31	0.97 ± 0.35	n.s.
GSH levels		4.29 ± 0.49	4.88 ± 0.82	n.s.

5.3.3. Rotenone decreased MAO-B activity and protein level

The effect of rotenone was studied over and above the effect of the vehicle, ethanol. After treatment with rotenone, no significant changes were observed in TH or AADC mRNA expression ***(Figure 5.1)***. Neither MAO-A activity nor its expression were affected by rotenone treatment ***(Figure 5.2)***. However, MAO-B activity decreased by 55% after rotenone treatment ***(Figure 5.3 A)*** and MAO-B protein expression was also lower in the rotenone-treated cells. This decrease was only significant after 3 h of L-DOPA, when MAO-B protein levels were 45% lower than those in the control ***(Figure 5.3 B)***. As for MAO-A, neither COMT protein nor mRNA expression varied after rotenone treatment ***(Figure 5.4)***.

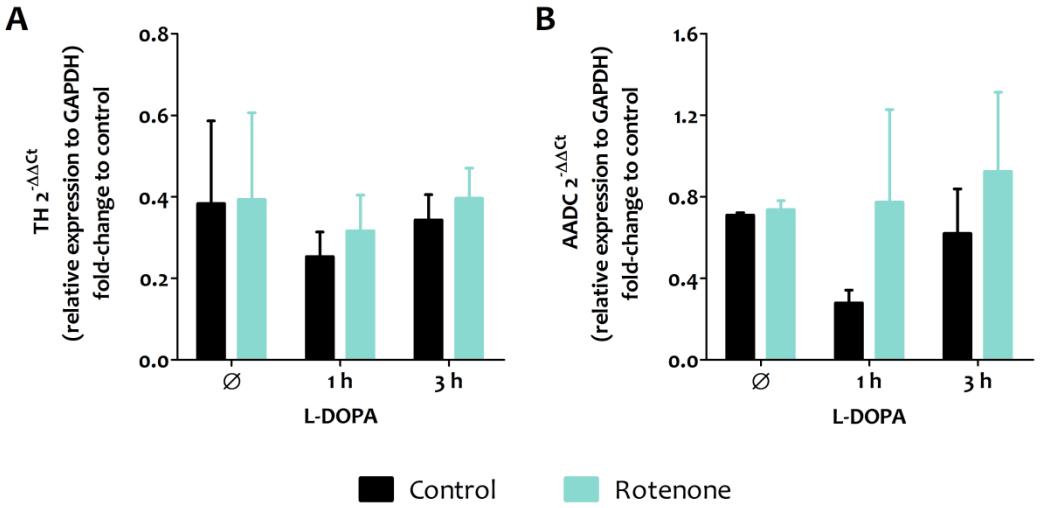

Figure 5.1 The effect of rotenone treatment on dopamine synthesis mRNA levels.
No changes were observed in TH (A) or AADC (B) mRNA levels after rotenone. Statistical analysis was carried out by unpaired Student t-test (n.s.). Data are presented as mean ± SEM (n = 3 experimental replicates).

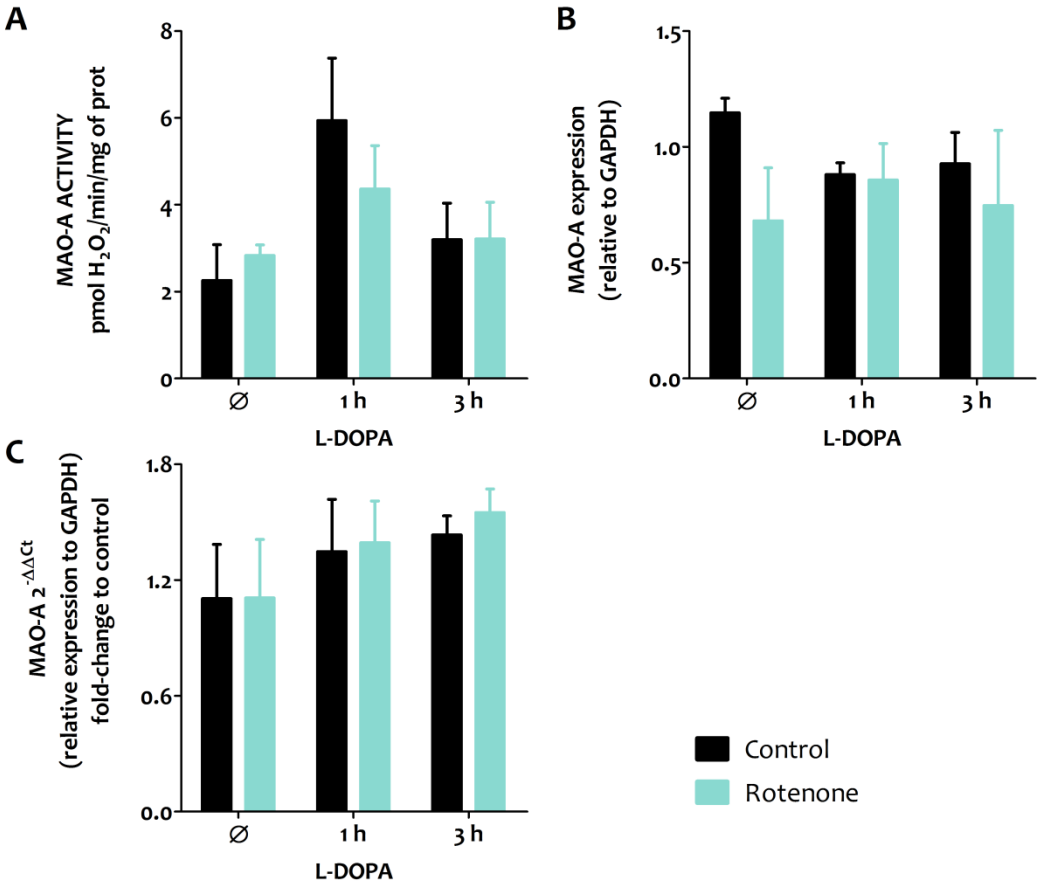

Figure 5.2 The effect of rotenone on MAO-A activity and expression.
No changes were observed in MAO-A activity (A), protein (B) or mRNA (C) levels in cells pre-treated with rotenone compared to levels in control (ethanol) cells. Statistical analysis was carried out by unpaired Student t-test (n.s.). Data are presented as mean ± SEM (n = 3 experimental replicates).

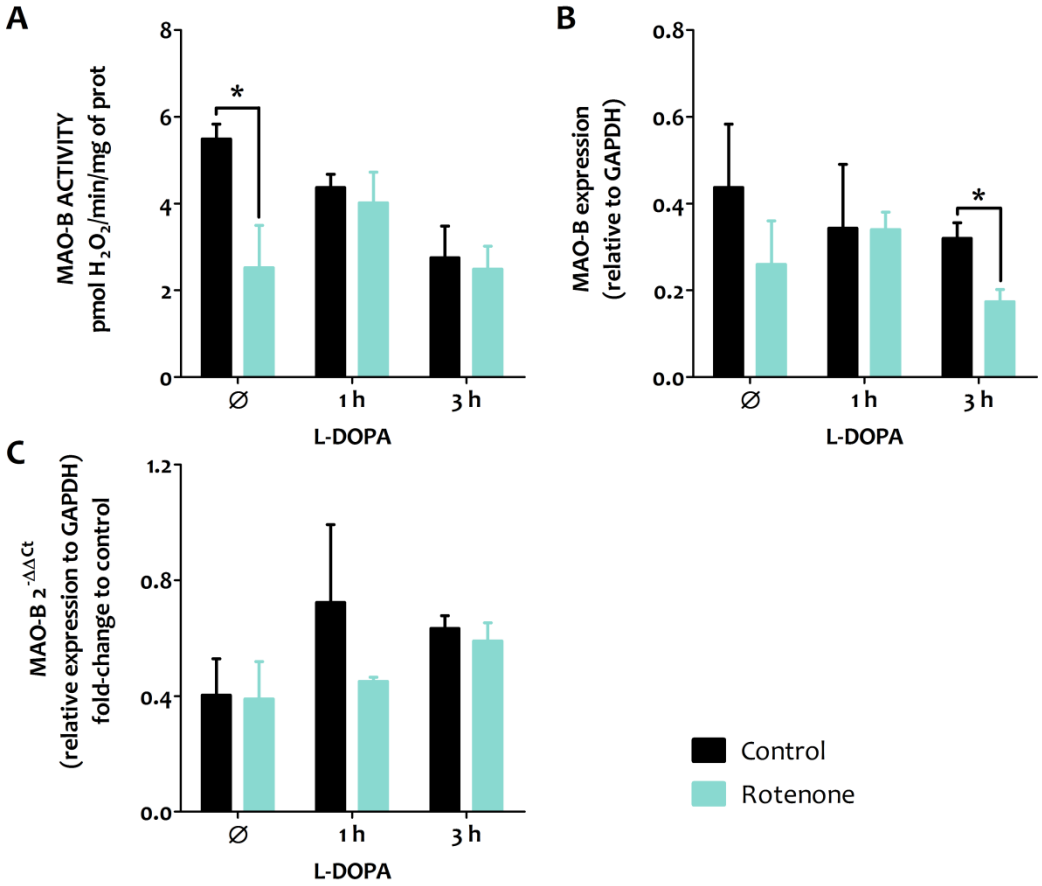

Figure 5.3 The effect of rotenone treatment on MAO-B activity and protein expression.
*MAO-B activity (A) and protein levels (B) were lower in the rotenone than in control (ethanol) cells. Decreased protein levels were observed when rotenone was followed by L-DOPA. No statistical differences were observed in its mRNA levels (C). Statistical analysis was carried out by unpaired Student t-test (*p≤0.05). Data are presented as mean ± SEM (n = 3 experimental replicates).*

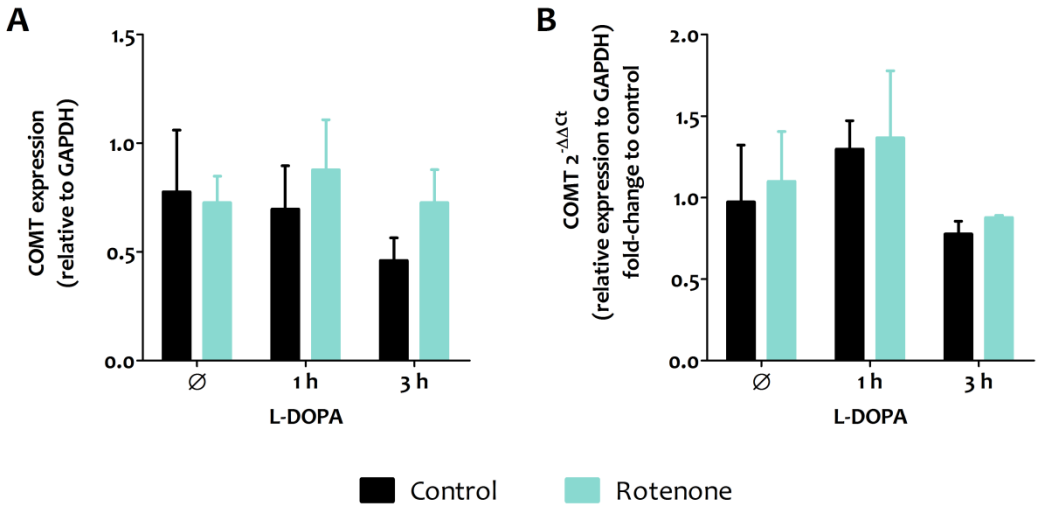

Figure 5.4 The effect of rotenone treatment on COMT expression.
Neither COMT protein (A) nor mRNA (B) levels differed from those in control (ethanol) cells. Statistical analysis was carried out by unpaired Student t-test (n.s.). Data are presented as mean ± SEM (n = 3 experimental replicates).

5.3.4. CBE treatment also decreased MAO-B activity

CBE did not alter the mRNA expression of the enzymes responsible for dopamine synthesis ***(Figure 5.5)***. Regarding its degradation, neither MAO-A activity, protein nor mRNA levels were affected by GBA1 inhibition ***(Figure 5.6)***. In contrast to MAO-A, MAO-B activity decreased by 40% when cells were treated with CBE followed by L-DOPA ***(Figure 5.7 A)***. This decrease in the enzymatic activity was not accompanied by changes in protein or mRNA levels ***(Figure 5.7 B-C)***. Also, no statistical differences were observed in COMT expression ***(Figure 5.8)***, although its mRNA levels tended to decrease after CBE treatment.

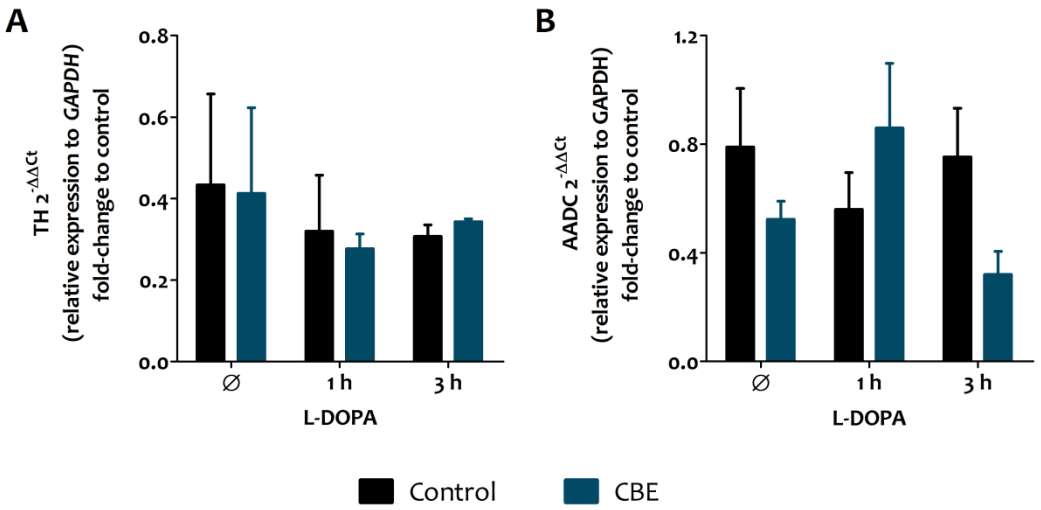

Figure 5.5 The effect of CBE on mRNA expression of the dopamine synthesis enzymes.
No changes were observed in TH (A) or AADC (B) mRNA levels after CBE compared to levels in control (untreated) cells. Statistical analysis was carried out by unpaired Student t-test (n.s.). Data are presented as mean ± SEM (n = 3 experimental replicates).

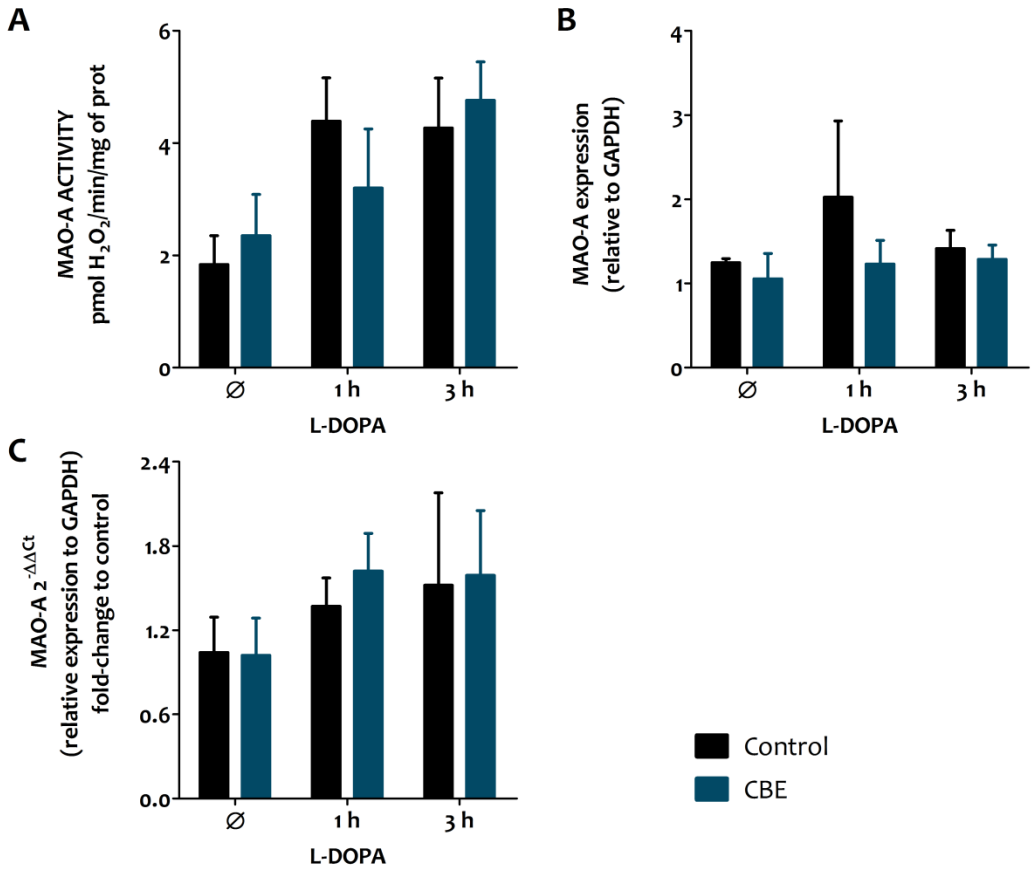

Figure 5.6 The effect of CBE on MAO-A activity and expression.
No differences were observed between control (untreated) and CBE cells in MAO-A activity (A), protein (B) or mRNA (C) levels. Statistical analysis was carried out by unpaired Student t-test (n.s.). Data are presented as mean ± SEM (n = 3 experimental replicates).

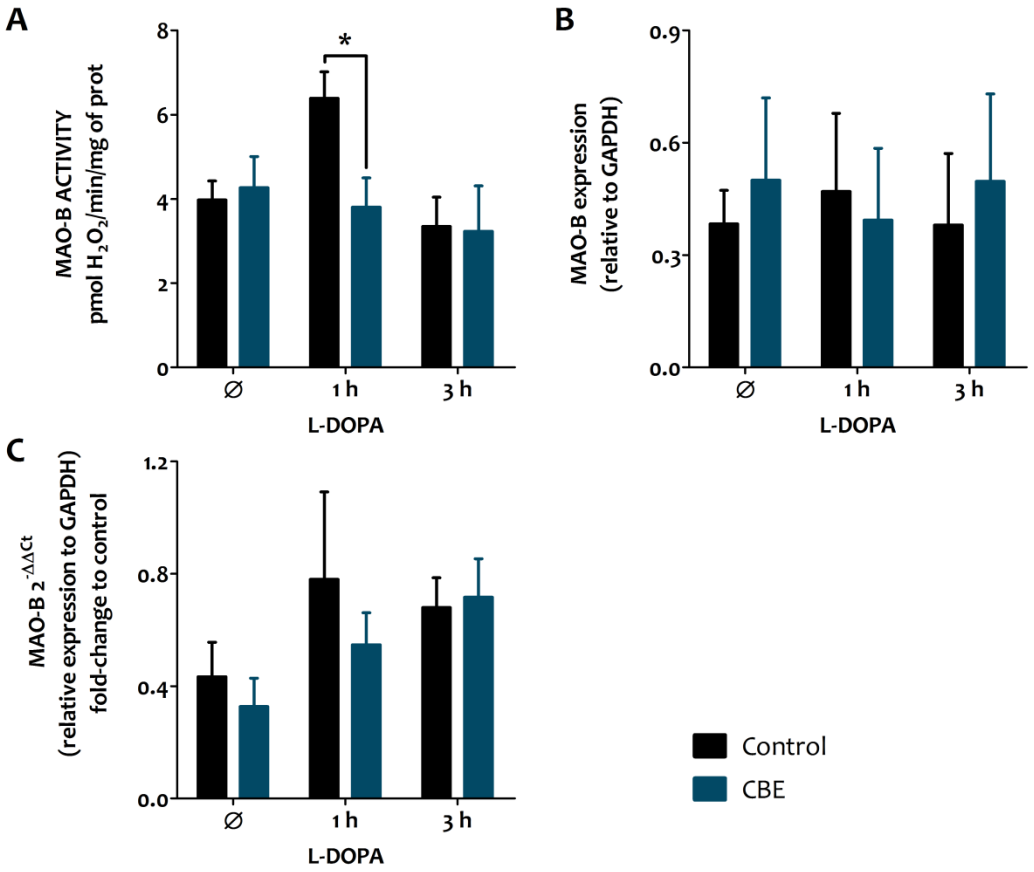

Figure 5.7 The effect of CBE treatment on MAO-B activity.
*The activity of MAO-B (A) decreased after consecutive treatment with CBE and L-DOPA. No statistical differences were observed in protein (B) or mRNA (C) levels after CBE treatment. Statistical analysis was carried out by unpaired Student t-test (*p≤0.05). Data are presented as mean ± SEM (n = 3 experimental replicates).*

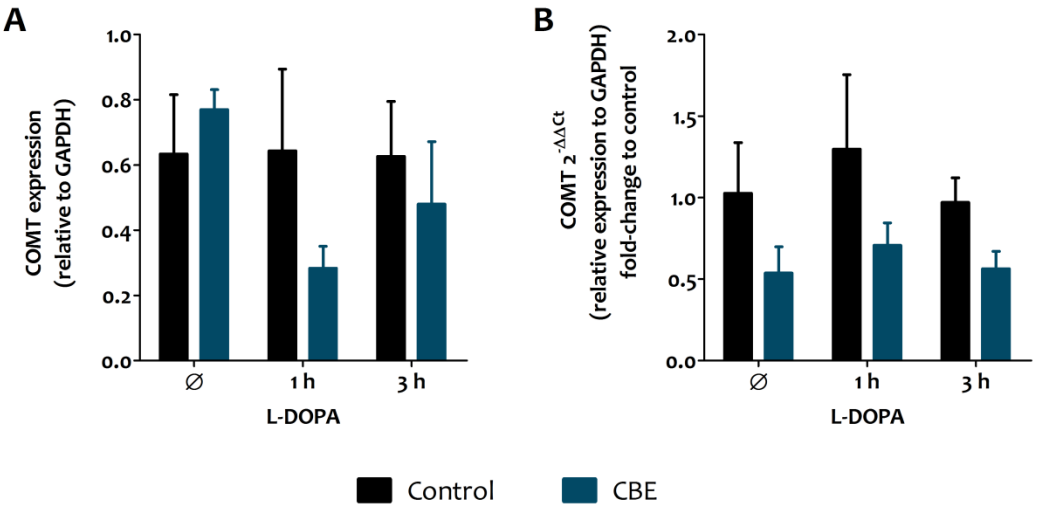

Figure 5.8 The effect of CBE treatment on COMT expression.
Protein (A) and mRNA (B) levels of COMT in CBE pre-treated cells did not show any statistical differences compared to levels in control (untreated) cells. Statistical analysis was carried out by unpaired Student t-test (n.s.). Data are presented as mean ± SEM (n = 3 experimental replicates).

5.3.5. Effect of NSD-1015 treatment on the dopamine degradation enzymes

The effect of inhibiting AADC was also studied. No differences were observed in the expression of TH or AADC after inhibiting the latter with NSD-1015 ***(Figure 5.9)***. This treatment did not have a statistically significant effect on MAO-A activity ***(Figure 5.10 A)***, although a decreased activity was noted when the pre-treatment was followed by L-DOPA. No changes were observed in MAO-A expression after NSD-1015 ***(Figure 5.10 B-C)***. MAO-B activity also decreased after NSD-1015 treatment ***(Figure 5.11 A)***, being significant after 1 h of L-DOPA treatment. As for MAO-A, this decreased activity was not preceded by any change in MAO-B protein or mRNA levels ***(Figure 5.11 B-C)***. Separately, COMT expression was affected by NSD-1015 treatment. Inhibition of AADC doubled COMT protein levels ***(Figure 5.12 A)***, while its mRNA levels decreased by 50% ***(Figure 5.12 B)***. In both cases, the effect was maintained after L-DOPA treatment.

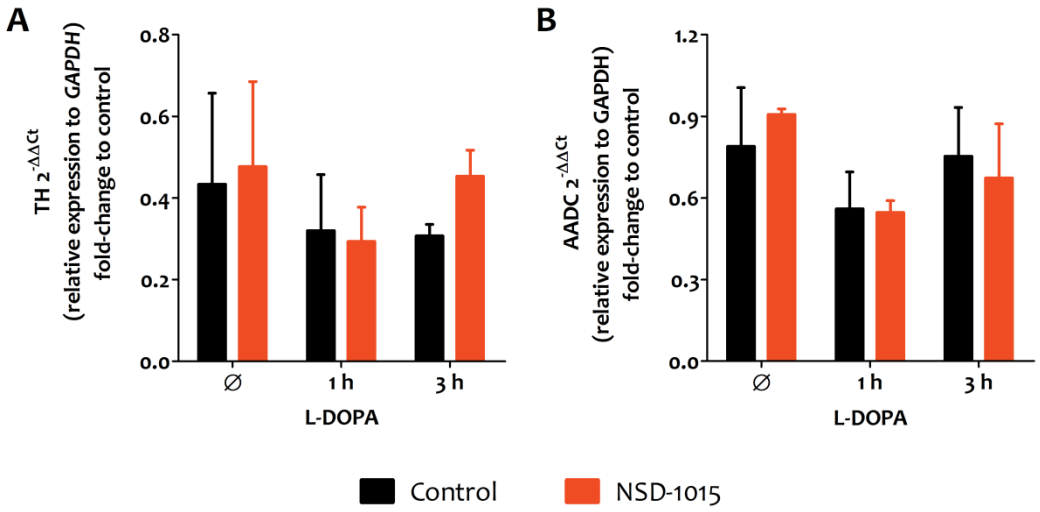

Figure 5.9 The effect of NSD-1015 on dopamine synthesis enzyme mRNA expression.
No changes were observed in TH (A) or AADC (B) mRNA levels after NSD-1015 treatment. Statistical analysis was carried out by unpaired Student t-test (n.s.). Data are presented as mean ± SEM (n = 3 experimental replicates).

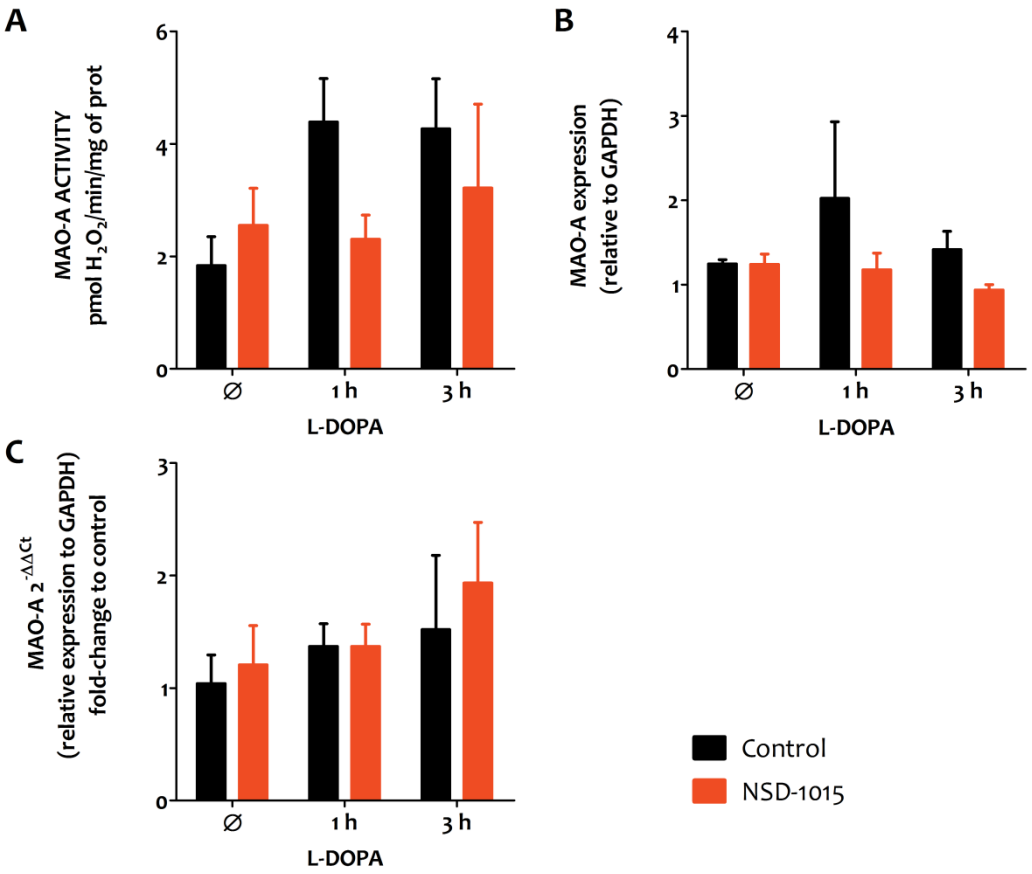

Figure 5.10 The effect of NSD-1015 on MAO-A activity and expression.
No differences were observed between control (untreated) and NSD-1015 cells in MAO-A activity (A), protein (B) or mRNA (C) levels. Statistical analysis was carried out by unpaired Student t-test (n.s.). Data are presented as mean ± SEM (n = 3 experimental replicates).

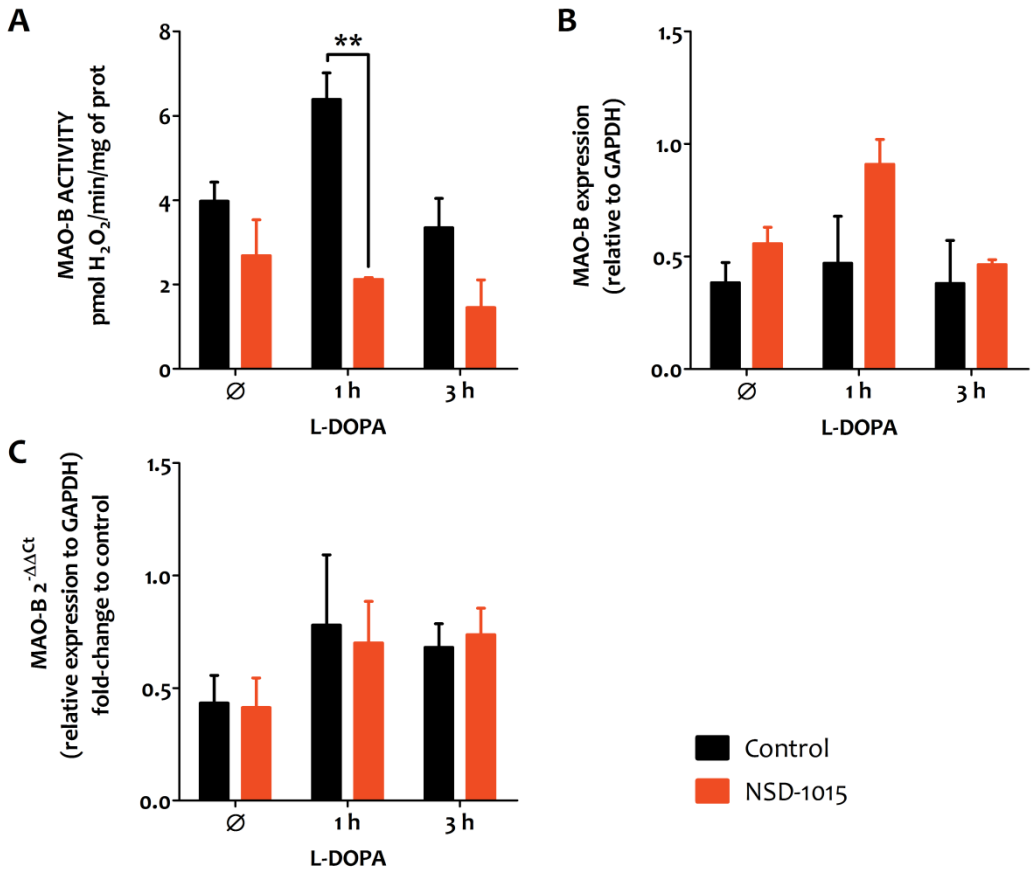

Figure 5.11 The effect of NSD-1015 on MAO-B activity.
*MAO-B activity (A) decreased after treatment with NSD-1015 followed by L-DOPA. No statistical differences were observed in protein (B) or mRNA (C) levels after NSD-1015 treatment. Statistical analysis was carried out by unpaired Student t-test (**p ≤ 0.01). Data are presented as mean ± SEM (n = 3 experimental replicates).*

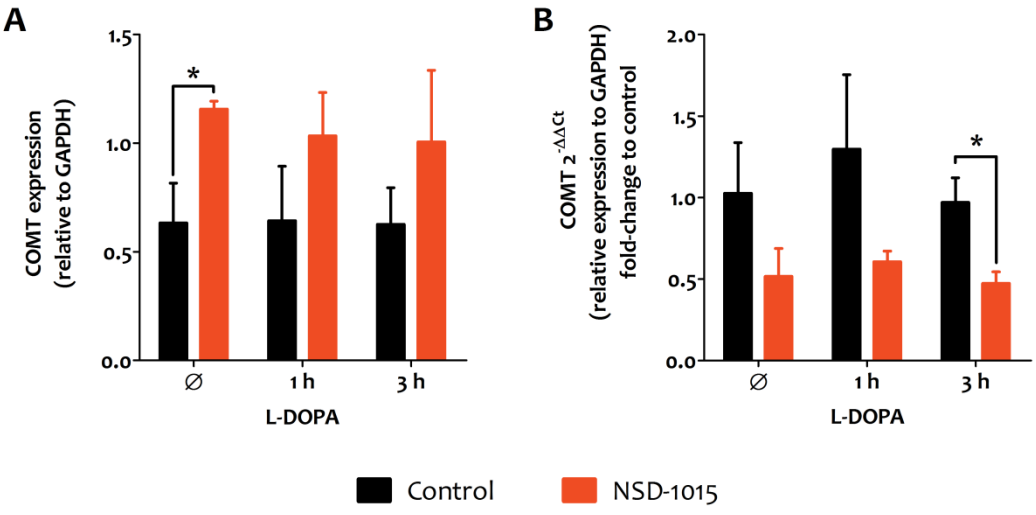

Figure 5.12 The effect of NSD-1015 treatment on COMT expression.
*NSD-1015 increased protein levels (A) and decreased mRNA levels (B). Statistical analysis was carried out by unpaired Student t-test (*p ≤ 0.05). Data are presented as mean ± SEM (n = 3 experimental replicates).*

5.3.6. Neither rotenone nor CBE treatment affected GSH levels

Intracellular GSH was quantified in the mitochondrial impairment and lysosomal dysfunction SH-SY5Y models. Rotenone treatment was compared to its vehicle control (ethanol) and CBE to untreated cells. In either case, no significant differences were observed in GSH levels due to rotenone ***(Figure 5.13)*** or CBE treatment ***(Figure 5.14)***.

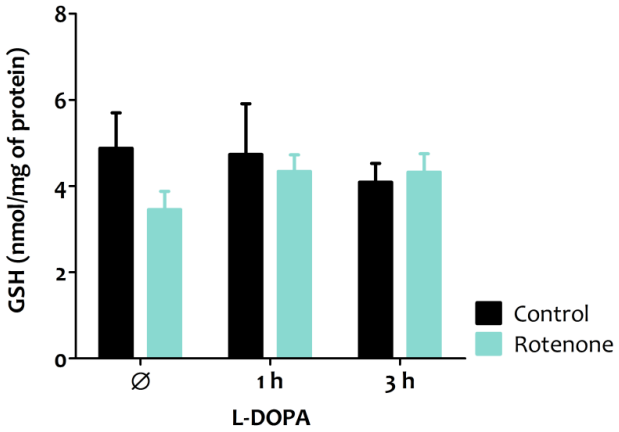

Figure 5.13 The effect of rotenone treatment on GSH levels.
No statistical differences were observed between control (ethanol) and rotenone-treated cells. Statistical analysis was carried out by unpaired Student t-test (n.s.). Data are presented as mean ± SEM (n = 3 experimental replicates).

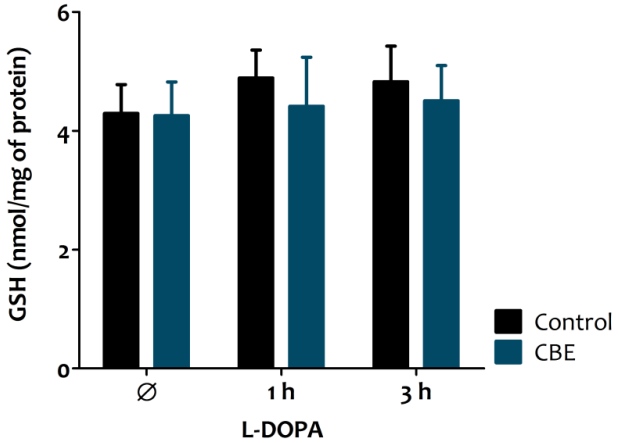

Figure 5.14 The effect of CBE treatment on GSH levels.
No statistical differences were observed between GBA1 inhibition and control cells. Statistical analysis was carried out by unpaired Student t-test (n.s.). Data are presented as mean ± SEM (n = 3 experimental replicates).

5.4. Discussion

5.4.1. Dopamine but not L-DOPA might induce its own degradation

Increasing dopamine availability by the treatment with L-DOPA and MAO-B/COMT inhibitors has been the gold-standard treatment for the dopamine deficiency characteristic of PD. However, the molecular consequences of increasing L-DOPA and dopamine on the enzymes involved in the dopamine pathway are not fully understood. Some theories suggest that chronic L-DOPA treatment increases toxicity and inflammation markers in idiopathic PD patients and impairs the metabolism of the biothiols; for example, GSH (reviewed by Dorszewska et al., 2014). Therefore, if the expression of dopamine pathway enzymes varies as consequence of L-DOPA administration, PD treatment could be more detrimental than beneficial.

In the present study, L-DOPA treatment did not modify mRNA or protein expression of any dopamine pathway enzymes. However, both MAO isoforms increased their activity because of L-DOPA treatment ***(Table 5.1)***. To analyse whether this increase was due to L-DOPA treatment or to dopamine synthesis, cells were treated with the AADC-inhibitor, NSD-1015. While MAO-A activity in the AADC-inhibited cells was comparable to that in control cells, MAO-B activity decreased ***(Figure 5.11 A)***. These results suggest that dopamine could be regulating its own degradation through MAO via a positive feedback. This is not the first time MAO and AADC have been related: Cumming et al. (1995) previously reported that inhibition of MAO could decrease AADC activity via the dopamine receptor in rat brain. In this case, decreased AADC activity resulted in decreased MAO-B activity. Further enzymatic studies in the presence of dopamine and/or L-DOPA are needed to confirm these observations, as a balance between AADC and MAO activities could be fundamental to maintain dopamine levels within a certain range, especially in PD.

While COMT protein and mRNA expression were unaffected by L-DOPA treatment ***(Table 5.1)***, its expression changed when AADC was inhibited ***(Figure 5.12)***. COMT mRNA concentration decreased after sequential NSD-1015 and L-DOPA treatments. Surprisingly, its protein expression increased when AADC was inhibited. Several factors could account for this; for example, dopamine or L-DOPA concentration, the L-DOPA:dopamine ratio or a direct interaction between AADC and COMT. Further work is needed to determine whether these changes in the expression of COMT are translated to differences in the enzymatic activity. This is of special importance as COMT is not only implicated in dopamine degradation, but also catalyses L-DOPA conversion to 3-OMD by an alternative route to dopamine (Hiroi et al., 1998).

Finally, it is known that TH activity is strongly regulated post-translationally by enzymes such as kinases and phosphatases, and molecules such as dopamine and its quinone derivate (Dorszewska et al., 2014). AADC can be regulated pre- and post-translationally, being long- and short-term solutions respectively. The first solution is slower and involves different gene expression while the latter is faster and includes phosphorylation and DA receptor signalling (Berry et al., 1996; Zhu and Juorio, 1995). Because of its broad substrate specificity, AADC is also regulated in a species- and tissue-dependent manner (Berry et al., 1996; Zhu and Juorio, 1995). Consequently, as both enzymes could potentially be regulated by dopamine, L-DOPA treatment could directly affect the expression of TH and/or AADC.

No changes were observed in the expression of these enzymes in the current L-DOPA treatment cell models. However, it is of note that the melting temperature, or threshold, of TH cDNA was reached on average around cycle 31 ***(Figure 5.15)***. This suggests a low yield of mRNA expression, in agreement with the absence of immunofluorescent TH-positive cells described in the Chapter 4 and with previous publications that

concluded that proliferative SH-SY5Y cells do not express TH (Lopes et al., 2010; Cui et al., 2015; McMillan et al., 2007). Additionally, inhibition of AADC activity did not affect TH or AADC mRNA expression ***(Figure 5.9 B)***. These findings differ from previously published data, which concludes that translation of these enzymes is affected by L-DOPA and/or dopamine levels (Daubner et al., 2011; Cumming et al., 1995). However, is not clear how dopamine and other catecholamines regulate their own synthesis (Flatmark, 2000). It should be noted that sample size in the current study is small and that further work is needed to confirm this observation.

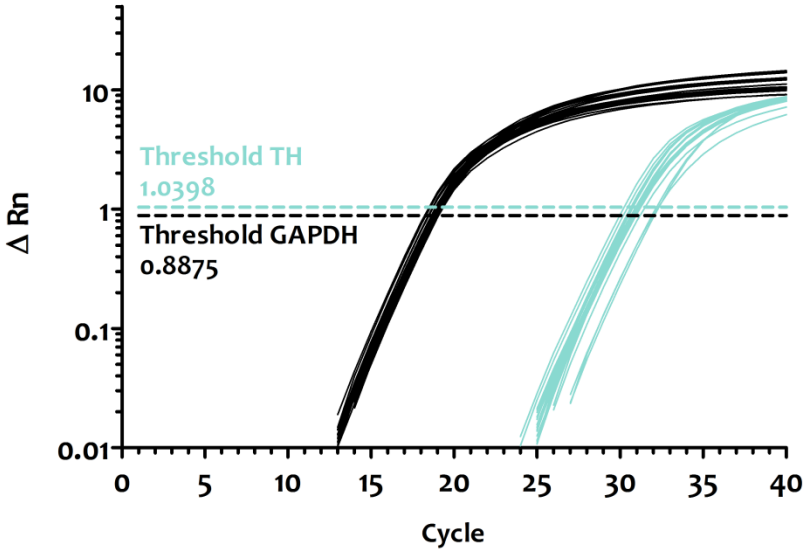

Figure 5.15 Profile of the qRT-PCR curve.
TH (blue) melting temperature (threshold) was reached on average around cycle 31, while other targets reached it much earlier; for example, GAPDH (black). Each line represents the average of sample triplicates (n = 24 experimental replicates). ΔRn: reporter signal normalised to the fluorescence signal of Applied Biosystems™ minus the baseline.

5.4.2. TH and AADC expression appeared not to be affected by mitochondrial or lysosomal impairment

Dopamine dyshomeostasis has been described as an early event in PD (Alberio et al., 2014), and the effect of dopamine on the molecular events of the disease has been studied in the last decades (for example, Aguirre et al., 2012; Alberio et al., 2014). In the

current study, TH and AADC mRNA levels in mitochondrial and lysosomal impairment were comparable to levels in control cells, even after treatment with L-DOPA. This is in accordance with the results obtained in chapter 4, as dopamine release was comparable to that in controls after rotenone and CBE treatment. However, these observations should be confirmed, especially those involving TH, due to the late melting point, where primer redesign should be considered.

5.4.3. Mitochondrial impairment could compromise the role of MAO-B

Neurons are highly dependent on correct mitochondrial function, and dopaminergic neurons are no exception (Abou-Sleiman et al., 2006). Nevertheless, the maintenance of mitochondria-dependent mechanisms could be more challenging in these neurons due to their complex morphology and to dopamine directly affecting the mitochondrial proteome and increasing mitochondrial-mediated apoptosis (Alberio et al., 2014). Some of the consequences of mitochondrial dysfunction are lower ATP synthesis with increased ROS production, as well as increased calcium release into the cytosol and dyshomeostasis of the apoptosis processes, all of which are described as molecular events in PD (Aguirre et al., 2012; Abou-Sleiman et al., 2006; Saffari et al., 2017). Additionally, it has been reported that mitophagy and mitochondrial turnover decrease with ageing (Mammucari and Rizzuto, 2010), making these changes more permanent. Despite all the work carried out in models with impaired mitochondria, it is not clear whether complex I dysfunction is contributing to dopamine dyshomeostasis. In the current study, cells with impaired mitochondria showed decreased MAO-B activity ***(Figure 5.3 A)***. MAO-B protein expression also decreased after L-DOPA treatment; however, this could be an indirect consequence of mitochondrial stress, as this enzyme is located in the outer mitochondrial membrane.

5.4.4. Lysosomal impairment and MAO-B activity

The relationship between GBA1 deficiency and other mechanisms altered in PD has also been studied (reviewed by Migdalska-Richards and Schapira, 2016). For example, animal and cellular models of GBA1 loss of function showed mitochondrial dysfunction and oxidative stress (Cleeter et al., 2013; Osellame et al., 2013). However, the effect of impairment GBA1 on dopamine metabolism has not yet been described. In the current study, lysosomal impairment alone did not modify the expression or activity of either MAO. However, when CBE treatment was followed by L-DOPA, MAO-B activity significantly decreased compared to that in control cells ***(Figure 5.7 A)***. This could lead to dopamine accumulation in the cytosol, increasing its oxidation and enhancing further GBA1 dysfunction, as proposed by Burbulla et al. (2017).

5.4.5. Decreased MAO-B activity as a possible common outcome of mitochondrial and lysosomal impairment

In contrast to the increased release of DOPAC described in Chapter 4, MAO-B activity significantly decreased after rotenone or CBE treatment. This could be a protective mechanism: cells try to compensate for increased oxidative stress caused by failure of the organelles by decreasing MAO activity, and consequently H_2O_2 production. However, this decreased activity would result in a higher concentration of dopamine in the cytosol, facilitating its oxidation and increasing oxidative stress (Munoz et al., 2012). Regarding COMT, no statistical differences were observed. However, a more thorough analysis of its activity and expression in these models is needed, as COMT expression tended to decrease after lysosomal impairment. Further work is necessary to confirm these findings. To summarise the conditions and the results obtained, a schematic review is presented in ***Table 5.3***.

Table 5.3 Summary of the effects of the different treatments on the catabolic enzymes. *Changes in mRNA, protein and activity levels are shown for MAO-A, MAO-B and COMT before (ø) and after L-DOPA treatment in all the models. Arrows in* **red** *are the significant changes between the treatment and its control (ethanol vs rotenone; control vs CBE; control vs NSD-1015); all other changes are not significant.*

		MAO-A			MAO-B			COMT		
	L-DOPA	Ø	1 h	3 h	Ø	1 h	3 h	Ø	1 h	3 h
Inhibited Complex I	mRNA	=	=	=	=	↓	=	=	=	=
	Protein	↓	=	↓	↓	=	↓	=	↑	↑
	Activity	↑	↓	=	↓	=	=			
Inhibited GBA1	mRNA	=	=	=	↓	↓	=	↓	↓	↓
	Protein	↓	↓	↓	↑	↓	↑	↑	↓	↓
	Activity	↑	↓	↑	=	↓	=			
Inhibited AADC	mRNA	=	=	↑	=	=	=	↓	↓	↓
	Protein	=	↓	↓	↑	↑	↑	↑	↑	↑
	Activity	↑	↓	↓	↓	↓	↓			

5.4.6. Neither L-DOPA nor mitochondrial/lysosomal dysfunction affected GSH levels

Oxidative stress has been described as a key molecular factor in the pathophysiology of PD (Blesa et al., 2015). Increased ROS production, iron accumulation and microglial activation are some of the events reported as contributors to oxidative stress in PD (Blesa et al., 2015; Aguirre et al., 2012; Munoz et al., 2012). GSH has been described as essential

to prevent mitochondrial damage by peroxynitrite and to carry out aminochrome excretion (Munoz et al., 2012; Heales et al., 1995). In the current study, GSH was detected in SH-SY5Y cells, although the values obtained were lower than the ones previously published in the literature (Allen et al., 2013). This could be due to the differences in the cell culture length or cell passage. L-DOPA treatment or mitochondrial/lysosomal impairment did not affect GSH concentration in the current study. Further work is needed to ascertain whether this is due to the absence of links between these events or to the nature of the model.

5.5. Conclusion

Although it is hard to conclude anything with certainty with this sample size, the results presented here suggest that dopamine could be regulating its own MAO-dependent degradation at post-translational level. However, COMT expression seems to be regulated by L-DOPA or AADC itself. Mitochondrial or lysosomal impairment decreased MAO-B activity in the SH-SY5Y cell line, in contrast to the increased DOPAC release described in Chapter 4. Undoubtedly, further work needs to be carried out to confirm these observations. However, these results support the hypothesis that defend there are mechanisms that have been not yet discovered in the already complex dopamine metabolism (Meiser et al., 2013).

CHAPTER 6

Monoamine Metabolism in Animal and Cellular Parkinsonism Models

6.1. Introduction

Several models of parkinsonism are available and have been used to study the possible causal relationship between the molecular and biochemical events related to PD. These models are also used to test the effects of potential drugs. While some systems provide faithful insights into the diseases, some animal models lead to mortality in a relatively short time, so may not give as good an insight into the disease. Creation of models require functional assays to assess their usefulness. HPLC coupled to an electrochemical detector is a suitable method for validating a dopamine/serotonin-related model at the functional level. In addition, dopamine and serotonin metabolism are directly or indirectly affected by the mutations causing some of these parkinsonism models; for example, GTPCH or DAT deficiency. In the present chapter, diverse parkinsonian model systems were studied, with the aim of gaining further mechanistic understanding of the diseases and to ascertain a possible commonality regarding monoamine metabolism. The following models were created by the collaborators as acknowledged:

A. *GTP cyclohydrolase 1 (GTPCH) deficiency in embryonic and adult zebrafish.* These animals expressed a loss-of-function mutation in the GTPCH gene (*GCHI*) suggested to lead to decreased synthesis of BH4. It has been reported before that mutations in this gene in the mouse model reduced GTPCH activity by 90% and BH4 concentration by 50% (Brand et al., 1996), although the effect on dopamine or serotonin pathways was not studied. It has been proposed that this decrease could lead to lower dopamine synthesis by the nigrostriatal cells in humans, resulting in L-DOPA responsive dystonia and parkinsonism (Mencacci et al., 2014).

B. *Deficiency of dopamine transporter.* This deficiency causes a parkinsonian syndrome known as DAT deficiency syndrome (DTDS) (Kurian et al., 2011b). DTDS patients show a characteristic increase in the concentration of dopamine metabolites in the CSF as a result of diminished dopamine recycling from the synaptic cleft. Due to lack of success in finding a treatment, gene replacement therapy is being explored to try to restore DAT. DTDS models studied here included cultured dopaminergic iPS-derived neurons, mice and zebrafish. In all cases, mutated DAT gene and decreased expression were confirmed. In addition, the effect of a novel gene replacement therapy on dopamine and serotonin homeostasis was studied in the murine model.

C. *Glucosylsphingosine (GlcSph) effect on dopamine reuptake by DAT.* Recent findings by Dr Michel Riese (TINTIN fellow, personal communication, University of Manchester, Manchester, UK) suggested a direct interaction between DAT and GlcSph ***(Figure 6.1)***. This is of special interest as glucosyl lipids accumulate in Gaucher disease due to dysfunctional GBA1. GlcSph has been proposed as an intracellular DAT antagonist that acts to regulate dopamine uptake (Dr Michel Riese, data not published). The non-dopaminergic cell line HEK-293 expressing human DAT (Hummerich et al., 2004) was used to explore this hypothesis.

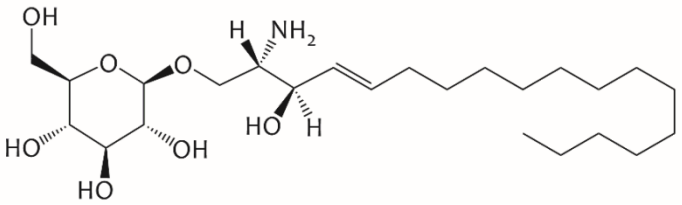

Figure 6.1 Glucosylsphingosine.
This molecule has been proposed as a competitive inhibitor of dopamine transport via DAT.

D. *Genetic models of Gaucher disease,* in contrast to the pharmacological cellular model used in chapters 4 and 5. One model consisted of GBA1 silencing in the SH-SY5Y cell line, the second was a mouse model of GD. The cell model was produced by transduction with lentiviruses containing interference RNA (iRNA) binding the mRNA of exon 4 from the human *GBA1*, resulting in a loss of function of the enzyme. The murine model was developed with a loxP-neo-loxP cassette in the intron 8, creating a splicing defect in one of the alleles of *GBA1* (Enquist et al., 2007). This cassette was present in all tissue except the skin, where the *Cre* gene was expressed, eliminating the cassette, producing normal GBA1 enzyme and allowing the mice to live longer than the day after birth.

Finally, the effect of differentiating the SH-SY5Y cell line to a more dopaminergic-like cell type was assessed. Even though it is the most commonly used cell model for this disease, several publications criticise this undifferentiated cell line as a PD model (Lopes et al., 2010; Biedler et al., 1978). Therefore, the extracellular levels of catecholamine and serotonin metabolite were studied before and after one week of differentiation by treatment with retinoic acid (RA) and brain-derived neurotrophic factor (BDNF) in order to investigate whether monoamine metabolism changes after differentiation. A summary of the models studied in this chapter can be found in ***Figure 6.2***.

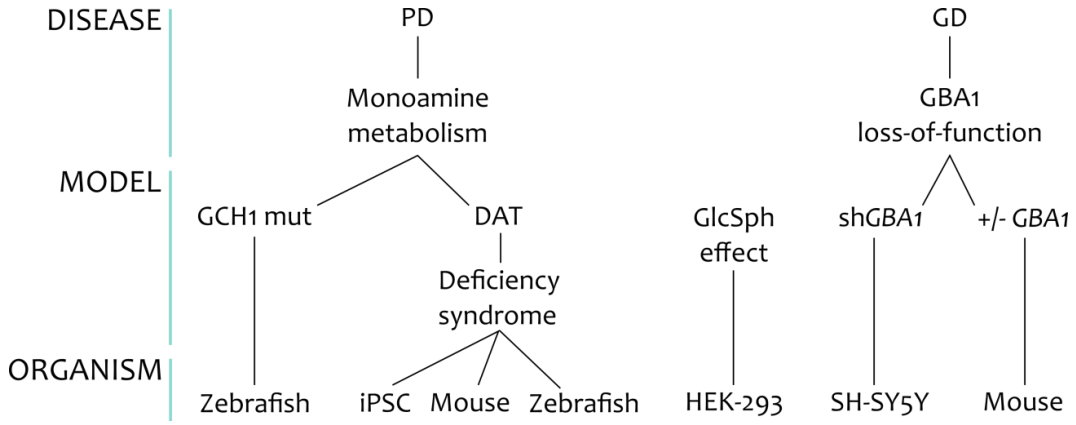

Figure 6.2 Summary of the cellular and animal models studied in Chapter 6.
The models were grouped by disease and phenotype. Each phenotype could be caused by more than one condition (model). Finally, several organisms, tissues or cell types were studied.

6.2. Methods

6.2.1. Pre-treatments

In the present chapter, models were produced and maintained by the collaborators. Most of the models were analysed in basal conditions, although in some cases, cellular models needed to be incubated or pre-treated before the samples were processed for HPLC measurement. The models pre-treated were the following.

6.2.1.1. iPS cells media incubation

iPS cells derived from two patients and a healthy individual (Kurian et al., 2011b). These cells were maintained with phenol-red-free medium for 48 h before collecting the samples on day 65 of the differentiation to dopaminergic neurons.

6.2.1.2. hDAT-HEK-293 treatments

HEK-293 cells expressing recombinant human DAT were incubated with 10 µM GlcSph for 10 min at 37 °C and 5% CO_2. Cells were then incubated with dopamine at 1 µM, 10 µM or 100 µM for 10 min at 37 °C and 5% CO_2. Before harvesting, cells were treated

with MAO inhibitors for 15 min to prevent any dopamine degradation. This protocol was carried out by Dr Yasmina Marti (Universität Mannheim, Mannheim, Germany).

6.2.1.3. L-DOPA incubation of GBA1-silenced SH-SY5Y cells

Cells were incubated for 24 h with the lentivirus at a multiplicity of infection of 3, i.e. 3 infective viral particles per cell. A scramble vector was used as a control. Scramble was not an empty vector, but a sequence bound to a non-relevant sequence in the human genome. Transduced cells were selected with puromycin and seeded at a density of 10^4 cells/cm^2 for the experiment. After 7 days, cells were incubated with 100 µM L-DOPA for 1 h in accordance with the method described in section 2.2.2.1. After silencing, these cells showed a 70% decrease in GBA1 mRNA expression and enzymatic activity. This protocol was carried out by Dr Maria Garcia-Gomez (UCL GOS Institute of Child Health, London, UK), who optimised the silencing and measured the enzymatic activity.

6.2.2. SH-SY5Y cell differentiation

Undifferentiated and differentiated SH-SY5Y cells followed the same path until and including puromycin selection. Cells were seeded in a collagen-A-coated plate at a confluence of 6×10^3 cells per cm^2 and allowed to attach overnight. The next day, the medium was changed to RA differentiating medium: DMEM/F-12-Glutamax medium supplemented with 2% FBS and 10 µM RA. The medium was changed every other day. Five days after the beginning of RA treatment, the medium was changed to BDNF differentiating medium: DMEM/F-12-Glutamax medium supplemented with 2% FBS and 50 ng/ml BDNF. The medium was changed every other day. Three days after the beginning of BDNF treatment, the cells were incubated with 100 µM L-DOPA for 1 h as described in section 2.2.2.1. This success of this differentiation protocol was evaluated by visual

identification. This protocol was carried out by Dr Maria Garcia-Gomez (UCL GOS Institute of Child Health, London, UK).

6.2.3. Intracellular and media sample preparation

Media samples were harvested and prepared by the collaborators as described in section 2.2.3.1. Intracellular monoamines were measured in the cell pellet of 10^5 HEK-293 cells. 400 µl of the isolation buffer used in section 2.2.3.3 was added to the pellet. The cells were re-suspended and immediately 400 µl of 0.8 M perchloric added before processing as described in section 2.2.3.1.

6.2.4. *GCH1* zebrafish sample preparation

Whilst zebrafish tails were used for genotyping, whole heads or brains were used for monoamine quantification in embryos and adults, respectively, as follows:

6.2.4.1. Zebrafish larvae

20 larvae were weighed and diluted 1:20 (weight to volume) in homogenisation buffer (0.2 M perchloric acid and 0.5 µM EDTA in ultrapure H_2O). This buffer was freshly made on the day of the experiment and kept on ice. The tissue was mechanically homogenised with glass homogeniser on ice and transferred to a centrifuge tube. It was incubated at 4 °C for 10 min and centrifuged at 13000 ×*g* for 5 min. The supernatant was collected and stored at –80 °C until HPLC analysis.

6.2.4.2. Adult zebrafish brain

In this model, three brains were mixed together taking into consideration genotype, gender and parents. The tissue was weighed and diluted 1:9 in homogenisation buffer following the protocol described in section 6.2.4.1. Supernatant was stored at –80 °C until HPLC analysis.

6.2.5. DAT KO mouse brain sample preparation

These animals were produced by Cre-lox homologous recombination (Giros et al., 1996), and genotyped after birth. *DAT* KO mice had a disrupted *DAT* gene, so they could not express the functional transporter and no dopamine reuptake could be accomplished. Gene therapy of KO animals started the day after genotyping and consisted of a bilateral injection in the brain ventricles with AAV9.hDAT. In both cases, mice were sacrificed 1 year after birth and the brain removed. Then, half a brain was weighed and diluted 1:9 in homogenisation buffer as described in section 6.2.4.2. The supernatant was collected and stored at –80 °C until HPLC analysis. This protocol was carried out by Dr Joanne Ng (UCL GOS Institute of Child Health, London, UK).

6.2.6. DAT KO embryo zebrafish brain sample preparation

To quantify dopamine metabolites within zebrafish brains, 10 brains were pooled together before the tissue was weighed and diluted 1:25 in homogenisation buffer. The protocol described in section 6.2.4.1 was then followed. The supernatant was collected and stored at –80 °C until HPLC analysis.

6.2.7. GD mouse brain sample preparation

As with DAT KO mice (section 6.2.5), half a brain was weighed and diluted 1:9 in homogenisation buffer. Then, the protocol described in section 6.2.4.1 was followed.

6.2.8. Monoamine measurement

In all cases, monoamines were quantified following the protocol described in Chapter 3.

6.3. Results

6.3.1. Monoamine status in GTPCH-mutated and wild-type zebrafish

Only 3-OMD, DOPAC and 5-HIAA were detected in zebrafish embryos ***(Figure 6.3)***. No statistical differences were observed in 3-OMD and DOPAC levels between the three groups: WT, heterozygote (GCH1 +/-) and homozygote (GCH1 -/-) embryos ***(Figure 6.3)***. Unexpectedly, serotonin catabolism was severely compromised in the KO animals, as 5-HIAA was only detected in WT and heterozygote embryos ***(Figure 6.3)***.

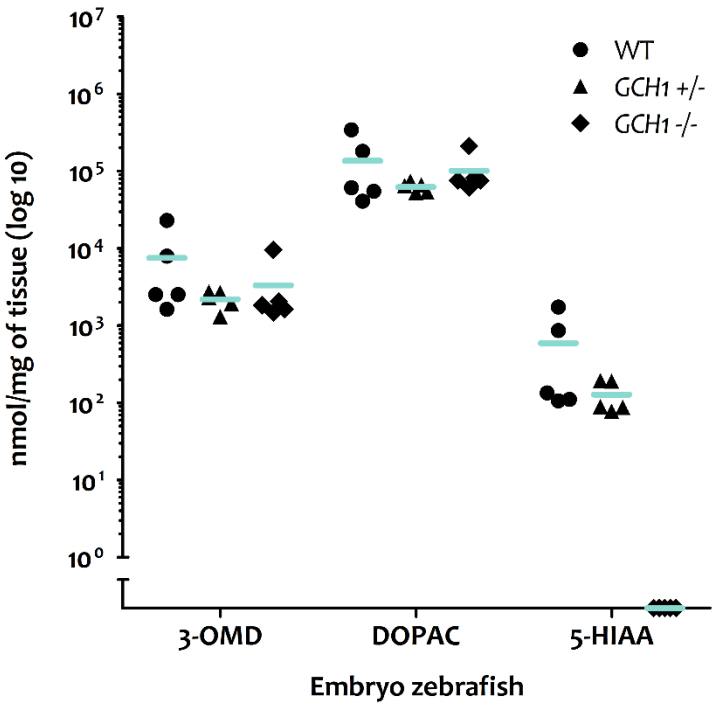

Figure 6.3 3-OMD, DOPAC and 5-HIAA levels in zebrafish embryos.
No statistical differences were found in the levels of 3-OMD, DOPAC and 5-HIAA between WT, GCH1 +/- or GCH1 -/-. Statistical analysis was carried out by one-way ANOVA with Tukey's post hoc *test. Data are presented as individual values and mean (n = 5 experimental replicates).*

In contrast to the embryos, dopamine was detected in adult zebrafish, along with HVA and 5-HIAA. Only WT and heterozygotes could be studied as KO embryos died 10 days post-fertilisation. It was not known whether zebrafish gender or progenitors had an

effect on monoamine metabolism, so samples were prepared taking those parameters into consideration. No differences were observed based on gender or tank ***(Table 6.1)***. Therefore, samples were grouped based on the genotype, and no differences were noted between WT and heterozygote animals ***(Figure 6.4)***.

Table 6.1 Monoamine levels in adult zebrafish brain based on tank origin and gender.
In addition to the separation by genotype, monoamine levels were studied grouping samples by tank (same progenitors) and by gender, and non-significant differences were obtained. Statistical analysis was carried out by unpaired Student t-test and data are presented as mean (nmol/mg of tissue) ± SEM.

		Tank A	Tank B	Male	Female
Dopamine	WT	1874 ± 582.5	1894 ± 222.7	2249 ± 207.5	1744 ± 247.2
	GCH1 +/-	1770 ± 176.2	1942 ± 328.1	1517 ± 320.6	2094 ± 240.1
HVA	WT	64 ± 35.5	69 ± 32.1	84 ± 15.5	61 ± 33.1
	GCH1 +/-	41 ± 18.6	60 ± 24.3	41 ± 18.1	60 ± 24.5
5-HIAA	WT	475 ± 193	526 ± 82.9	650 ± 18.5	457 ± 90
	GCH1 +/-	447 ± 48.8	405 ± 69.1	399 ± 94	434 ± 53.8

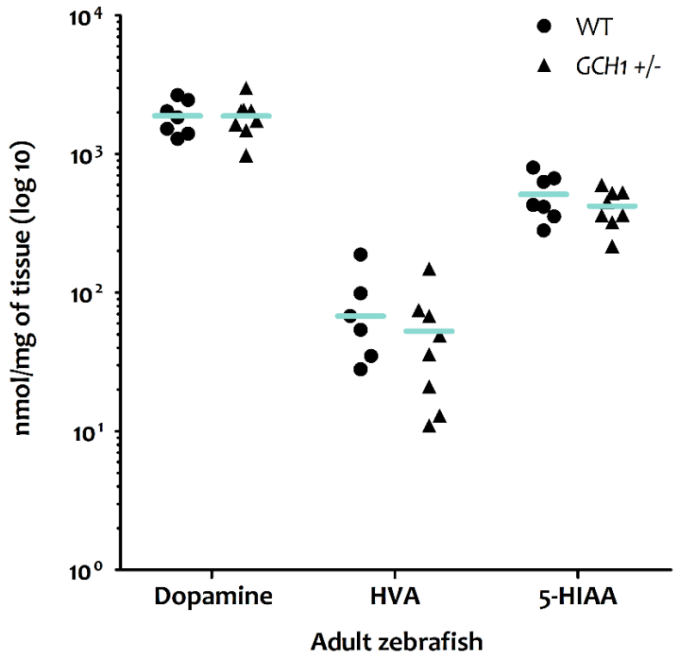

Figure 6.4 Levels of dopamine, HVA and 5-HIAA in WT and GCH1 heterozygote adults.
Only dopamine, HVA and 5-HIAA were detected in adult zebrafish brain. No differences were observed in the quantity of analytes between WT (n = 7 experimental replicates) and GCH1 heterozygote (GCH1 +/-, n = 8 experimental replicates) adults. Statistical analysis was carried out by unpaired Student t-test. Data are presented as individual values and mean.

6.3.2. iPS-derived neurons from DTDS patients and dopamine metabolism

Dopamine, DOPAC and HVA were detected in the culture media ***(Figure 6.5)***. No statistical differences were observed between cells derived from the control (n = 9 experimental replicates) and the two DTDS patients (n = 4 experimental replicates for each patient) in dopamine or DOPAC levels. However, HVA levels were significantly increased in the extracellular media of the iPS cells derived from DTDS patients compared to levels in the control cells ***(Figure 6.5)***.

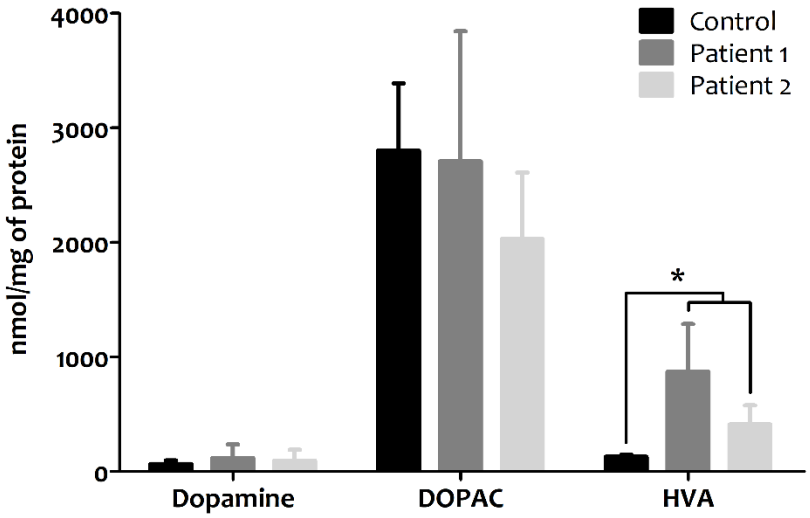

Figure 6.5 Extracellular dopamine and its metabolites in DTDS iPS cells on day 65 of differentiation.
*Dopamine and DOPAC levels remained constant in control (n = 9 experimental replicates) and the two DTDS (patient 1 and 2, n = 4 experimental replicates each) samples. On the contrary, HVA levels were higher in the DTDS samples. Statistical analysis was carried out by unpaired Student t-test compared with the control (*p<0.05). Data are presented as mean ± SEM.*

6.3.3. Brain monoamine metabolism in DTDS mice

Dopamine levels in KO mice (n = 4 experimental replicates) were markedly lower than levels in the brains of WT animals (n = 8 experimental replicates) (***Table 6.2 and Figure 6.6***). The levels of dopamine and serotonin metabolites HVA and 5-HIAA were significantly higher in KO mice than in WT ***(Table 6.2 and Figure 6.6)***. This increase of the

metabolites resulted in a significant increase in all three ratios ***(Table 6.2)***. After gene therapy (n = 4 experimental replicates), dopamine levels decreased compared to those of untreated KO animals ***(Figure 6.6)***. The decreases in both MAO-dependent metabolites DOPAC and 5-HIAA were such that the levels were below those of WT. Finally, HVA levels also decreased after gene therapy yet remained significantly higher than WT ***(Figure 6.6)***. Whilst not significant, the values of dopamine and serotonin metabolites decreased after the treatment with gene therapy; hence, the values of those metabolites were closer to WT than those of the untreated KO. However, the genotypes could be distinguished when the ratios were calculated ***(Figure 6.7)***. Untreated and treated KO mice showed similar values for all the ratios calculated here, suggesting that the DAT derived from the gene therapy might not be functional as DAT in WT animals. HVA:5-HIAA, HVA:dopamine and turnover ratios were 2, 19 and 13 times higher respectively in both KO animals compared to WT.

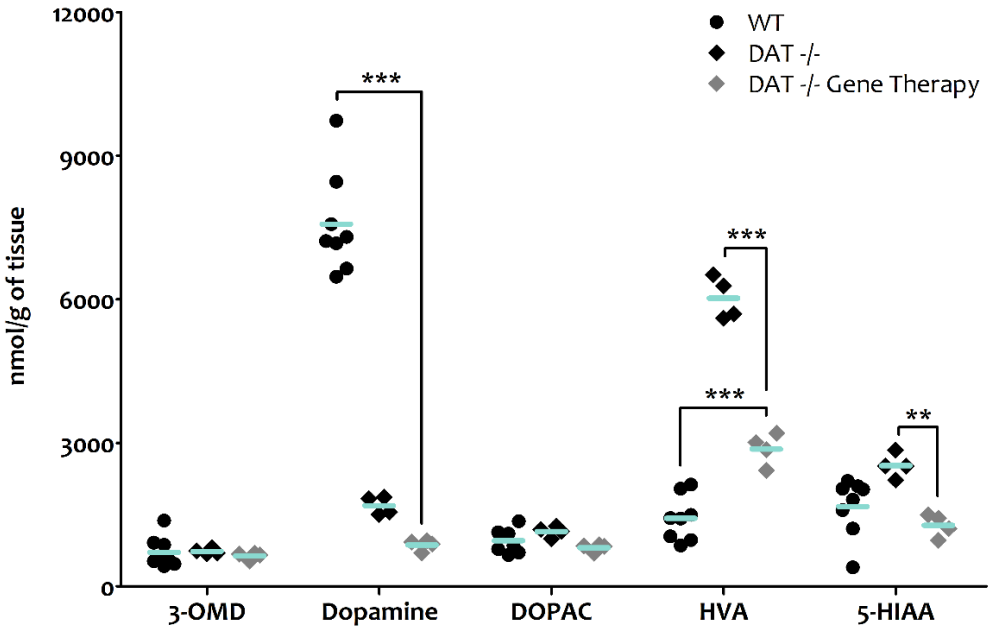

Figure 6.6 Brain dopamine and serotonin metabolism in DAT KO mice with and without gene therapy.
*DAT KO mice (DAT -/-, n = 4 experimental replicates) displayed lower levels of dopamine and higher HVA than WT (n = 8 experimental replicates). Animals treated with gene therapy (DAT -/- Gene Therapy, n = 4 experimental replicates) showed values closer to the WT, except for dopamine. Statistical analysis was carried out by one-way ANOVA with Tukey's post hoc test (**p < 0.01; ***p < 0.0001). Data are presented as individual values and mean.*

Table 6.2 Comparison of WT versus DAT KO mouse brain tissue.
Statistical analysis was carried out by unpaired Student t-test. Turnover = (DOPAC+HVA)/dopamine. Data are presented as mean (nmol/mg of tissue) ± SEM.

	WT	DAT KO	p-value
3-OMD	712 ± 113.7	731 ± 29.1	n.s.
Dopamine	7572 ± 375.5	1687 ± 92.2	**<0.001**
DOPAC	957 ± 87.0	1147 ± 55.1	n.s.
HVA	1423 ± 166.8	6024 ± 222.2	**<0.001**
5-HIAA	1672 ± 215	2525 ± 127.7	**<0.05**
HVA:5-HIAA	1.03 ± 0.240	2.37 ± 0.064	**<0.001**
HVA:Dopamine	0.19 ± 0.017	3.59 ± 0.058	**<0.001**
Turnover	0.31 ± 0.020	4.30 ± 0.092	**<0.001**

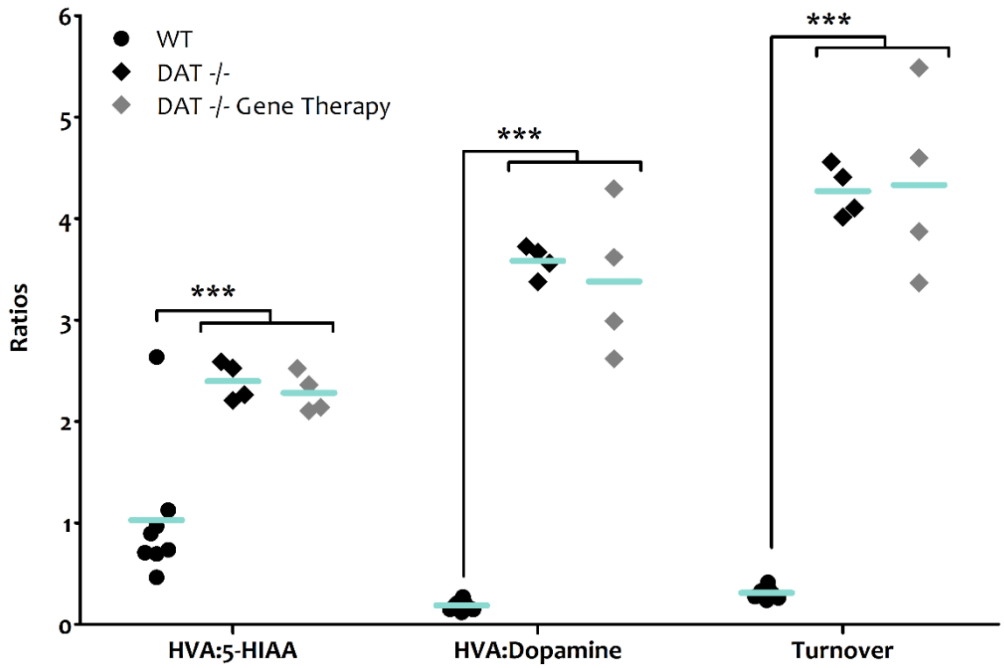

Figure 6.7 Catecholamine ratios showed differences between WT and DAT KO mice.
*The two genotypes could be separated into two groups after calculating the ratios, including those with gene therapy (DAT -/- Gene Therapy). Statistical analysis was carried out after square root transformation of the ratios followed by one-way ANOVA with Tukey's post hoc test (***p < 0.0001). Turnover = (DOPAC+HVA)/dopamine. Data are presented as individual values and mean.*

6.3.4. Monoamine metabolism in heterozygote and DTDS zebrafish

Genotyping was carried out in the tail, while the brain was used to measure monoamine levels. Only 3-OMD, DOPAC and 5-HIAA were detected in this model ***(Figure 6.8)***. None of the molecules showed any differences between the three genotypes.

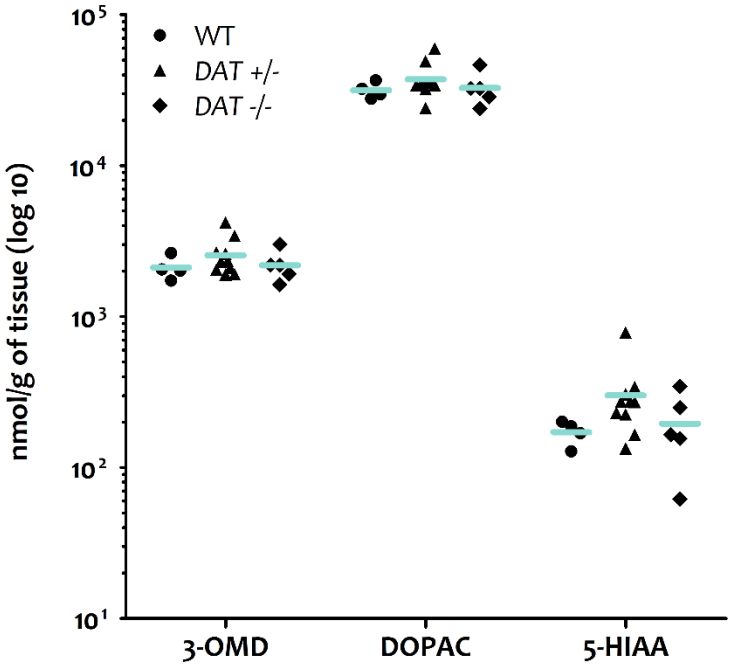

Figure 6.8 Differences in metabolite levels between DTDS zebrafish model and WT. *Zebrafish embryos of WT (n = 4 experimental replicates), DAT heterozygote (DAT +/-, n = 10 experimental replicates) and DAT homozygote (DAT -/-, n = 5 experimental replicates) were studied and no differences were observed between groups. Statistical analysis was carried out by one-way ANOVA with Tukey's* post hoc *test. Data are presented as individual values and mean.*

6.3.5. Dopamine reuptake in HEK-293 cells expressing human DAT

Intracellular dopamine could only be detected in HEK-293 cells that were incubated at a concentration of 10 µM or higher ***(Figure 6.9)***, and no differences were observed in dopamine reuptake between control and GlcSph groups.

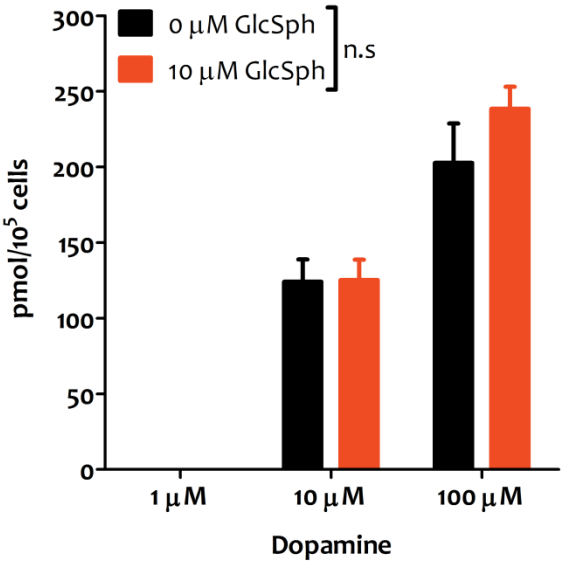

Figure 6.9 The effect of treatment of hDAT HEK-293 with GlcSph on dopamine reuptake. *GlcSph treatment did not disrupt dopamine reuptake through DAT. Statistical analysis was carried out by unpaired Student t-test to compare control to GlcSph treatment (n.s.). Data are presented as mean ± SEM (n = 3 experimental replicates).*

6.3.6. GBA1 silencing and monoamine metabolism

SH-SY5Y cells with silenced GBA1 (iGBA1) exhibited decreased extracellular levels of dopamine compared to those in control cells ***(Figure 6.10)***. Although not significant, it was noted that iGBA1 cells showed decreased levels of all the other measured metabolites. When looking at the ratios, the HVA:5-HIAA ratio was increased in the iGBA1 cells ***(Figure 6.11)*** and the HVA:dopamine ratio tended to be higher in iGBA1 cells, although neither increase was statistically significant. Dopamine turnover was comparable in both groups.

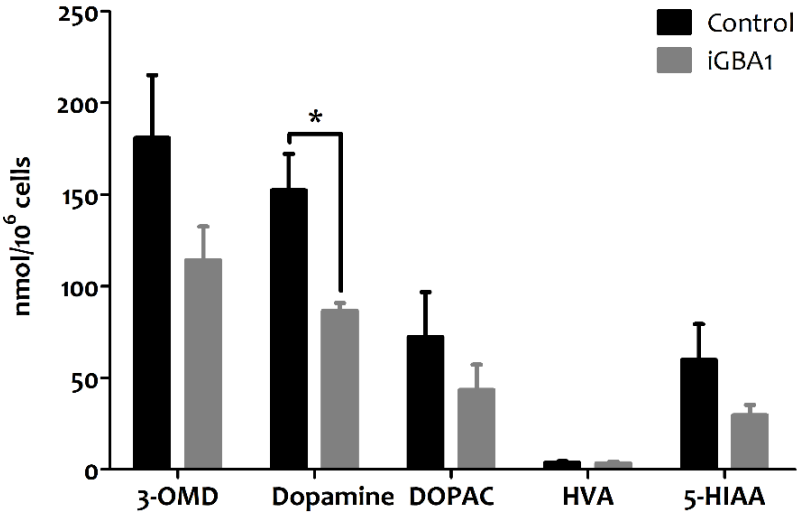

Figure 6.10 The effect of silencing GBA1 on extracellular dopamine levels.
*SH-SY5Y cells transduced with iGBA1 showed significantly lower dopamine levels. Although not significant, the levels of dopamine metabolites were lower in iGBA1 cells. Statistical analysis was carried out by unpaired Student t-test (*p < 0.05). Data are presented as mean ± SEM (n = 5 experimental replicates).*

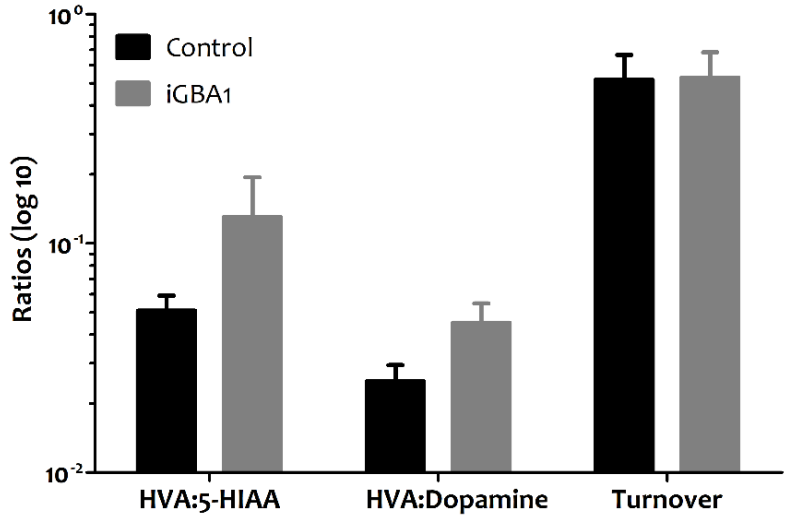

Figure 6.11 The effect of silencing GBA1 on catecholamine turnover.
Statistical analysis was carried out, after the transformation of the ratios, by unpaired Student t-test. Turnover = (DOPAC+HVA)/dopamine. Data are presented as mean ± SEM (n = 5 experimental replicates).

6.3.7. Brain monoamine levels in heterozygote GD murine model

After studying the neurotransmitters in two GD cell models, a murine model was studied. In this case, the animals were heterozygote for a *GBA1* mutation and showed decreased GBA1 enzymatic activity within the brain (Enquist et al., 2007). Heterozygote animals were studied, as carriers of *GBA1* mutations have also shown higher probability of developing PD (Neumann et al., 2009). No differences were observed between WT (n = 3 experimental replicates) and heterozygotes (*GBA1* +/-, n = 7 experimental replicates) in the levels of either dopamine and its metabolites, or serotonin metabolites ***(Figure 6.12)***. Ratios also had similar values in both groups ***(Figure 6.13)***.

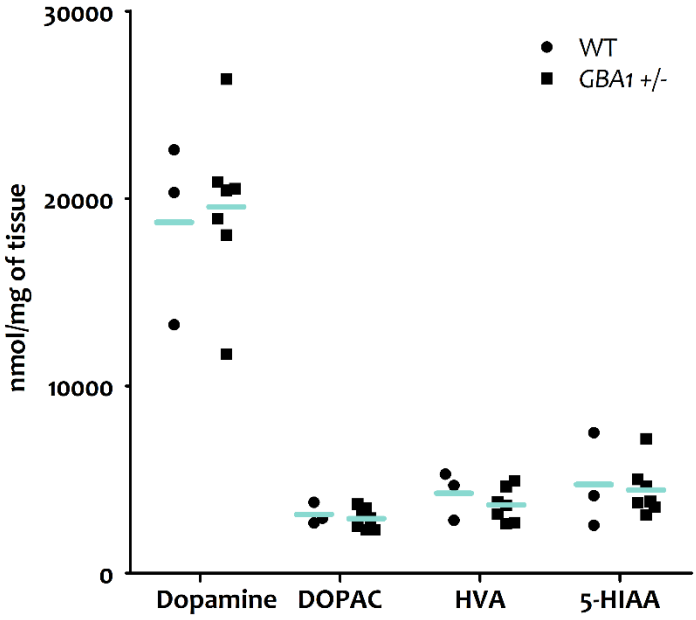

Figure 6.12 Changes in monoamine levels in the brains of heterozygote GBA1 mutant mouse model compared to WT.
Dopamine, DOPAC, HVA and 5-HIAA showed similar values in the brains of WT and GBA1 +/- mice. Statistical analysis was carried out by unpaired Student t-test. Data are presented as individual values and mean.

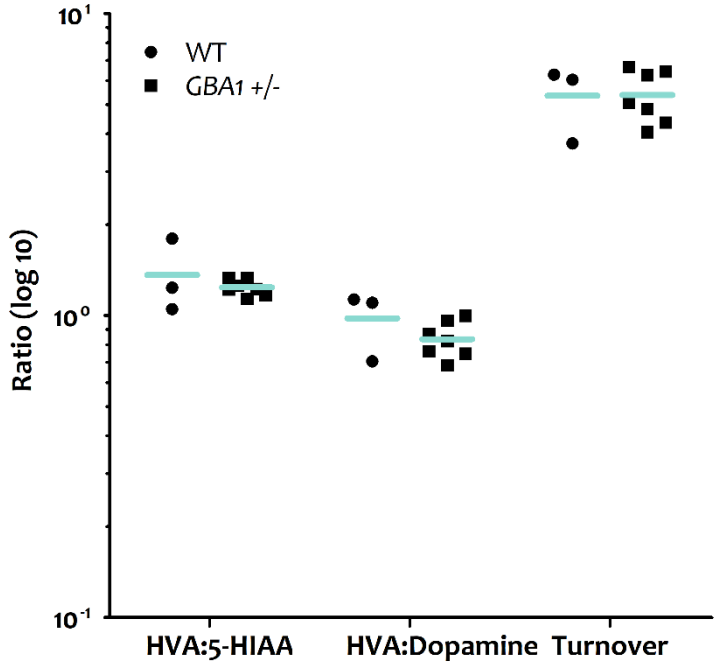

Figure 6.13 Differences in ratios between heterozygote GBA1 mutant mouse and WT. *None of the ratios showed statistical differences between WT and GBA1 +/- mice. Statistics were performed after transforming the ratio values to a normal distribution and completed using unpaired Student's t-test. Turnover = (DOPAC+HVA)/dopamine. Data are presented as individual values and mean.*

6.3.8. Monoamine metabolism after SH-SY5Y differentiation

SH-SY5Y differentiation to a dopaminergic neuron-like cell type, i.e. expressing TH, is described in the literature (for example, Kovalevich and Langford, 2013). After L-DOPA treatment, differentiated SH-SY5Y cells showed decreased extracellular dopamine levels compared to non-differentiated cells, in contrast to the significant increase in 3-OMD ***(Figure 6.14)***. Although not statistically significant, the levels of dopamine metabolites were higher after differentiation. The serotonin metabolite 5-HIAA was significantly increased in medium from the differentiated cells. All these changes resulted in a decreased ratio HVA:5-HIAA and increased dopamine turnover ***(Figure 6.15)***.

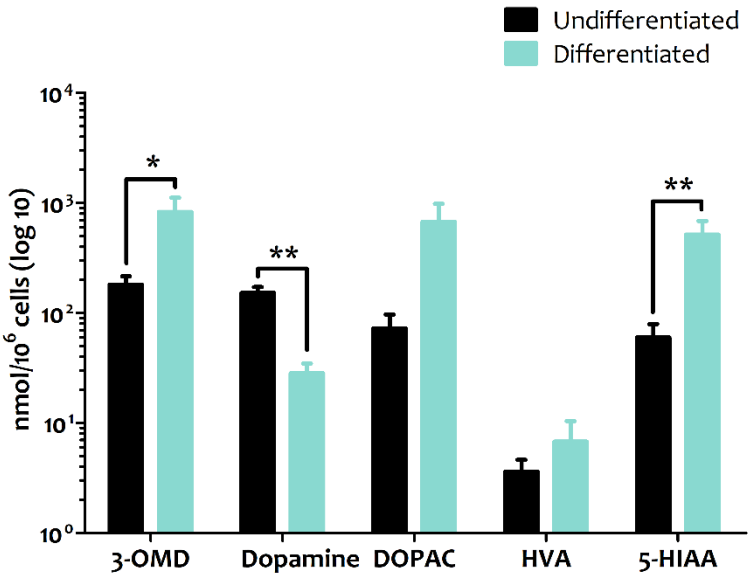

Figure 6.14 Changes in extracellular dopamine levels after SH-SY5Y differentiation.
*Undifferentiated (n = 5 experimental replicates) and differentiated (n = 4 experimental replicates) SH-SY5Y cells were compared. Dopamine significantly decreased after differentiation. On the contrary, differentiated cells significantly increased the levels of 3-OMD and 5-HIAA. Statistical analysis was carried out by unpaired Student t-test (*p < 0.05; **p < 0.01). Data are presented as mean ± SEM.*

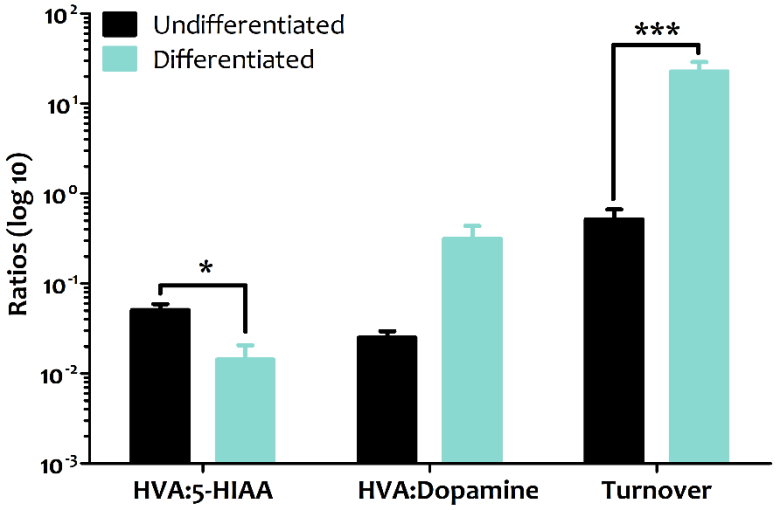

Figure 6.15 The effect of differentiation on dopamine turnover.
*While differentiated cells showed a decreased HVA:5-HIAA ratio, overall dopamine turnover increased 43-fold compared to undifferentiated cells. Statistical analysis was carried out, after transformation of the ratios, by unpaired Student t-test (*p < 0.05; ***p < 0.001). Turnover = (DOPAC+HVA)/dopamine. Data are presented as mean ± SEM.*

6.4. Discussion

6.4.1. BH4 deficiency effects on dopamine and serotonin metabolism

Zebrafish have been used as a model in several diseases, mostly in the developmental stages due to the characteristics of the egg, allowing observation of embryo development as it is "external and visually accessible" (Veldman and Lin, 2008). This is also very convenient for the study of diseases with a low or null survival rate after birth, such as homozygous *GCH1* mutation where zebrafish die 10 days post-fertilisation (Dr Marcus Keatinge, personal communication, University of Sheffield, Sheffield, UK). In the current study, both embryo and adult zebrafish were studied as a model of BH4 deficiency by GTPCH mutation.

While dopamine and serotonin metabolites were measurable in embryos, no dopamine was detected. This suggested that the zebrafish embryos might have been able to synthesise dopamine but were not mature enough to accumulate it. The high levels of DOPAC support this theory, as dopamine may be degraded to this metabolite. However, no differences in monoamine levels between WT and GTPCH deficient embryos were found. Surprisingly, 5-HIAA could not be detected in GCH1 -/- embryos although it was detectable in WT embryos, suggesting that serotonin metabolism is severely compromised. This observation may be independent of MAO expression and activity because DOPAC, the dopamine product produced by MAO, was not affected in the same way.

As the total absence of GTPCH was lethal shortly after fertilisation, only WT and heterozygote adults were studied. In humans, mutations in GTPCH are inherited in an autosomal dominant way, with a proposed female predominance (Steinberger et al., 1998; Furukawa et al., 1998) although this has been disputed, as some authors have reported no

gender imbalance (Wider et al., 2009). The animals studied here showed no differences in dopamine and serotonin metabolites between genders. Although dopamine could be detected in adult zebrafish, no differences between WT and heterozygotes were observed in its synthesis or degradation. Similarly, no differences in serotonin degradation were detected between the two groups. These results suggest that one allele might be sufficient for dopamine synthesis in zebrafish. Indeed, Brand et al. (1995) reported that the mutation of one *GCH1* allele in a murine model would result in half of the BH4 concentration of a WT. Therefore, it was hypothesised that a system with GTPCH deficiency might need to be stressed to show any changes in dopamine synthesis due to decreased BH4 levels. For instance, L-DOPA-responsive dystonia is caused by an autosomal dominant mutation of the gene *GCH1*, and the BH4 system needs to be stressed for the diagnosis (Saunders-Pullman et al., 2004). Phenylalanine loading is the established and most reliable diagnostic tool to distinguish L-DOPA-responsive dystonia of early onset PD (Hyland et al., 1997). In this test, patients with mutant GTPCH show an increased phenylalanine/tyrosine ratio, as BH4 is required to transform phenylalanine to tyrosine by phenylalanine hydroxylase. Further experimentation needs to be carried out to explore this theory in the zebrafish model.

6.4.2. Mammalian DTDS models mimic human patients

DTDS patients show high levels of dopamine metabolites in the CSF due to loss of function of DAT (Kurian et al., 2011b). This is a characteristic and possibly critical phenotype for the development and evolution of the symptoms in these patients. In order to validate the models, it is therefore important to assess whether the disease models also reflect this feature.

For the study of iPS cells, monoamine concentration in the medium was normalised against cell protein content, as the number of patient-derived cells was decreased by

almost half (Dr Serena Barral, personal communication, UCL GOS Institute of Child Health, London, UK). Both control and patient cells were able to release dopamine to the medium, confirming their dopaminergic phenotype. However, although the iPS differentiation protocol was designed to produce dopaminergic neurons (Dr Serena Barral, personal communication, UCL GOS Institute of Child Health, London, UK), some of the samples were serotoninergic, suggesting incomplete differentiation. Patient cells showed increased levels of HVA, as observed in the CSF of the DTDS patients (Kurian et al., 2011b). Dopamine levels were also higher in the media of patients' cells, although this difference was not significant, supporting the view that the absence of DAT can cause accumulation of dopamine in the synaptic cleft of DTDS patients due to impaired reuptake of the neurotransmitter.

DTDS mice were dwarf and showed hyperlocomotor behaviour, as well as reduced survival (by 10 weeks) compared to DAT heterozygotes (Giros et al., 1996). As in the iPS cell model and in the CSF of patients, high HVA levels were observed in the brains of KO mice, suggesting that this murine model is a suitable organism for the study of this disease. These animals also displayed significantly higher levels of 5-HIAA. This observation could be a result of enhanced MAO activity, as DOPAC levels in KO animals were also higher, although this difference not significant. The differences in the levels of these two MAO-dependent molecules could be due to the fact that, in the dopamine pathway, DOPAC is further metabolised by COMT to produce HVA, while 5-HIAA is the end product of the serotonin pathway. In addition, dopamine levels in the brain of the KO animals were decreased, possibly due to the emptied intracellular dopamine storage vesicles. Therefore, the maintenance of dopamine levels in these animals is presumably dependent exclusively on *de novo* dopamine synthesis. This appears to be the first time a decrease in dopamine levels has been reported in the brains of DTDS mice. This depletion also agrees with the increased prolactin levels reported in DTDS patients (Kurian et al., 2011b), as dopamine

negatively regulates the exocytosis of this hormone (reviewed by Fitzgerald and Dinan, 2008).

Modification of DAT expression in the murine model by gene therapy was followed by decreased degradation of dopamine and serotonin. Surprisingly, this decrease in dopamine degradation did not result in increased levels of dopamine, as the neurotransmitter levels were lower than those of untreated KO. Examining the ratios of the metabolites, it is noticeable that animals after one year of treatment showed similar values to those without treatment, and different values to WT mice, despite the changes in HVA levels after therapy. The results observed here suggest that the compensation by gene therapy has not been sufficient yet, as dopamine levels are still significantly decreased. This could be due to the fact that dopamine connections are made before birth (Stott and Ang, 2013) and these animals were treated after birth. Therefore, treatment could be increasing the expression of DAT, but the dopaminergic network could possibly be too weak to respond accordingly. However, it is of note that the values obtained from the murine model were a result of experiments in half brain formed by a mix of cell types. It would be of interest to examine different regions within the brain to determine whether gene therapy results in any localised improvements in dopamine levels.

Finally, no dopamine was detected in the zebrafish embryo model. However, dopamine metabolites were present, suggesting that the system is able to synthesise dopamine but that it is degraded. The serotonin metabolite 5-HIAA was also detected in this developmental stage, as in the other embryonic zebrafish model used here, the GTPCH model. In the DTDS zebrafish model, no differences were observed between control and heterozygote or homozygote animals in the metabolites that were detected. Therefore, although this model expresses the same mutation as the iPS cells and mice, zebrafish was not mimicking the phenotype of the patients, suggesting that dopamine

synthesis in zebrafish embryos is either very slow so that residual enzyme activity on the DTDS in zebrafish is sufficient, or that there are differences in the dopamine synthesis pathway in zebrafish embryos.

In conclusion, only mammalian models of DTDS displayed quantifiable dopamine levels. In addition, and despite the fact that monoamine levels were measured extracellularly in the iPS cell model and intracellularly in the murine model, they both showed increased HVA levels, as described in the CSF of patients, suggesting these models are more suitable than zebrafish for study of the disease. To my knowledge, this is the first time that DTDS has been shown to be a deficiency state of dopamine, possibly leading to the dysregulation of other cellular functions, such as the release of prolactin.

6.4.3. Dopamine reuptake in HEK-293 cells after GlcSph treatment

HEK-239 is a human embryonic kidney cell line, therefore its phenotype is neither neuronal nor dopaminergic (Thomas and Smart, 2005). Therefore, these cells were modified to artificially express human DAT in order to study transporter functionality by analysing dopamine reuptake before and after incubation with GlcSph. This molecule is of special interest as increased levels of GlcSph and low GBA1 activity have been related to lower neuronal viability (de la Mata et al., 2016). Cells were also treated with MAO inhibitors to prevent dopamine degradation and allow intracellular dopamine accumulation. Under the current conditions, no differences were observed between control and GlcSph-treated cells. This could be due to the extracellular application of the DAT regulator that might act intracellularly. Another possible explanation is that there are small changes in dopamine, but more data would be necessary to detect these changes.

6.4.4. Genetic GBA1 loss of function and monoamine metabolism

Since GD is related to PD, several pharmacological and genetic models of GD have been established (Farfel-Becker et al., 2011; Santos and Tiscornia, 2017). An example of a pharmacological model is the cellular model described in Chapter 4. GBA1 silenced cells showed decreased levels of dopamine in the media. In fact, all the metabolites were lower (albeit non-significantly) in the GD genetic model, including serotonin-derived 5-HIAA. This contrasts with the results obtained in the CBE cell model, where only dopamine and serotonin metabolites were affected by the treatment. However, it is of note that pharmacological GBA1 inhibition possibly affects other enzymes, in contrast to more-focused genetic methods, as CBE could be interacting with other cell targets (Rempel and Withers, 2008).

In the genetic murine model of GD, heterozygote GBA1 mice showed very similar values to WT. This would agree with the observation that not all the carriers of a mutated GBA1 develop parkinsonian symptoms (Migdalska-Richards and Schapira, 2016). Also, age is a key predisposing factor in the development of neurodegeneration, and these animals were young at the time of measurement; it would have been interesting to determine dopamine metabolism in aged mice. However, a slight non-significant increase in dopamine levels and a decrease in its metabolites were observed, leading to decreased HVA:5-HIAA and HVA:dopamine ratios. Further work needs to be done with GBA1 KO mice to better characterise dopamine metabolism in this model, as changes in dopamine degradation could be a possible early event in the development of the disease.

6.4.5. Effect of SH-SY5Y cell differentiation on dopamine and serotonin metabolism

The suitability of the SH-SY5Y cell line as a dopaminergic model has been widely discussed (Xicoy et al., 2017). The expression and functionality of some of the dopaminergic cell-type features are absent in the proliferative or undifferentiated SH-SY5Y cells, as indicated by the absence of TH reported in this study and by others (Lopes et al., 2010; Cui et al., 2015; McMillan et al., 2007). Some publications have concluded that differentiating the SH-SY5Y cell line to a more neuron-like cell type would be a more appropriate model of PD (Nishida et al., 2008). SH-SY5Y differentiation decreased extracellular levels of dopamine. In contrast, the levels of dopamine and serotonin metabolites increased, that of MAO-dependent metabolites being the most noticeable. This could be due to changes in the expression of the enzymes, for instance increased expression and/or activity of MAO. The ratios confirmed that overall dopamine turnover increased in the differentiated cells, suggesting that this differentiation could be regulating dopamine release and/or its extracellular concentration more carefully. However, it remains to be confirmed whether this controlled release is more similar to physiological events in the human brain.

6.5. Conclusion

The aim of this chapter was to identify the biochemical characteristics and to ascertain whether different parkinsonian models present common features regarding monoamine metabolism. While dopamine was detected in several models, confirming their dopaminergic nature; for example, iPS cell media and mouse brain, in others the neurotransmitter was undetectable; for example, zebrafish embryo (summarised in ***Table***

6.3). It is also reported here that the DTDS mouse model showed a deficiency in intracellular dopamine, opening new possibilities for the development of new therapies. It is hypothesised that the zebrafish embryo models studied here, *GCHI* and *DAT* mutants, could have an immature storage system as dopamine was not detected but dopamine metabolites were. Examination of this pathway could be enhanced by studying adult animals, but mammalian models remain the most suitable. Regarding SH-SY5Y differentiation, changes in monoamine turnover prove the need for extended investigation, as these cells can give more accurate insights into monoamine metabolism in dopaminergic neurons.

Table 6.3 Is there commonality in dopamine and serotonin metabolism?
Data summarised here show the statistically significant observations reported in Chapter 6. All models are compared to its control/WT, except for the DTDS mice treated with gene therapy, which are compared to untreated KO animals. GlcSph: glucosylsphingosine; mut.: mutant; NA: not applicable; ND: not detected; T: treated; UT: untreated; ZF: zebrafish.

Model	Organism	3-OMD	DA	DOPAC	HVA	5-HIAA	Turnover
GTPCH mut.	ZF het embryo	=	ND	=	ND	=	NA
	ZF KO embryo	=	ND	=	ND	ND	NA
	ZF het adult	ND	=	ND	=	=	NA
DTDS	iPS cells	ND	=	=	↑	ND	NA
	KO mice	=	↓	=	↑	↑	↑
	T KO mice (vs UT)	=	=	=	↓	↓	=
	ZF embryo	=	ND	=	ND	=	NA
GlcSph	HEK-293	NA	=	NA	NA	NA	NA
GD	iGBA1 SH-SY5Y	=	↓	=	=	=	=
	Mice	ND	=	=	=	=	=
Differentiation	SH-SY5Y	↑	↓	=	=	↑	↑

CHAPTER 7

CSF Glycoprotein Profile in Individuals with Parkinsonism

7.1. Introduction

Protein post-translational modifications and their role in different pathologies have received more and more attention in recent years (Santos and Lindner, 2017). Glycosylation, the addition of carbohydrates (glycans) to form glycoproteins, is a major post-translational modification of proteins. The physiological roles of glycosylation include correct protein folding, stability and location; for example, mannose-6-phosphate acts as a lysosomal location tag (reviewed by Hwang et al., 2010). Glycans are divided in two groups, *N*- and *O*-linked, based on how the glycan is linked to the protein (***Figure 7.1***). While in the former, glycans are attached to an asparagine residue by a nitrogen atom, in the latter they are linked to a serine or threonine by an oxygen atom. Another difference is that *N*-linked glycans are usually more complex and branched. Although both types are found on the membrane proteins and on the glycoproteins secreted to biological fluids, *N*-linked glycans are more widely studied due to the lack of enzymes able to release *O*-linked glycans.

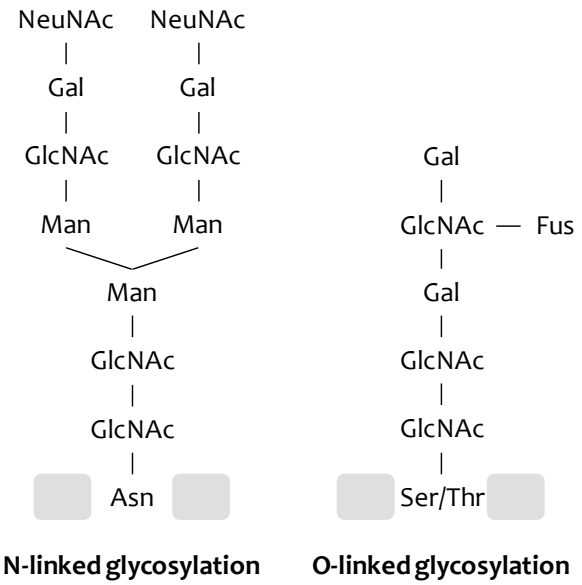

Figure 7.1 Types of glycan based on their linkage.
Asn: asparagine; Ser/Thr: serine/threonine; GlcNAc: N-acetylglucosamine; Man: mannose; Gal: galactose; Fus: fucose; NeuNAc: sialic acid.

Glycoprotein synthesis is an intricate process that involves several organelles, including the endoplasmic reticulum and Golgi apparatus, and sequential addition of monosaccharaides (Ohtsubo and Marth, 2006). Glycoprotein degradation occurs mainly in lysosomes (Winchester, 2005; Freeze et al., 2015). Lysosomal glycosidases are a large group of soluble hydrolases with a low optimum pH that, despite accomplishing similar reactions, have a structural similarity of less than 20%. These enzymes are classified into two groups, exo- and endoglycosidases, based on the position of the glycosidic link that they cleave. While exoglycosidases are specific to monosaccharides in a terminal position, endoglycosidases cleave internal glycosidic bonds of longer chains of glycans.

In the search for early diagnostic markers for neurodegenerative diseases, protein glycosylation has been proposed as a possible biomarker. Changes in glycan degradation might yield a suitable biomarker, as lysosomes are involved in both glycan degradation and parkinsonism (Ohtsubo and Marth, 2006; Lynch-Day et al., 2012). Changes in the CSF glycoprofile are already used as a diagnostic tool in some neurological diseases, including schizophrenia and leukodystrophies (Stanta et al., 2010; Fogli et al., 2012). Comprehensive glycosylation analysis might therefore offer new insights into biomarker discovery, as changes in the glycoprofile could be an indicator of the actual state of the underlying biochemical mechanisms. Therefore, the aim of this study was to explore whether there were any differences in the glycan profile of CSF from patients with parkinsonism, defined as low CSF HVA levels, compared with disease control samples, i.e. non-parkinsonian, defined as normal CSF HVA levels.

7.2. Methods

7.2.1. Secondment

This study took place at the National Institute for Bioprocessing Research & Training (NIBRT, Dublin, Ireland) in early May 2016. NIBRT was founded in 2011 as a collaboration between University College Dublin, Trinity College Dublin, Dublin City University and the Institute of Technology. This centre is notable for its training courses and research in bioprocessing, specialising in the analytical study of biological processes such as post-translational modifications; for example glycosylation. This industrial placement was part of the TINTIN project. The protocol used during the secondment was established at NIBRT by Prof Jonathan Bones and supervised by TINTIN fellow Dr Csaba Varadi.

7.2.2. Sample selection criteria

Residual anonymised CSF samples were evaluated in accordance with Royal College of Pathologists guidelines (2012). Three samples of CSF with evidence of low HVA, i.e. parkinsonism, and ten CSF samples with normal HVA, i.e. disease control, were selected for study of the glycan profile. These were provided by the Neurometabolic unit of the National Hospital (London, UK).

7.2.3. Glycan purification

CSF samples were reduced and alkylated with DTT and iodoacetamide respectively, both prepared at a 10x concentration in 8 M urea. 50 µl CSF were placed on a 10 kDa filter and mixed with DTT at a final concentration of 2 mM and incubated at room temperature in the dark for 30 min. Then, a final concentration of 10 mM iodoacetamide was added to the previous mixture, and incubated at room temperature in the dark for 30 min. The reduced and alkylated sample was washed with water and centrifuged at 12000 rpm for

25 min at room temperature. The flow-through was discarded and 400 µl of 50 mM ammonium hydrogen carbonate added before centrifuging at 12000 rpm for 25 min at room temperature. Ammonium hydrogen carbonate was used as a volatile exchange buffer to eliminate the remaining urea and DTT. At this stage, glycans are still attached to the proteins and retained in the filter. To isolate the *N*-linked glucans from the proteins, samples were digested with 2 U of recombinant Peptide-N-Glycosidase F (PNGase F) and incubated overnight at 37 °C. 400 µl of the sample mix were added to each filter before samples were centrifuged at 12000 rpm for 10 min at room temperature. The flow-through was then dried in a centrifugal vacuum evaporator for around 2 h to prepare the glycans for labelling.

7.2.4. Glycan labelling

The dried glycans were derivatised in order to provide them with adequate charge and fluorescent properties. In this case, sugars were labelled via reductive amination by incubation overnight at 37 °C with 6 µl of 20 mM 9-aminopyrene-1,4,6-trisulfonic acid (APTS) in 15% v/v acetic acid and 2 µl of 1 M sodium cyanoborohydride. The following day, 22 µl of water were added before eliminating the excess dye from labelled glycans by ultra-HPLC. The mobile phase consisted of 50 mM ammonium formate (pH 4.4) and was kept at 40 °C. The flow rate was set at 0.5 ml/min. 30 µl sample mixed with 70 µl of acetonitrile were injected into the system, and only the labelled peak was collected. Samples were then dried in the vacuum centrifuge to prepare samples for analysis of the glycoprofile.

7.2.5. Glycoprofile measurement by capillary electrophoresis

Once the sample is dry, derivatised sugars were suspended in 15 µl of water before being analysed by capillary electrophoresis. The equipment used was a PA800 *Plus*

automated capillary electrophoresis instrument (SCIEX) coupled to a solid-state laser based fluorescent detector (excitation: 488 nm; emission: 520 nm).

Samples were injected at a pressure of 1 psi for 5 sec in a N-CHO coated 50 µm capillary, 50 cm effective length, maintained at 25 °C. The electric field applied was 500 V/cm with the anode at the detection side (reversed polarity). For electropherogram alignment and relative quantification purposes, APTS-labelled maltose was co-injected with each sample as an internal standard. Karat 32 version 7.0 (SCIEX) software was used for data acquisition and analysis.

7.3. Results

The glycoprofile of anonymised CSF was analysed and the resulting electropherograms are shown in ***Figure 7.2***. The samples analysed were divided into two groups: disease control and parkinsonian patients with clear impairment of dopamine metabolism, i.e. low HVA levels. CSF from control patients showed peaks of variable sizes at constant retention times. Samples from parkinsonian patients showed much lower glycan content.

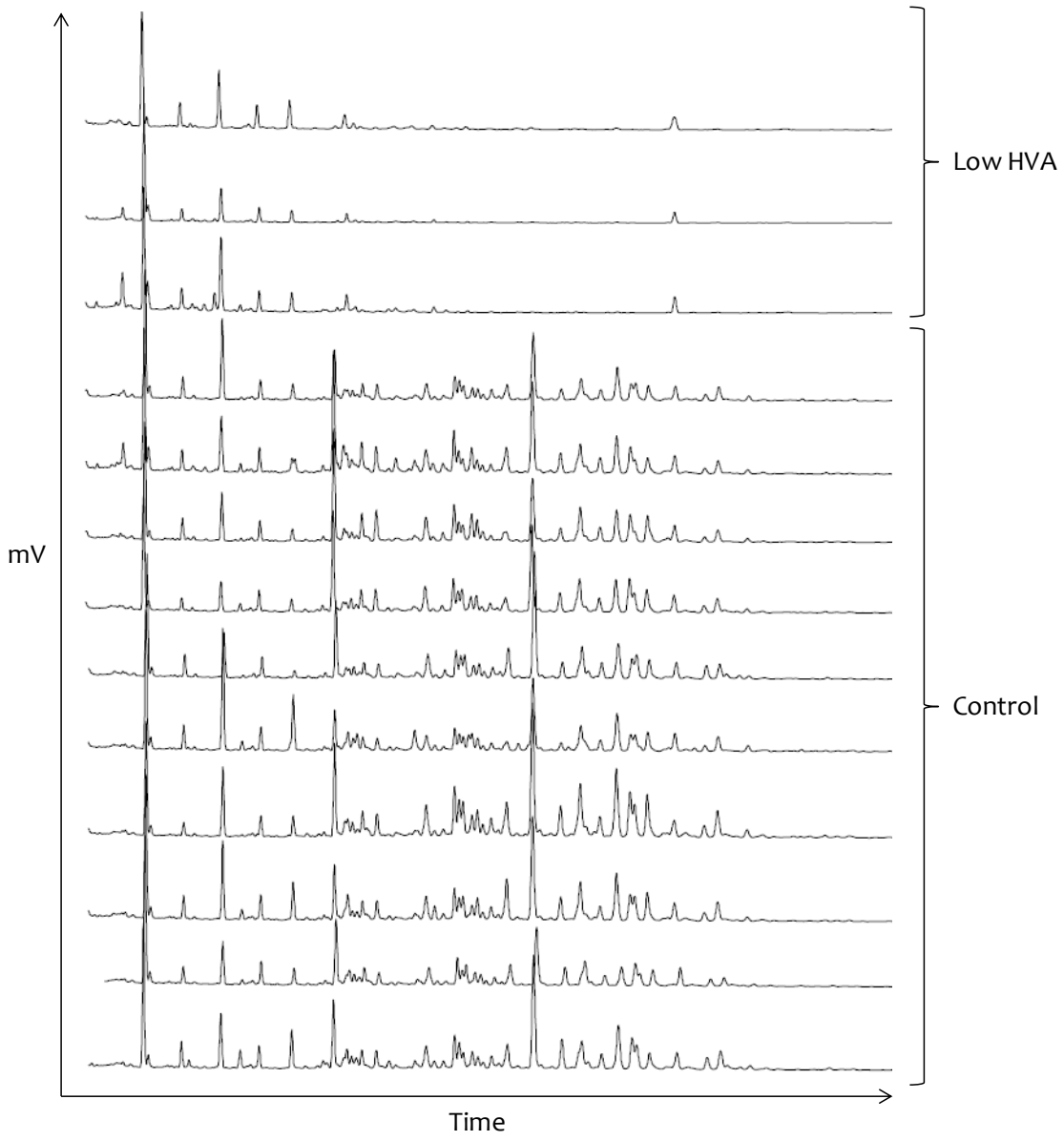

Figure 7.2 Glycoprofiles of CSF from control and low HVA patients.
CSF of patients with low HVA levels (n = 3 experimental replicates) showed a smoother glycoprofile compared to control samples (n = 10 experimental replicates). Time = 20 min.

7.4. Discussion and Further Work

The use of differences in the glycan profile as biomarkers for the diagnosis and progression of neurodegenerative diseases is an expanding field. The heterogeneity of glycans is thought to be due to the expression level and activity of glycosidases and glycosyl-transferases, which can be altered in pathological conditions (Ohtsubo and

Marth, 2006). Although there are currently no reliable early-stage biomarkers for the diagnosis of parkinsonism, two recent publications have reported changes in glycosylation in PD patients. One reported decreased levels of the glycan-isoform of the brain-derived transferrin in the CSF of PD patients (Hoshi et al., 2017), and the other proposed changes on the *N*-glycans of the fragment crystallisable region of the IgG as a biomarker of PD (Russell et al., 2017). Changes in the glycan levels could also be a consequence of altered degradation due to lysosomal dysfunction. In PD, studies have shown that lysosomal enzymes fail to degrade other molecules such as glucosylceramide (Gegg et al., 2012; Migdalska-Richards and Schapira, 2016). As lysosomal dysfunction in the cell model reported in Chapter 4 resulted in low HVA levels, it was hypothesised here that the low HVA levels seen in the CSF could be accompanied by lysosomal dysfunction and changes in glycan degradation. To investigate this, CSF samples from patients with reported low HVA levels were compared to control samples from patients with no evidence of dopamine metabolism impairment. As a precursor, commercial CSF was measured following the protocol described in section 6.2 in order to validate the application of the previously established method to CSF samples (data not shown). Once the suitability of the protocol was confirmed for this sample type, patient samples were measured. Samples of CSF from control patients showed diverse peaks with different heights, probably due to their primary non-parkinsonian pathology. However, the CSF glycoprofile of patients with impaired dopamine metabolism was missing numerous peaks, suggesting that glycan metabolism could be also impaired. Further work needs to be carried out to identify the missing peaks in the low HVA patients. Although, it was not anticipated that the differences in the glycoprofile would be so dramatic when comparing parkinsonian and non-parkinsonian patients, the results obtained in this preliminary study support the reports that proposed glycans as PD biomarkers (Russell et al., 2017; Hoshi et al., 2017).

CHAPTER 8

Discussion

8.1. Discussion

PD is a neurodegenerative disorder caused by a substantial loss of dopaminergic neurons in the substantia nigra. Despite being the second most common neurodegenerative disease, the causes underlying this degeneration are unknown. A multifactorial pathogenesis has been proposed as the cause of PD (Fujita et al., 2014), complicating the development of a cure. Dopamine deficiency in PD is asymptomatic until dopamine levels decrease by 60–80% and dopaminergic denervation occurs (Klebe et al., 2013). At diagnosis, patients usually start treatment with L-DOPA and dopamine catabolism inhibitors. However, the efficacy of this PD gold-standard treatment decreases over time for reasons unknown. It is possible that this loss of efficacy could be due to changes in the dopamine pathway caused by the treatment itself.

Before studying the effect of L-DOPA on dopamine metabolism, dopamine metabolism was characterised in the cell model used, as its suitability as a PD model system has been widely discussed. As shown by immunofluorescence and qRT-PCR ***(4.3.1)***, SH-SY5Y cells do not express TH, the first enzyme of the dopamine pathway under the conditions employed. My findings are in agreement with previous publications (Lopes et al., 2010; Cui et al., 2015; McMillan et al., 2007). However, SH-SY5Y cells do express the other enzymes of the classical pathway as shown by monoamine extracellular detection, western blotting and qRT-PCR. Dopamine production is highly regulated, as its accumulation can lead to the formation of oxidative molecules (reviewed by Munoz et al., 2012). The intermediate product of dopamine oxidation, aminochrome, is highly reactive and can oxidise different proteins; for example, complex I, and modifies the expression of others, such as iron transporters (Aguirre et al., 2012), further enhancing the optimum conditions for dopamine oxidation.

Previous studies have reported that dopamine regulates the activity of enzymes upstream; for example, TH is regulated by the neurotransmitter via negative feedback (reviewed by Daubner et al., 2011). In this study, incubation with L-DOPA and consequent dopamine production had no effect on mRNA expression of dopamine synthesis enzymes. However, incubation with L-DOPA altered dopamine degradation by increasing the activity of MAO-B. Indeed, when considering the HVA:DA and turnover ratios, maintenance of overall dopamine degradation after acute L-DOPA incubation would rely on a higher production of DOPAC by MAO ***(Figure 8.1)***. These results suggest that L-DOPA and/or dopamine could play a role in the regulation of dopamine degradation. In addition, it is hypothesised here that changes in AADC expression and/or activity could also affect the expression of other enzymes downstream in the dopamine pathway. Lovenberg et al. (1962) suggested that an excess of substrate could inhibit AADC activity. In PD, L-DOPA is administered externally, so the treatment itself could reduce the activity of AADC. The effect of loss of AADC activity was examined in the current study by chemical inhibition of AADC activity. This inhibition did not affect MAO-B activity, but did lead to an increase in COMT protein ***(Figure 8.1)***. Although increased COMT expression might result in higher production of 3-OMD, preventing L-DOPA oxidation and its cytosolic accumulation (Munoz et al., 2012), this seems unlikely because of the absence of changes in any of the COMT-dependent metabolites in the current study. Nonetheless, the changes observed in COMT protein expression could be due to an AADC-mediated regulation, as it is known that AADC regulates other proteins of the dopamine pathway (Cartier et al., 2010). In addition, it is possible that the AADC inhibitor used in this study blocked the interaction of AADC with one or more transcription factors, thereby affecting COMT expression.

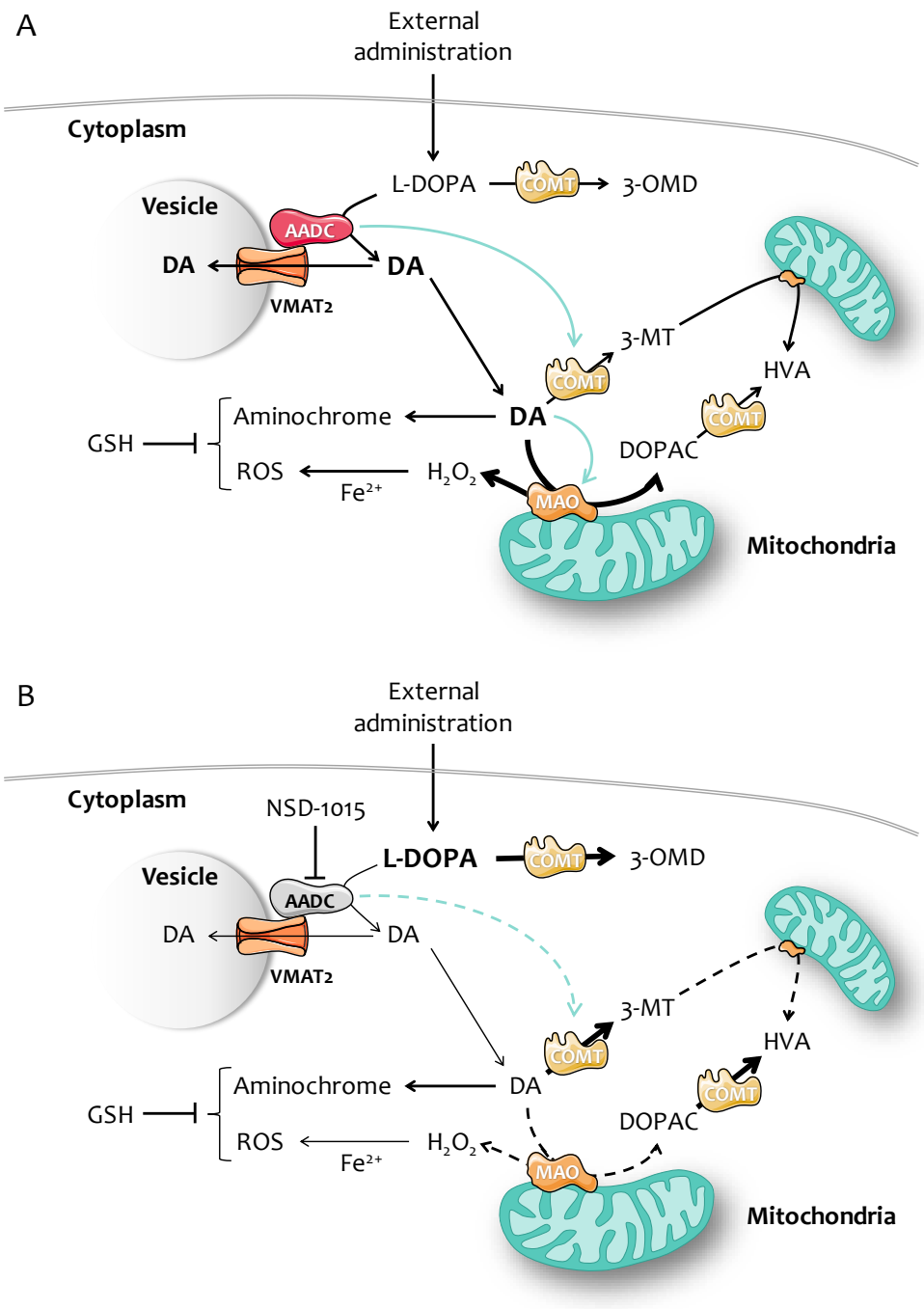

Figure 8.1 Effect of L-DOPA incubation on the dopamine pathway in the proliferative SH-SY5Y cell model.

(A) Treatment with L-DOPA could be modifying dopamine metabolism, as MAO-B activity increased after L-DOPA incubation. (B) Inhibition of AADC by NSD-1015 changed COMT expression, suggesting it might be regulated by AADC. Dashed lines: possibly affected activity/production. Bold lines/molecules: increased production. Thin lines: decreased activity/production. Blue lines: hypothesised regulation of activity/expression.

In summary, considering that L-DOPA incubation and consequent dopamine synthesis increased MAO-B activity, and that MAO-B activity did not increase when AADC was chemically blocked, I hypothesise that dopamine could play a role in up-regulation of MAO-B activity, and therefore its own degradation. In addition, AADC could act as a regulator of COMT activity and/or expression, as inhibition of AADC greatly affected COMT mRNA and protein expression. This interaction would be of great interest in PD treatment, as both AADC and COMT use L-DOPA as a substrate in the synthesis of dopamine and 3-OMD, respectively.

Mitochondria have frequently been associated with neurodegenerative and oxidative diseases. Since complex I deficiency was reported to be present in the brains of PD patients (Schapira et al., 1990), the mitochondrion became the focus of studies aiming to find the trigger for dopaminergic degeneration (reviewed by Abou-Sleiman et al., 2006). In fact, several genes reported to be involved in both idiopathic and familial PD are related to mitochondrial function (see section 1.2.6). In the current study, rotenone was used to inhibit mitochondrial complex I and model the mitochondrial impairment described in PD patients. While mitochondrial impairment alone or in combination with L-DOPA incubation did not affect dopamine synthesis, it did alter neurotransmitter degradation. It is of note that ethanol was used as vehicle for rotenone. The possible side-effects of this carrier have been studied before and, although there is no agreement, several studies have concluded that there is a positive relationship between alcohol intake and increased dopamine release (reviewed by Ma and Zhu, 2014). Here, incubation with ethanol had no effect on MAO-B activity or on the extracellular monoamine concentration. Therefore, it was concluded that any changes observed after rotenone treatment were due to the effect of rotenone itself and not the vehicle.

As GD and mutations in GBA1 are the most common genetic risk factors for PD development, the effect of GBA1 inhibition on dopamine metabolism was also studied. It has been proposed in the literature that lysosomal dysfunction can cause a secondary mitochondrial impairment (de la Mata et al., 2016; Plotegher and Duchen, 2017). In parallel, it has been reported that mitochondrial damage can impair lysosomal function (Demers-Lamarche et al., 2016). Although the mechanisms by which this occurs are not known, impairment of mitophagy has been proposed as a possible mechanism, since glucocerebroside, the substrate for GBA1, is present in the inner and outer mitochondrial membrane (Vielhaber et al., 2001). This would result in accumulation of damaged mitochondria in GD as lysosomes are not capable of maintaining mitochondrial quality control. Here, changes in extracellular levels of dopamine and its metabolites in SH-SY5Y cells with inhibited GBA1 were similar to the changes seen in cells with mitochondrial complex I inhibition. However, it was noted that the overall turnover was significantly higher in the cells with lysosomal impairment compared to the other groups, suggesting that lysosomal dysfunction could indeed cause secondary mitochondrial impairment.

The similar changes in DOPAC and HVA levels in complex I and GBA1 impairment are thought to be due to changes in dopamine degradation. The observed results could be due to increased MAO and/or decreased COMT expression/activity; although this seems unlikely as no changes were observed in levels of 3-OMD, the other COMT-dependent metabolite, when rotenone or CBE treatments were compared to control cells. However, 3-OMD levels were significantly lower after CBE treatment than after rotenone treatment, suggesting further COMT impairment in those cells. Therefore, the increased extracellular concentration of DOPAC in both models lead to the hypothesis of increased MAO expression and/or activity. This was in accordance with increased MAO-B activity in the substantia nigra of PD patients previously reported by Birkmayer et al. (1975). However, that increased activity would be a result of transcriptional or post-translational

modifications as (Molochnikov et al., 2012) concluded that MAO expression does not vary in the substantia nigra of PD patients. Additionally, it is known that MAO-B activity can be affected by environmental factors. For instance, Launay et al. (2009) found that smoking inhibits MAO-B activity and to compensate for this activity loss, synthesis is increased, and the effect maintained even after smoking cessation. The increased MAO-B activity observed in PD patients is possibly an early event in the disease pathology, as it has also been reported as increased in several post-mortem brain regions of elderly and senile humans with no nervous system involvement (Volchegorskii et al., 2001). In addition, MAO-B involvement could be a common event in the development of neurodegenerative diseases as increased activity has been reported in the platelets of AD patients (Bortolato and Shih, 2011). In this study, involvement of increased MAO-B activity was supported by an increased extracellular concentration of DOPAC. However, both MAO-B expression and activity significantly decreased, rather than increased as hypothesised. Although a possible compensatory role for MAO-A has been proposed (Bortolato and Shih, 2011), this isoform did not show an increase in activity or expression.

Therefore, it is hypothesised that lysosomal dysfunction could lead to secondary impairment of mitochondrial complex I (de la Mata et al., 2016; Plotegher and Duchen, 2017) possibly resulting in accumulation of damaged mitochondria and consequently affecting other ATP-dependent processes. Vacuolar adenosine triphosphatase (V-ATPase) activity could be diminished due to impaired ATP production, potentially leading to lower VMAT2 activity and increased dopamine concentration in the cytosol. The decreased activity of complex I could further damage mitochondria because of ROS production and affect other enzymes in mitochondria, such as MAO (Binda et al., 2004), also affecting dopamine metabolism. This is not the first time complex I and dopamine metabolism have been related, as previous publications have reported that incubation of SH-SY5Y cells with extracellular dopamine increased complex I activity (Allen et al., 2013). This is of interest

as antioxidant mechanisms can be also compromised in PD. Indeed, lower GSH levels and decreased SOD activity have been reported in the substantia nigra of PD brains (Sian et al., 1994; Volchegorskii et al., 2001). Whether that decrease is due to lower cell number is unclear. In addition, iron, necessary for the Fenton reaction, and ROS have been described as increased in the substantia nigra of PD patients (Riederer et al., 1989; Dias et al., 2013). Sai et al. (2013) reported an increase in cytosolic calcium after treatment with rotenone, leading to a further increase in oxidative stress. In the current study, no alterations in GSH levels were observed following L-DOPA incubation and/or rotenone or CBE treatment.

Crosstalk between dopamine and serotonin pathways has been previously proposed. Studies in rats with a chemically impaired dopaminergic system reported that these animals could maintain dopamine homeostasis after L-DOPA treatment via the serotoninergic network (reviewed by Stansley and Yamamoto, 2015). Other studies have proposed that these pathways are related by the heteromerisation of enzymes of both pathways, such as TH and TPH (Mockus et al., 1997), and their post-synaptic receptors (Albizu et al., 2011). In this study, SH-SY5Y cells were not only capable of tryptophan uptake (Kollalpitiya and Wimalasena, 2008), but also able to metabolise it through the whole serotonin pathway, as 5-HIAA could be detected in the extracellular media of these cells. It has been reported that chronic L-DOPA treatment can lead to a deficiency in serotonin metabolism and transmission (Stansley and Yamamoto, 2015). However, in this study, incubation with L-DOPA did not affect serotonin homeostasis in the SH-SY5Y cell line as judged by the release of its metabolite. This could be because of the model system used or because the SH-SY5Y cells were incubated with L-DOPA for a relatively short time compared to the incubation time in previous studies (Stansley and Yamamoto, 2015). In this study, extracellular 5-HIAA levels increased when mitochondrial or lysosomal function was disrupted. This increase could be a consequence of changes to MAO activity and/or expression, as suggested for dopamine metabolites. However, the activity and

expression of these isoenzymes did not vary after the treatments, as described in this study. Nevertheless, the increased extracellular levels of 5-HIAA support MAO involvement in PD pathogenesis as, unlike DOPAC, this metabolite is not influenced by COMT. The absence of changes in MAO isozyme suggests that there may be another link between dopamine and serotonin pathways.

Finally, further research into pathological biomarkers in the CSF of patients with impaired dopamine metabolism was carried out at NIBRT (Dublin, Ireland). When glycan content in the CSF of these patients was assessed by capillary electrophoresis, numerous peaks in the electropherogram of patients with low levels of HVA, i.e. parkinsonian, were absent in comparison to controls, i.e. non-parkinsonian. Although this was a preliminary study, these differences could be a result of lysosomal dysfunction, as this organelle, which is responsible for glycan catabolism, has been implicated in PD (Lynch-Day et al., 2012). Although further work is needed to identify and validate the specific glycan changes observed, these results are promising as glycans could potentially be used as pathologic biomarkers.

8.2. Conclusion

The suitability of the SH-SY5Y cell line as an *in vitro* model for the study of PD has been widely discussed. Although no TH was detected, meaning that the cells cannot normally synthesise dopamine (Lopes et al., 2010; Cui et al., 2015; McMillan et al., 2007), these cells can synthesise and metabolise dopamine when L-DOPA is administered exogenously. Dopamine and its metabolites were detected in the media of SH-SY5Y cells along with the serotonin metabolite 5-HIAA. The current treatment of PD is symptomatic and works for a limited time. However, the consequences of this treatment and the reason

for its loss of efficacy are not known. The acute effects of L-DOPA treatment on a parkinsonism cell model were considered here. It is hypothesised that while L-DOPA accumulation decreases MAO-B activity, the activity of this enzyme would increase when dopamine is present, with consequent higher H_2O_2 production ***(Figure 8.2)***. Also, a possible regulatory role is proposed here for AADC, as the expression of COMT appeared to depend on AADC.

Cells with either mitochondrial or lysosomal impairment were shown to be affected in a similar way, i.e. they exhibited altered dopamine degradation. It was hypothesised that the increased levels of DOPAC and 5-HIAA were due to an increased role for MAO in the pathway. However, no changes in MAO activity or expression were observed, raising the possibility of an unknown step common to both pathways. When PD patients are treated, MAO inhibitors are given to increase the half-life of dopamine, and decrease H_2O_2 production simultaneously. However, if mitochondria are impaired, this will result in further accumulation of dopamine in the cytosol, further increasing oxidative stress ***(Figure 8.2)***. In addition, cells with dysfunctional lysosomes could present decreased COMT expression/activity, enhancing the observed DOPAC accumulation and HVA decrease. To determine whether the hypothesised increased oxidative stress decreased antioxidant mechanisms, intracellular GSH levels were quantified but no changes were noted due to L-DOPA incubation or mitochondrial/lysosomal dysfunction. This could be due to the acute treatment times, as oxidative stress may require chronic accumulation of dopamine-derived molecules such as neuromelanin. If these molecules accumulate excessively due to deficient degradation or excessive synthesis, eventually release of bound pro-oxidant species, such as Fe^{2+}, could leave the cell in a critical oxidative state.

In summary, data presented here suggest there is a potential common effect on dopamine and serotonin metabolism caused by two of the events described as key in the

pathogenesis of PD: mitochondrial complex I impairment and lysosomal GBA1 dysfunction. These findings shed some light on dopamine metabolism in a parkinsonian context. However, the question is: does the therapy administered to control symptoms in PD also have detrimental effects on disease progression?

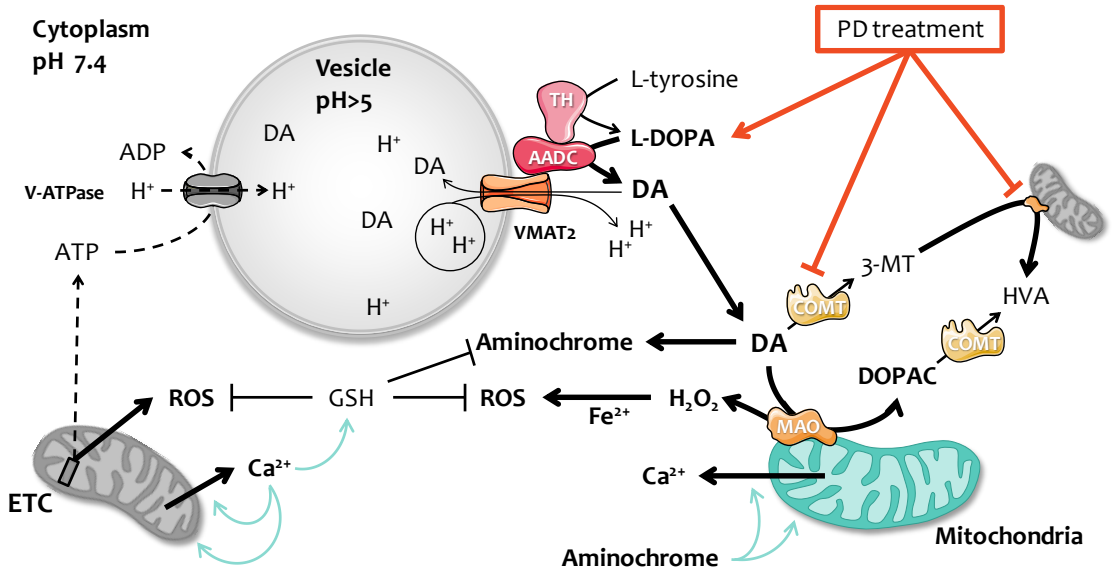

Figure 8.2 Dopamine metabolism in PD.
PD gold-standard treatment consists of L-DOPA administration along with systemic AADC inhibitors and MAO-B and/or COMT inhibitors, to increase the reservoir and half-life of dopamine in the substantia nigra of the patients. Dashed lines: hypothesised affected activity/production. Bold lines/molecules: increased production. Thin lines: hypothesised decreased activity.

8.3. Further Work

To confirm the data and the hypotheses presented in this thesis, and continue the study of dopamine and serotonin metabolisms in PD, the following experiments may be considered:

- To further explore the interplay between dopamine and serotonin by further developing the HPLC method to analyse concomitantly other molecules of the serotonin pathway, such as 5-hydroxytryptophan and serotonin itself.

Additionally, it would be interesting to analyse the intracellular monoamine levels to study whether the extracellular changes reflect intracellular changes.

- To further study the effect of L-DOPA and dopamine on the catabolic enzymes of the pathway, as well as the relationship between enzymes, in order to ascertain whether there are other unknown regulatory mechanisms. For instance, whether COMT is regulated via AADC and whether decreased COMT protein level results in decreased enzymatic activity.

- To differentiate the SH-SY5Y cells to study the release of dopamine and serotonin metabolites, and expression and activity of the enzymes involved in the pathway, as differentiated cells showed different levels of monoamine release to that seen in proliferative SH-SY5Y cells. To avoid controversy regarding the phenotype of the cell model used, dopaminergic neurons derived from iPS cells should be eventually considered.

- In addition to the analysis of the individual effect of either mitochondrial impairment or lysosomal dysfunction on monoamine metabolism, the interaction between these organelles at a functional level should be assessed as both are involved in PD neurodegeneration and affected by dopamine oxidation, so there may be cumulative effects (Burbulla et al., 2017).

- Identify the glycans that are deficient in the CSF of patients with low HVA, as they could be used as pathological biomarkers. Additionally, exploring the interplay between glycan degradation and lysosomal dysfunction in a parkinsonian context would be interesting, as the involvement of lysosomes could be key to the differences observed between the glycoprofiles of the CSF of disease control individuals and patients with parkinsonism.

Annex

I. Published journal articles related to this thesis

de la Fuente, C; Burke, D. G; Eaton, S; & Heales, S. J. (2017). *Inhibition of neuronal mitochondrial complex I or lysosomal glucocerebrosidase is associated with increased dopamine and serotonin turnover.* Neurochem Int. doi:10.1016 j.neuint.2017.02.013

Barral, S; Erdem, F; Wallings, R; **de la Fuente Barrigon, C**; Lignani, G; Privolizzi, R; Alrashidi, H; Heasman, S; Ngoh, A; Ng, J; Meyer, E; Waddington, S; Schorge, S; Cowley, S. A; Sucic, S; Freissmuth, M; Heales, S. J; Wade-Martins, R; Bencze, M; & Kurian, M. A. *An iPSC-Derived Dopaminergic Model of Genetic Parkinsonism Reveals Key Mediators of Neurodegeneration and Precision Therapies.* Submitted to Nature Medicine.

II. Oral communications at international conferences

Inhibition of Lysosomal Glucocerebrosidase is Associated with Altered Dopamine Turnover. A Mechanistic Insight into the Link between Gaucher and Parkinson's disease, **de la Fuente Barrigon, C**; Eaton, S; Burke, D; Heales, S. Presented at the Lysosomal Diseases Research & Conference, WORLDSymposium 2018, San Diego, USA, by Prof Heales.

Dopamine metabolism analysis in different cellular models of Parkinson's disease, **de la Fuente Barrigon, C**; Eaton, S; Heales, S. Presented at Mediterranean Neuroscience Society (MNS), St Julian's, Malta 2017.

Gaucher and Parkinson's Disease. Cell models and disease modifying factors. Burke, D; **de la Fuente Barrigon, C**; Garcia-Gomez, M; Heales, S. Presented at the European Working Group on Gaucher disease (EWGGD) 2016, Zaragoza, Spain, by Dr Burke.

III. Posters presented at international conferences

Modelling Childhood Parkinsonism with Patient-Derived Induced Pluripotent Stem Cells. Barral, S; Erdem, F; Lignani, G; **de la Fuente Barrigon, C;** Bencze, M; Heasman, S; Ng, J; Meyer, E; Cowley, S.A; Wade-Martins, R; Heales, S; Kurian, M. Presented at the International Society for Stem Cell Research (ISSCR) 2017, Boston, USA, by Dr Barral.

Dopamine and serotonin turnover in neuronal cell models of mitochondrial complex I deficiency and Gaucher disease. **de la Fuente Barrigon, C;** Garcia-Gomez, M; Burke, D; Eaton, S; Heales, S. Presented at the Society for the Study of Inborn Errors of Metabolism (SSIEM) 2016, Rome, Italy.

The measurement of dopamine metabolites in model systems. **de la Fuente Barrigon, C;** Eaton, S; Heales, S. Presented at the Federation of European Neuroscience Societies (FENS) 2016, Copenhagen, Denmark.

Gaucher and Parkinson's Disease. Cell models and disease modifying factors. Burke, D; **de la Fuente Barrigon, C;** Garcia-Gomez, M; Heales, S. Presented at the European Working Group on Gaucher disease (EWGGD) 2016, Zaragoza, Spain, by Dr Burke.

Studying the link between Gaucher and Parkinson's Disease. Cell models and disease-modifying factors. Garcia-Gomez, M; Burke, D; **de la Fuente Barrigon, C;** Heales, S. Presented at the *Chemical and Biological Therapeutics Approaches to Neurological Disorders III* (2016) hosted by the Royal Society of Chemistry, London, UK.

References

Abou-Sleiman, P. M., Muqit, M. M. & Wood, N. W. 2006. Expanding Insights Of Mitochondrial Dysfunction In Parkinson's Disease. *Nat Rev Neurosci,* 7, 207-19.

Aguirre, P., Urrutia, P., Tapia, V., Villa, M., Paris, I., Segura-Aguilar, J. & Nunez, M. T. 2012. The Dopamine Metabolite Aminochrome Inhibits Mitochondrial Complex I And Modifies The Expression Of Iron Transporters Dmt1 And Fpn1. *Biometals,* 25, 795-803.

Akao, Y., Maruyama, W., Yi, H., Shamoto-Nagai, M., Youdim, M. B. & Naoi, M. 2002. An Anti-Parkinson's Disease Drug, N-Propargyl-1(R)-Aminoindan (Rasagiline), Enhances Expression Of Anti-Apoptotic Bcl-2 In Human Dopaminergic Sh-Sy5y Cells. *Neurosci Lett,* 326, 105-8.

Alberio, T., Bondi, H., Colombo, F., Alloggio, I., Pieroni, L., Urbani, A. & Fasano, M. 2014. Mitochondrial Proteomics Investigation Of A Cellular Model Of Impaired Dopamine Homeostasis, An Early Step In Parkinson's Disease Pathogenesis. *Mol Biosyst,* 10, 1332-44.

Albizu, L., Holloway, T., Gonzalez-Maeso, J. & Sealfon, S. C. 2011. Functional Crosstalk And Heteromerization Of Serotonin 5-Ht2a And Dopamine D2 Receptors. *Neuropharmacology,* 61, 770-7.

Allen, G. F., Ullah, Y., Hargreaves, I. P., Land, J. M. & Heales, S. J. 2013. Dopamine But Not L-Dopa Stimulates Neural Glutathione Metabolism. Potential Implications For Parkinson's And Other Dopamine Deficiency States. *Neurochem Int,* 62, 684-94.

Alter, S. P., Lenzi, G. M., Bernstein, A. I. & Miller, G. W. 2013. Vesicular Integrity In Parkinson's Disease. *Curr Neurol Neurosci Rep,* 13, 362.

Anderson, M. C., Hasan, F., Mccrodden, J. M. & Tipton, K. F. 1993. Monoamine Oxidase Inhibitors And The Cheese Effect. *Neurochem Res,* 18, 1145-9.

Aylett, S. B., Neergheen, V., Hargreaves, I. P., Eaton, S., Land, J. M., Rahman, S. & Heales, S. J. 2013. Levels Of 5-Methyltetrahydrofolate And Ascorbic Acid In Cerebrospinal Fluid Are Correlated: Implications For The Accelerated Degradation Of Folate By Reactive Oxygen Species. *Neurochem Int,* 63, 750-5.

Azevedo, F. A., Carvalho, L. R., Grinberg, L. T., Farfel, J. M., Ferretti, R. E., Leite, R. E., Jacob Filho, W., Lent, R. & Herculano-Houzel, S. 2009. Equal Numbers Of Neuronal And Nonneuronal Cells Make The Human Brain An Isometrically Scaled-Up Primate Brain. *J Comp Neurol,* 513, 532-41.

Bae, E. J., Yang, N. Y., Lee, C., Lee, H. J., Kim, S., Sardi, S. P. & Lee, S. J. 2015. Loss Of Glucocerebrosidase 1 Activity Causes Lysosomal Dysfunction And Alpha-Synuclein Aggregation. *Exp Mol Med,* 47, E153.

Balasooriya, I. S. & Wimalasena, K. 2007. Are Sh-Sy5y And Mn9d Cell Lines Truly Dopaminergic? *Faseb J,* 21.

Barker, J. E., Bolanos, J. P., Land, J. M., Clark, J. B. & Heales, S. J. 1996. Glutathione Protects Astrocytes From Peroxynitrite-Mediated Mitochondrial Damage: Implications For Neuronal/Astrocytic Trafficking And Neurodegeneration. *Dev Neurosci,* 18**,** 391-6.

Bendor, J. T., Logan, T. P. & Edwards, R. H. 2013. The Function Of Alpha-Synuclein. *Neuron,* 79**,** 1044-66.

Berry, M. D., Juorio, A. V., Li, X. M. & Boulton, A. A. 1996. Aromatic L-Amino Acid Decarboxylase: A Neglected And Misunderstood Enzyme. *Neurochem Res,* 21**,** 1075-87.

Betarbet, R., Sherer, T. B. & Greenamyre, J. T. 2005. Ubiquitin-Proteasome System And Parkinson's Diseases. *Exp Neurol,* 191 Suppl 1**,** S17-27.

Betarbet, R., Sherer, T. B., Mackenzie, G., Garcia-Osuna, M., Panov, A. V. & Greenamyre, J. T. 2000. Chronic Systemic Pesticide Exposure Reproduces Features Of Parkinson's Disease. *Nat Neurosci,* 3**,** 1301-6.

Beyer, K. 2007. Mechanistic Aspects Of Parkinson's Disease: Alpha-Synuclein And The Biomembrane. *Cell Biochem Biophys,* 47**,** 285-99.

Bialecka, M., Klodowska-Duda, G., Honczarenko, K., Gawronska-Szklarz, B., Opala, G., Safranow, K. & Drozdzik, M. 2007. Polymorphisms Of Catechol-O-Methyltransferase (Comt), Monoamine Oxidase B (Maob), N-Acetyltransferase 2 (Nat2) And Cytochrome P450 2d6 (Cyp2d6) Gene In Patients With Early Onset Of Parkinson's Disease. *Parkinsonism Relat Disord,* 13**,** 224-9.

Biedler, J. L., Roffler-Tarlov, S., Schachner, M. & Freedman, L. S. 1978. Multiple Neurotransmitter Synthesis By Human Neuroblastoma Cell Lines And Clones. *Cancer Res,* 38**,** 3751-7.

Binda, C., Hubalek, F., Li, M., Edmondson, D. E. & Mattevi, A. 2004. Crystal Structure Of Human Monoamine Oxidase B, A Drug Target Enzyme Monotopically Inserted Into The Mitochondrial Outer Membrane. *Febs Letters,* 564**,** 225-228.

Birkmayer, W., Riederer, P., Youdim, M. B. & Linauer, W. 1975. The Potentiation Of The Anti Akinetic Effect After L-Dopa Treatment By An Inhibitor Of Mao-B, Deprenil. *J Neural Transm,* 36**,** 303-26.

Blesa, J. & Przedborski, S. 2014. Parkinson's Disease: Animal Models And Dopaminergic Cell Vulnerability. *Front Neuroanat,* 8**,** 155.

Blesa, J., Trigo-Damas, I., Quiroga-Varela, A. & Jackson-Lewis, V. R. 2015. Oxidative Stress And Parkinson's Disease. *Front Neuroanat,* 9**,** 91.

Bolanos, J. P., Almeida, A., Stewart, V., Peuchen, S., Land, J. M., Clark, J. B. & Heales, S. J. 1997. Nitric Oxide-Mediated Mitochondrial Damage In The Brain: Mechanisms And Implications For Neurodegenerative Diseases. *J Neurochem,* 68**,** 2227-40.

Bolanos, J. P. & Heales, S. J. 2010. Persistent Mitochondrial Damage By Nitric Oxide And Its Derivatives: Neuropathological Implications. *Front Neuroenergetics,* 2, 1.

Bolanos, J. P., Heales, S. J., Land, J. M. & Clark, J. B. 1995. Effect Of Peroxynitrite On The Mitochondrial Respiratory Chain: Differential Susceptibility Of Neurones And Astrocytes In Primary Cultures. *Journal Of Neurochemistry,* 64, 8.

Bolanos, J. P., Peuchen, S., Heales, S. J., Land, J. M. & Clark, J. B. 1994. Nitric Oxide-Mediated Inhibition Of The Mitochondrial Respiratory Chain In Cultured Astrocytes. *J Neurochem,* 63, 910-6.

Bortolato, M. & Shih, J. C. 2011. Behavioral Outcomes Of Monoamine Oxidase Deficiency: Preclinical And Clinical Evidence. *Int Rev Neurobiol,* 100, 13-42.

Bradford, M. M. 1976. A Rapid And Sensitive Method For The Quantitation Of Microgram Quantities Of Protein Utilizing The Principle Of Protein-Dye Binding. *Anal Biochem,* 72, 248-54.

Brand, M. P., Heales, S. J., Land, J. M. & Clark, J. B. 1995. Tetrahydrobiopterin Deficiency And Brain Nitric Oxide Synthase In The Hph1 Mouse. *J Inherit Metab Dis,* 18, 33-9.

Brand, M. P., Hyland, K., Engle, T., Smith, I. & Heales, S. J. 1996. Neurochemical Effects Following Peripheral Administration Of Tetrahydropterin Derivatives To The Hph-1 Mouse. *J Neurochem,* 66, 1150-6.

Bromek, E., Haduch, A., Golembiowska, K. & Daniel, W. A. 2011. Cytochrome P450 Mediates Dopamine Formation In The Brain In Vivo. *J Neurochem,* 118, 806-15.

Burbulla, L. F., Song, P., Mazzulli, J. R., Zampese, E., Wong, Y. C., Jeon, S., Santos, D. P., Blanz, J., Obermaier, C. D., Strojny, C., Savas, J. N., Kiskinis, E., Zhuang, X., Kruger, R., Surmeier, D. J. & Krainc, D. 2017. Dopamine Oxidation Mediates Mitochondrial And Lysosomal Dysfunction In Parkinson's Disease. *Science*.

Burlina, A. B., Celato, A., Polo, G., Edini, C. & Burlina, A. P. 2017. The Utility Of Csf For The Diagnosis Of Primary And Secondary Monoamine Neurotransmitter Deficiencies. *Ejifcc,* 28, 64-76.

Butler, B., Saha, K., Rana, T., Becker, J. P., Sambo, D., Davari, P., Goodwin, J. S. & Khoshbouei, H. 2015. Dopamine Transporter Activity Is Modulated By Alpha-Synuclein. *J Biol Chem,* 290, 29542-54.

Cartier, E. A., Parra, L. A., Baust, T. B., Quiroz, M., Salazar, G., Faundez, V., Egana, L. & Torres, G. E. 2010. A Biochemical And Functional Protein Complex Involving Dopamine Synthesis And Transport Into Synaptic Vesicles. *J Biol Chem,* 285, 1957-66.

Chaudhry, F. A., Edwards, R. H. & Fonnum, F. 2008. Vesicular Neurotransmitter Transporters As Targets For Endogenous And Exogenous Toxic Substances. *Annu Rev Pharmacol Toxicol,* 48, 277-301.

Chen, J., Lipska, B. K., Halim, N., Ma, Q. D., Matsumoto, M., Melhem, S., Kolachana, B. S., Hyde, T. M., Herman, M. M., Apud, J., Egan, M. F., Kleinman, J. E. & Weinberger, D. R. 2004. Functional Analysis Of Genetic Variation In Catechol-O-Methyltransferase (Comt): Effects On Mrna, Protein, And Enzyme Activity In Postmortem Human Brain. *Am J Hum Genet,* 75**,** 807-21.

Chen, Y. A. & Scheller, R. H. 2001. Snare-Mediated Membrane Fusion. *Nat Rev Mol Cell Biol,* 2**,** 98-106.

Choi, W. S., Kim, H. W. & Xia, Z. 2015. Jnk Inhibition Of Vmat2 Contributes To Rotenone-Induced Oxidative Stress And Dopamine Neuron Death. *Toxicology,* 328**,** 75-81.

Choi, W. S., Palmiter, R. D. & Xia, Z. 2011. Loss Of Mitochondrial Complex I Activity Potentiates Dopamine Neuron Death Induced By Microtubule Dysfunction In A Parkinson's Disease Model. *J Cell Biol,* 192**,** 873-82.

Cleeter, M. W., Chau, K. Y., Gluck, C., Mehta, A., Hughes, D. A., Duchen, M., Wood, N. W., Hardy, J., Mark Cooper, J. & Schapira, A. H. 2013. Glucocerebrosidase Inhibition Causes Mitochondrial Dysfunction And Free Radical Damage. *Neurochem Int,* 62**,** 1-7.

Compton, S. J. & Jones, C. G. 1985. Mechanism Of Dye Response And Interference In The Bradford Protein Assay. *Anal Biochem,* 151**,** 369-74.

Connolly, B. S. & Lang, A. E. 2014. Pharmacological Treatment Of Parkinson Disease: A Review. *Jama,* 311**,** 1670-83.

Conway, K. A., Rochet, J. C., Bieganski, R. M. & Lansbury, P. T., Jr. 2001. Kinetic Stabilization Of The Alpha-Synuclein Protofibril By A Dopamine-Alpha-Synuclein Adduct. *Science,* 294**,** 1346-9.

Coskun, O. 2016. Separation Techniques: Chromatography. *North Clin Istanb,* 3**,** 156-160.

Costa, P., Checkoway, H., Levy, D., Smith-Weller, T., Franklin, G. M., Swanson, P. D. & Costa, L. G. 1997. Association Of A Polymorphism In Intron 13 Of The Monoamine Oxidase B Gene With Parkinson Disease. *Am J Med Genet,* 74**,** 154-6.

Coune, P. G., Schneider, B. L. & Aebischer, P. 2012. Parkinson's Disease: Gene Therapies. *Cold Spring Harb Perspect Med,* 2**,** A009431.

Cui, X., Pertile, R., Liu, P. & Eyles, D. W. 2015. Vitamin D Regulates Tyrosine Hydroxylase Expression: N-Cadherin A Possible Mediator. *Neuroscience,* 304**,** 90-100.

Cumming, P., Kuwabara, H., Ase, A. & Gjedde, A. 1995. Regulation Of Dopa Decarboxylase Activity In Brain Of Living Rat. *J Neurochem,* 65**,** 1381-90.

Daubner, S. C., Le, T. & Wang, S. 2011. Tyrosine Hydroxylase And Regulation Of Dopamine Synthesis. *Arch Biochem Biophys,* 508**,** 1-12.

Dauer, W. & Przedborski, S. 2003. Parkinson's Disease: Mechanisms And Models. *Neuron,* 39**,** 889-909.

Davey, G. P., Peuchen, S. & Clark, J. B. 1998. Energy Thresholds In Brain Mitochondria. Potential Involvement In Neurodegeneration. *J Biol Chem,* 273, 12753-7.

Davis, G. C., Williams, A. C., Markey, S. P., Ebert, M. H., Caine, E. D., Reichert, C. M. & Kopin, I. J. 1979. Chronic Parkinsonism Secondary To Intravenous Injection Of Meperidine Analogues. *Psychiatry Res,* 1, 249-54.

Dawson, T. M. & Dawson, V. L. 2010. The Role Of Parkin In Familial And Sporadic Parkinson's Disease. *Mov Disord,* 25 Suppl 1, S32-9.

De La Mata, M., Cotan, D., Villanueva-Paz, M., De Lavera, I., Alvarez-Cordoba, M., Luzon-Hidalgo, R., Suarez-Rivero, J. M., Tiscornia, G. & Oropesa-Avila, M. 2016. Mitochondrial Dysfunction In Lysosomal Storage Disorders. *Diseases,* 4.

Dehay, B., Martinez-Vicente, M., Ramirez, A., Perier, C., Klein, C., Vila, M. & Bezard, E. 2012. Lysosomal Dysfunction In Parkinson Disease: Atp13a2 Gets Into The Groove. *Autophagy,* 8, 1389-91.

Demers-Lamarche, J., Guillebaud, G., Tlili, M., Todkar, K., Belanger, N., Grondin, M., Nguyen, A. P., Michel, J. & Germain, M. 2016. Loss Of Mitochondrial Function Impairs Lysosomes. *J Biol Chem,* 291, 10263-76.

Dias, V., Junn, E. & Mouradian, M. M. 2013. The Role Of Oxidative Stress In Parkinson's Disease. *J Parkinsons Dis,* 3, 461-91.

Dolan, J. W. 2008. Ion Pairing — Blessing Or Curse? *Lcgc Europe,* 21.

Dorszewska, J., Prendecki, M., Lianeri, M. & Kozubski, W. 2014. Molecular Effects Of L-Dopa Therapy In Parkinson's Disease. *Curr Genomics,* 15, 11-7.

Double, K. L., Ben-Shachar, D., Youdim, M. B., Zecca, L., Riederer, P. & Gerlach, M. 2002. Influence Of Neuromelanin On Oxidative Pathways Within The Human Substantia Nigra. *Neurotoxicol Teratol,* 24, 621-8.

Enquist, I. B., Lo Bianco, C., Ooka, A., Nilsson, E., Mansson, J. E., Ehinger, M., Richter, J., Brady, R. O., Kirik, D. & Karlsson, S. 2007. Murine Models Of Acute Neuronopathic Gaucher Disease. *Proc Natl Acad Sci U S A,* 104, 17483-8.

Eriksen, J., Jorgensen, T. N. & Gether, U. 2010. Regulation Of Dopamine Transporter Function By Protein-Protein Interactions: New Discoveries And Methodological Challenges. *J Neurochem,* 113, 27-41.

Espinoza, S., Manago, F., Leo, D., Sotnikova, T. D. & Gainetdinov, R. R. 2012. Role Of Catechol-O-Methyltransferase (Comt)-Dependent Processes In Parkinson's Disease And L-Dopa Treatment. *Cns Neurol Disord Drug Targets,* 11, 251-63.

Farfel-Becker, T., Vitner, E. B. & Futerman, A. H. 2011. Animal Models For Gaucher Disease Research. *Dis Model Mech,* 4, 746-52.

Finch, C. C., Ho, S. L., Williams, A. C. & Billett, E. E. 1995. Platelet Mao Activities And Mao-B Protein Concentrations In Parkinson's Disease And Controls. *Prog Brain Res,* 106**,** 85-90.

Fitzgerald, P. & Dinan, T. G. 2008. Prolactin And Dopamine: What Is The Connection? A Review Article. *J Psychopharmacol,* 22**,** 12-9.

Flatmark, T. 2000. Catecholamine Biosynthesis And Physiological Regulation In Neuroendocrine Cells. *Acta Physiol Scand,* 168**,** 1-17.

Fogli, A., Merle, C., Roussel, V., Schiffmann, R., Ughetto, S., Theisen, M. & Boespflug-Tanguy, O. 2012. Csf N-Glycan Profiles To Investigate Biomarkers In Brain Developmental Disorders: Application To Leukodystrophies Related To Eif2b Mutations. *Plos One,* 7**,** E42688.

Freeze, H. H., Kinoshita, T. & Schnaar, R. L. 2015. Genetic Disorders Of Glycan Degradation. *In:* Rd, Varki, A., Cummings, R. D., Esko, J. D., Stanley, P., Hart, G. W., Aebi, M., Darvill, A. G., Kinoshita, T., Packer, N. H., Prestegard, J. H., Schnaar, R. L. & Seeberger, P. H. (Eds.) *Essentials Of Glycobiology.* Cold Spring Harbor (Ny).

Fujita, K. A., Ostaszewski, M., Matsuoka, Y., Ghosh, S., Glaab, E., Trefois, C., Crespo, I., Perumal, T. M., Jurkowski, W., Antony, P. M., Diederich, N., Buttini, M., Kodama, A., Satagopam, V. P., Eifes, S., Del Sol, A., Schneider, R., Kitano, H. & Balling, R. 2014. Integrating Pathways Of Parkinson's Disease In A Molecular Interaction Map. *Mol Neurobiol,* 49**,** 88-102.

Furukawa, Y., Lang, A. E., Trugman, J. M., Bird, T. D., Hunter, A., Sadeh, M., Tagawa, T., St George-Hyslop, P. H., Guttman, M., Morris, L. W., Hornykiewicz, O., Shimadzu, M. & Kish, S. J. 1998. Gender-Related Penetrance And De Novo Gtp-Cyclohydrolase I Gene Mutations In Dopa-Responsive Dystonia. *Neurology,* 50**,** 1015-20.

Gegg, M. E., Beltran, B., Salas-Pino, S., Bolanos, J. P., Clark, J. B., Moncada, S. & Heales, S. J. R. 2004. Differential Effect Of Nitric Oxide On Glutathione Metabolism And Mitochondrial Function In Astrocytes And Neurones: Implications For Neuroprotection/Neurodegeneration? *Journal Of Neurochemistry,* 86**,** 228-237.

Gegg, M. E., Burke, D., Heales, S. J., Cooper, J. M., Hardy, J., Wood, N. W. & Schapira, A. H. 2012. Glucocerebrosidase Deficiency In Substantia Nigra Of Parkinson Disease Brains. *Ann Neurol,* 72**,** 455-63.

Gerlach, M., Double, K. L., Ben-Shachar, D., Zecca, L., Youdim, M. B. H. & Riederer, P. 2003. Neuromelanin And Its Interaction With Iron As A Potential Risk Factor For Dopaminergic Neurodegeneration Underlying Parkinson's Disease. *Neurotoxicity Research,* 5**,** 35-43.

Giros, B., Jaber, M., Jones, S. R., Wightman, R. M. & Caron, M. G. 1996. Hyperlocomotion And Indifference To Cocaine And Amphetamine In Mice Lacking The Dopamine Transporter. *Nature,* 379**,** 606-12.

Gleichmann, M. & Mattson, M. P. 2011. Neuronal Calcium Homeostasis And Dysregulation. *Antioxid Redox Signal,* 14**,** 1261-73.

Glick, D., Barth, S. & Macleod, K. F. 2010. Autophagy: Cellular And Molecular Mechanisms. *J Pathol,* 221, 3-12.

Gopisankar, M. G. 2017. Cyp2d6 Pharmacogenomics. *The Egyptian Journal Of Medical Human Genetics,* 18, 5.

Graumann, R., Paris, I., Martinez-Alvarado, P., Rumanque, P., Perez-Pastene, C., Cardenas, S. P., Marin, P., Diaz-Grez, F., Caviedes, R., Caviedes, P. & Segura-Aguilar, J. 2002. Oxidation Of Dopamine To Aminochrome As A Mechanism For Neurodegeneration Of Dopaminergic Systems In Parkinson's Disease. Possible Neuroprotective Role Of Dt-Diaphorase. *Pol J Pharmacol,* 54, 573-9.

Grosch, J., Winkler, J. & Kohl, Z. 2016. Early Degeneration Of Both Dopaminergic And Serotonergic Axons - A Common Mechanism In Parkinson's Disease. *Front Cell Neurosci,* 10, 293.

Guillot, T. S. & Miller, G. W. 2009. Protective Actions Of The Vesicular Monoamine Transporter 2 (Vmat2) In Monoaminergic Neurons. *Mol Neurobiol,* 39, 149-70.

Hadjiconstantinou, M. & Neff, N. H. 2008. Enhancing Aromatic L-Amino Acid Decarboxylase Activity: Implications For L-Dopa Treatment In Parkinson's Disease. *Cns Neurosci Ther,* 14, 340-51.

Halliday, G. M., Blumbergs, P. C., Cotton, R. G., Blessing, W. W. & Geffen, L. B. 1990. Loss Of Brainstem Serotonin- And Substance P-Containing Neurons In Parkinson's Disease. *Brain Res,* 510, 104-7.

Hauser, D. N. & Hastings, T. G. 2013. Mitochondrial Dysfunction And Oxidative Stress In Parkinson's Disease And Monogenic Parkinsonism. *Neurobiol Dis,* 51, 35-42.

Heales, S. J., Barker, J. E., Stewart, V. C., Brand, M. P., Hargreaves, I. P., Foppa, P., Land, J. M., Clark, J. B. & Bolanos, J. P. 1997. Nitric Oxide, Energy Metabolism And Neurological Disease. *Biochem Soc Trans,* 25, 939-43.

Heales, S. J. & Bolanos, J. P. 2001. Impairment Of Brain Mitochondrial Function By Reactive Nitrogen Species: The Role Of Gluathione In Dictating Susceptibility. *Neurochemistry International,* 40, 469-474.

Heales, S. J., Bolanos, J. P. & Clark, J. B. 1995. Glutathione Depletion Is Accompanied By Increased Neuronal Nitric Oxide Synthase Activity. *Neurochem Research,* 21, 5.

Heales, S. J., Bolanos, J. P., Land, J. M. & Clark, J. B. 1994. Trolox Protects Mitochondrial Complex Iv From Nitric Oxide-Mediated Damage In Astrocytes. *Brain Res,* 668, 243-5.

Heales, S. J., Bolanos, J. P., Stewart, V. C., Brookes, P. S., Land, J. M. & Clark, J. B. 1999. Nitric Oxide, Mitochondria And Neurological Disease. *Biochim Biophys Acta,* 1410, 215-28.

Hernan, M. A., Checkoway, H., O'brien, R., Costa-Mallen, P., De Vivo, I., Colditz, G. A., Hunter, D. J., Kelsey, K. T. & Ascherio, A. 2002. Maob Intron 13 And Comt Codon

158 Polymorphisms, Cigarette Smoking, And The Risk Of Pd. *Neurology,* 58**,** 1381-7.

Hiroi, T., Imaoka, S. & Funae, Y. 1998. Dopamine Formation From Tyramine By Cyp2d6. *Biochem Biophys Res Commun,* 249**,** 838-43.

Hirst, J. & Roessler, M. M. 2016. Energy Conversion, Redox Catalysis And Generation Of Reactive Oxygen Species By Respiratory Complex I. *Biochim Biophys Acta,* 1857**,** 872-83.

Ho, S. L., Kapadi, A. L., Ramsden, D. B. & Williams, A. C. 1995. An Allelic Association Study Of Monoamine Oxidase B In Parkinson's Disease. *Ann Neurol,* 37**,** 403-5.

Horváth, C. 1988. *High-Performance Liquid Chromatography,* San Diego,Ca, Academic Press.

Hoshi, K., Matsumoto, Y., Ito, H., Saito, K., Honda, T., Yamaguchi, Y. & Hashimoto, Y. 2017. A Unique Glycan-Isoform Of Transferrin In Cerebrospinal Fluid: A Potential Diagnostic Marker For Neurological Diseases. *Biochim Biophys Acta,* 1861**,** 2473-2478.

Howard, G. A. & Martin, A. J. 1950. The Separation Of The C12-C18 Fatty Acids By Reversed-Phase Partition Chromatography. *Biochem J,* 46**,** 532-8.

Hummerich, R., Reischl, G., Ehrlichmann, W., Machulla, H. J., Heinz, A. & Schloss, P. 2004. Dasb -In Vitro Binding Characteristics On Human Recombinant Monoamine Transporters With Regard To Its Potential As Positron Emission Tomography (Pet) Tracer. *J Neurochem,* 90**,** 1218-26.

Hwang, H., Zhang, J., Chung, K. A., Leverenz, J. B., Zabetian, C. P., Peskind, E. R., Jankovic, J., Su, Z., Hancock, A. M., Pan, C., Montine, T. J., Pan, S., Nutt, J., Albin, R., Gearing, M., Beyer, R. P., Shi, M. & Zhang, J. 2010. Glycoproteomics In Neurodegenerative Diseases. *Mass Spectrom Rev,* 29**,** 79-125.

Hyland, K., Fryburg, J. S., Wilson, W. G., Bebin, E. M., Arnold, L. A., Gunasekera, R. S., Jacobson, R. D., Rost-Ruffner, E. & Trugman, J. M. 1997. Oral Phenylalanine Loading In Dopa-Responsive Dystonia: A Possible Diagnostic Test. *Neurology,* 48**,** 1290-7.

Iversen, S. D. & Iversen, L. L. 2007. Dopamine: 50 Years In Perspective. *Trends Neurosci,* 30**,** 188-93.

Jacobson, J., Duchen, M. R., Hothersall, J., Clark, J. B. & Heales, S. J. 2005. Induction Of Mitochondrial Oxidative Stress In Astrocytes By Nitric Oxide Precedes Disruption Of Energy Metabolism. *J Neurochem,* 95**,** 388-95.

Jiang, H., Ren, Y., Yuen, E. Y., Zhong, P., Ghaedi, M., Hu, Z., Azabdaftari, G., Nakaso, K., Yan, Z. & Feng, J. 2012. Parkin Controls Dopamine Utilization In Human Midbrain Dopaminergic Neurons Derived From Induced Pluripotent Stem Cells. *Nat Commun,* 3**,** 668.

Jimenez-Jimenez, F. J., Alonso-Navarro, H., Garcia-Martin, E. & Agundez, J. A. 2014. Comt Gene And Risk For Parkinson's Disease: A Systematic Review And Meta-Analysis. *Pharmacogenet Genomics,* 24, 331-9.

Kang, S. J., Scott, W. K., Li, Y. J., Hauser, M. A., Van Der Walt, J. M., Fujiwara, K., Mayhew, G. M., West, S. G., Vance, J. M. & Martin, E. R. 2006. Family-Based Case-Control Study Of Maoa And Maob Polymorphisms In Parkinson Disease. *Mov Disord,* 21, 2175-80.

Kapatos, G. 2013. The Neurobiology Of Tetrahydrobiopterin Biosynthesis: A Model For Regulation Of Gtp Cyclohydrolase I Gene Transcription Within Nigrostriatal Dopamine Neurons. *Iubmb Life,* 65, 323-33.

Khwanraj, K., Phruksaniyom, C., Madlah, S. & Dharmasaroja, P. 2015. Differential Expression Of Tyrosine Hydroxylase Protein And Apoptosis-Related Genes In Differentiated And Undifferentiated Sh-Sy5y Neuroblastoma Cells Treated With Mpp(.). *Neurol Res Int,* 2015, 734703.

Kilpatrick, I. C., Jones, M. W. & Phillipson, O. T. 1986. A Semiautomated Analysis Method For Catecholamines, Indoleamines, And Some Prominent Metabolites In Microdissected Regions Of The Nervous System: An Isocratic Hplc Technique Employing Coulometric Detection And Minimal Sample Preparation. *J Neurochem,* 46, 1865-76.

Kirkeby, A., Grealish, S., Wolf, D. A., Nelander, J., Wood, J., Lundblad, M., Lindvall, O. & Parmar, M. 2012. Generation Of Regionally Specified Neural Progenitors And Functional Neurons From Human Embryonic Stem Cells Under Defined Conditions. *Cell Rep,* 1, 703-14.

Klebe, S., Golmard, J. L., Nalls, M. A., Saad, M., Singleton, A. B., Bras, J. M., Hardy, J., Simon-Sanchez, J., Heutink, P., Kuhlenbaumer, G., Charfi, R., Klein, C., Hagenah, J., Gasser, T., Wurster, I., Lesage, S., Lorenz, D., Deuschl, G., Durif, F., Pollak, P., Damier, P., Tison, F., Durr, A., Amouyel, P., Lambert, J. C., Tzourio, C., Maubaret, C., Charbonnier-Beaupel, F., Tahiri, K., Vidailhet, M., Martinez, M., Brice, A., Corvol, J. C., French Parkinson's Disease Genetics Study, G. & International Parkinson's Disease Genomics, C. 2013. The Val158met Comt Polymorphism Is A Modifier Of The Age At Onset In Parkinson's Disease With A Sexual Dimorphism. *J Neurol Neurosurg Psychiatry,* 84, 666-73.

Kollalpitiya, Y. & Wimalasena, K. Transport Of Tryptophan Into Sh-Sy5y Neuronal Cells. 4th Annual Grasp Symposium, 2008 Wichita State University.

Korecka, J. A., Van Kesteren, R. E., Blaas, E., Spitzer, S. O., Kamstra, J. H., Smit, A. B., Swaab, D. F., Verhaagen, J. & Bossers, K. 2013. Phenotypic Characterization Of Retinoic Acid Differentiated Sh-Sy5y Cells By Transcriptional Profiling. *Plos One,* 8, E63862.

Kovalevich, J. & Langford, D. 2013. Considerations For The Use Of Sh-Sy5y Neuroblastoma Cells In Neurobiology. *Methods Mol Biol,* 1078, 9-21.

Kurian, M. A., Gissen, P., Smith, M., Heales, S., Jr. & Clayton, P. T. 2011a. The Monoamine Neurotransmitter Disorders: An Expanding Range Of Neurological Syndromes. *Lancet Neurol,* 10**,** 721-33.

Kurian, M. A., Li, Y., Zhen, J., Meyer, E., Hai, N., Christen, H. J., Hoffmann, G. F., Jardine, P., Von Moers, A., Mordekar, S. R., O'callaghan, F., Wassmer, E., Wraige, E., Dietrich, C., Lewis, T., Hyland, K., Heales, S., Jr., Sanger, T., Gissen, P., Assmann, B. E., Reith, M. E. & Maher, E. R. 2011b. Clinical And Molecular Characterisation Of Hereditary Dopamine Transporter Deficiency Syndrome: An Observational Cohort And Experimental Study. *Lancet Neurol,* 10**,** 54-62.

Kurth, J. H., Kurth, M. C., Poduslo, S. E. & Schwankhaus, J. D. 1993. Association Of A Monoamine Oxidase B Allele With Parkinson's Disease. *Ann Neurol,* 33**,** 368-72.

Launay, J. M., Del Pino, M., Chironi, G., Callebert, J., Peoc'h, K., Megnien, J. L., Mallet, J., Simon, A. & Rendu, F. 2009. Smoking Induces Long-Lasting Effects Through A Monoamine-Oxidase Epigenetic Regulation. *Plos One,* 4**,** E7959.

Longo, N. 2009. Disorders Of Biopterin Metabolism. *J Inherit Metab Dis,* 32**,** 333-42.

Lopes, F. M., Schroder, R., Da Frota, M. L., Jr., Zanotto-Filho, A., Muller, C. B., Pires, A. S., Meurer, R. T., Colpo, G. D., Gelain, D. P., Kapczinski, F., Moreira, J. C., Fernandes Mda, C. & Klamt, F. 2010. Comparison Between Proliferative And Neuron-Like Sh-Sy5y Cells As An In Vitro Model For Parkinson Disease Studies. *Brain Res,* 1337**,** 85-94.

Lotta, T., Vidgren, J., Tilgmann, C., Ulmanen, I., Melen, K., Julkunen, I. & Taskinen, J. 1995. Kinetics Of Human Soluble And Membrane-Bound Catechol O-Methyltransferase: A Revised Mechanism And Description Of The Thermolabile Variant Of The Enzyme. *Biochemistry,* 34**,** 4202-10.

Lovenberg, W., Weissbach, H. & Udenfriend, S. 1962. Aromatic L-Amino Acid Decarboxylase. *J Biol Chem,* 237**,** 89-93.

Lynch-Day, M. A., Mao, K., Wang, K., Zhao, M. & Klionsky, D. J. 2012. The Role Of Autophagy In Parkinson's Disease. *Cold Spring Harb Perspect Med,* 2**,** A009357.

Ma, H. & Zhu, G. 2014. The Dopamine System And Alcohol Dependence. *Shanghai Arch Psychiatry,* 26**,** 61-8.

Majors, R. E. 1994. Twenty-Five Years Of Hplc Column Development—A Commercial Perspective. *Lcgc,* 12**,** 11.

Mammucari, C. & Rizzuto, R. 2010. Signaling Pathways In Mitochondrial Dysfunction And Aging. *Mech Ageing Dev,* 131**,** 536-43.

Mandel, S., Weinreb, O., Amit, T. & Youdim, M. B. 2005. Mechanism Of Neuroprotective Action Of The Anti-Parkinson Drug Rasagiline And Its Derivatives. *Brain Res Brain Res Rev,* 48**,** 379-87.

Manning-Bog, A. B., Schule, B. & Langston, J. W. 2009. Alpha-Synuclein-Glucocerebrosidase Interactions In Pharmacological Gaucher Models: A Biological Link Between Gaucher Disease And Parkinsonism. *Neurotoxicology,* 30**,** 1127-32.

Mannisto, P. T. & Kaakkola, S. 1999. Catechol-O-Methyltransferase (Comt): Biochemistry, Molecular Biology, Pharmacology, And Clinical Efficacy Of The New Selective Comt Inhibitors. *Pharmacol Rev,* 51**,** 593-628.

Martin, A. J. & Synge, R. L. 1941. A New Form Of Chromatogram Employing Two Liquid Phases: A Theory Of Chromatography. 2. Application To The Micro-Determination Of The Higher Monoamino-Acids In Proteins. *Biochem J,* 35**,** 1358-68.

Mazzulli, J. R., Mishizen, A. J., Giasson, B. I., Lynch, D. R., Thomas, S. A., Nakashima, A., Nagatsu, T., Ota, A. & Ischiropoulos, H. 2006. Cytosolic Catechols Inhibit Alpha-Synuclein Aggregation And Facilitate The Formation Of Intracellular Soluble Oligomeric Intermediates. *J Neurosci,* 26**,** 10068-78.

Mazzulli, J. R., Xu, Y. H., Sun, Y., Knight, A. L., Mclean, P. J., Caldwell, G. A., Sidransky, E., Grabowski, G. A. & Krainc, D. 2011. Gaucher Disease Glucocerebrosidase And Alpha-Synuclein Form A Bidirectional Pathogenic Loop In Synucleinopathies. *Cell,* 146**,** 37-52.

Mcmillan, C. R., Sharma, R., Ottenhof, T. & Niles, L. P. 2007. Modulation Of Tyrosine Hydroxylase Expression By Melatonin In Human Sh-Sy5y Neuroblastoma Cells. *Neurosci Lett,* 419**,** 202-6.

Meiser, J., Weindl, D. & Hiller, K. 2013. Complexity Of Dopamine Metabolism. *Cell Commun Signal,* 11**,** 34.

Mencacci, N. E., Isaias, I. U., Reich, M. M., Ganos, C., Plagnol, V., Polke, J. M., Bras, J., Hersheson, J., Stamelou, M., Pittman, A. M., Noyce, A. J., Mok, K. Y., Opladen, T., Kunstmann, E., Hodecker, S., Munchau, A., Volkmann, J., Samnick, S., Sidle, K., Nanji, T., Sweeney, M. G., Houlden, H., Batla, A., Zecchinelli, A. L., Pezzoli, G., Marotta, G., Lees, A., Alegria, P., Krack, P., Cormier-Dequaire, F., Lesage, S., Brice, A., Heutink, P., Gasser, T., Lubbe, S. J., Morris, H. R., Taba, P., Koks, S., Majounie, E., Raphael Gibbs, J., Singleton, A., Hardy, J., Klebe, S., Bhatia, K. P., Wood, N. W., International Parkinson's Disease Genomics, C. & Consortium, U. C.-E. 2014. Parkinson's Disease In Gtp Cyclohydrolase 1 Mutation Carriers. *Brain,* 137**,** 2480-92.

Michel, T. M., Kasbauer, L., Gsell, W., Jecel, J., Sheldrick, A. J., Cortese, M., Nickl-Jockschat, T., Grunblatt, E. & Riederer, P. 2014. Aldehyde Dehydrogenase 2 In Sporadic Parkinson's Disease. *Parkinsonism Relat Disord,* 20 Suppl 1**,** S68-72.

Migdalska-Richards, A. & Schapira, A. H. 2016. The Relationship Between Glucocerebrosidase Mutations And Parkinson Disease. *J Neurochem,* 139 Suppl 1**,** 77-90.

Miksys, S., Rao, Y., Hoffmann, E., Mash, D. C. & Tyndale, R. F. 2002. Regional And Cellular Expression Of Cyp2d6 In Human Brain: Higher Levels In Alcoholics. *J Neurochem,* 82**,** 1376-87.

Mockus, S. M., Kumer, S. C. & Vrana, K. E. 1997. A Chimeric Tyrosine/Tryptophan Hydroxylase. The Tyrosine Hydroxylase Regulatory Domain Serves To Stabilize Enzyme Activity. *J Mol Neurosci,* 9, 35-48.

Mockus, S. M., Yohrling, G. J. T. & Vrana, K. E. 1998. Tyrosine Hydroxylase And Tryptophan Hydroxylase Do Not Form Heterotetramers. *J Mol Neurosci,* 10, 45-51.

Molochnikov, L., Rabey, J. M., Dobronevsky, E., Bonucelli, U., Ceravolo, R., Frosini, D., Grunblatt, E., Riederer, P., Jacob, C., Aharon-Peretz, J., Bashenko, Y., Youdim, M. B. & Mandel, S. A. 2012. A Molecular Signature In Blood Identifies Early Parkinson's Disease. *Mol Neurodegener,* 7, 26.

Moors, T., Paciotti, S., Chiasserini, D., Calabresi, P., Parnetti, L., Beccari, T. & Van De Berg, W. D. 2016. Lysosomal Dysfunction And Alpha-Synuclein Aggregation In Parkinson's Disease: Diagnostic Links. *Mov Disord,* 31, 791-801.

Munoz, P., Huenchuguala, S., Paris, I. & Segura-Aguilar, J. 2012. Dopamine Oxidation And Autophagy. *Parkinsons Dis,* 2012, 920953.

Muramatsu, S. 2010. [Gene Therapy For Parkinson Disease]. *Nihon Rinsho,* 68 Suppl 8, 646-9.

Nackley, A. G., Shabalina, S. A., Lambert, J. E., Conrad, M. S., Gibson, D. G., Spiridonov, A. N., Satterfield, S. K. & Diatchenko, L. 2009. Low Enzymatic Activity Haplotypes Of The Human Catechol-O-Methyltransferase Gene: Enrichment For Marker Snps. *Plos One,* 4, E5237.

Neumann, J., Bras, J., Deas, E., O'sullivan, S. S., Parkkinen, L., Lachmann, R. H., Li, A., Holton, J., Guerreiro, R., Paudel, R., Segarane, B., Singleton, A., Lees, A., Hardy, J., Houlden, H., Revesz, T. & Wood, N. W. 2009. Glucocerebrosidase Mutations In Clinical And Pathologically Proven Parkinson's Disease. *Brain,* 132, 1783-94.

Ng, J., Heales, S. J. & Kurian, M. A. 2014. Clinical Features And Pharmacotherapy Of Childhood Monoamine Neurotransmitter Disorders. *Paediatr Drugs,* 16, 275-91.

Nirenberg, M. J., Vaughan, R. A., Uhl, G. R., Kuhar, M. J. & Pickel, V. M. 1996. The Dopamine Transporter Is Localized To Dendritic And Axonal Plasma Membranes Of Nigrostriatal Dopaminergic Neurons. *J Neurosci,* 16, 436-47.

Nishida, Y., Adati, N., Ozawa, R., Maeda, A., Sakaki, Y. & Takeda, T. 2008. Identification And Classification Of Genes Regulated By Phosphatidylinositol 3-Kinase- And Trkb-Mediated Signalling Pathways During Neuronal Differentiation In Two Subtypes Of The Human Neuroblastoma Cell Line Sh-Sy5y. *Bmc Res Notes,* 1, 95.

Ohtsubo, K. & Marth, J. D. 2006. Glycosylation In Cellular Mechanisms Of Health And Disease. *Cell,* 126, 855-67.

Ormazabal, A., Garcia Cazorla, A., Perez Duenas, B., Pineda, M., Ruiz, A., Lopez Laso, E., Garcia Silva, M., Carilho, I., Barbot, C., Cormand, B., Ribases, M., Moller, L., Fernandez Alvarez, E., Campistol, J. & Artuch, R. 2006. [Usefulness Of Analysis Of Cerebrospinal Fluid For The Diagnosis Of Neurotransmitters And Pterin Defects

And Glucose And Folate Transport Deficiencies Across Blood Brain Barrier]. *Med Clin (Barc),* 127, 81-5.

Osellame, L. D., Rahim, A. A., Hargreaves, I. P., Gegg, M. E., Richard-Londt, A., Brandner, S., Waddington, S. N., Schapira, A. H. & Duchen, M. R. 2013. Mitochondria And Quality Control Defects In A Mouse Model Of Gaucher Disease--Links To Parkinson's Disease. *Cell Metab,* 17, 941-53.

Percudani, R. & Peracchi, A. 2003. A Genomic Overview Of Pyridoxal-Phosphate-Dependent Enzymes. *Embo Rep,* 4, 850-4.

Plotegher, N. & Duchen, M. R. 2017. Mitochondrial Dysfunction And Neurodegeneration In Lysosomal Storage Disorders. *Trends Mol Med,* 23, 116-134.

Reinhardt, P., Schmid, B., Burbulla, L. F., Schondorf, D. C., Wagner, L., Glatza, M., Hoing, S., Hargus, G., Heck, S. A., Dhingra, A., Wu, G., Muller, S., Brockmann, K., Kluba, T., Maisel, M., Kruger, R., Berg, D., Tsytsyura, Y., Thiel, C. S., Psathaki, O. E., Klingauf, J., Kuhlmann, T., Klewin, M., Muller, H., Gasser, T., Scholer, H. R. & Sterneckert, J. 2013. Genetic Correction Of A Lrrk2 Mutation In Human Ipscs Links Parkinsonian Neurodegeneration To Erk-Dependent Changes In Gene Expression. *Cell Stem Cell,* 12, 354-67.

Rempel, B. P. & Withers, S. G. 2008. Covalent Inhibitors Of Glycosidases And Their Applications In Biochemistry And Biology. *Glycobiology,* 18, 570-86.

Ridley, C. M., Thur, K. E., Shanahan, J., Thillaiappan, N. B., Shen, A., Uhl, K., Walden, C. M., Rahim, A. A., Waddington, S. N., Platt, F. M. & Van Der Spoel, A. C. 2013. Beta-Glucosidase 2 (Gba2) Activity And Imino Sugar Pharmacology. *J Biol Chem,* 288, 26052-66.

Riederer, P. & Laux, G. 2011. Mao-Inhibitors In Parkinson's Disease. *Exp Neurobiol,* 20, 1-17.

Riederer, P., Sofic, E., Rausch, W. D., Schmidt, B., Reynolds, G. P., Jellinger, K. & Youdim, M. B. 1989. Transition Metals, Ferritin, Glutathione, And Ascorbic Acid In Parkinsonian Brains. *J Neurochem,* 52, 515-20.

Ruottinen, H. M. & Rinne, U. K. 1998. Comt Inhibition In The Treatment Of Parkinson's Disease. *J Neurol,* 245, P25-34.

Russell, A. C., Simurina, M., Garcia, M. T., Novokmet, M., Wang, Y., Rudan, I., Campbell, H., Lauc, G., Thomas, M. G. & Wang, W. 2017. The N-Glycosylation Of Immunoglobulin G As A Novel Biomarker Of Parkinson's Disease. *Glycobiology,* 27, 501-510.

Saffari, A., Kolker, S., Hoffmann, G. F. & Ebrahimi-Fakhari, D. 2017. Linking Mitochondrial Dysfunction To Neurodegeneration In Lysosomal Storage Diseases. *J Inherit Metab Dis*.

Sai, Y., Chen, J., Ye, F., Zhao, Y., Zou, Z., Cao, J. & Dong, Z. 2013. Dopamine Release Suppression Dependent On An Increase Of Intracellular Ca(2+) Contributed To Rotenone-Induced Neurotoxicity In Pc12 Cells. *J Toxicol Pathol,* 26**,** 149-57.

Sai, Y., Wu, Q., Le, W., Ye, F., Li, Y. & Dong, Z. 2008. Rotenone-Induced Pc12 Cell Toxicity Is Caused By Oxidative Stress Resulting From Altered Dopamine Metabolism. *Toxicol In Vitro,* 22**,** 1461-8.

Santos, A. L. & Lindner, A. B. 2017. Protein Posttranslational Modifications: Roles In Aging And Age-Related Disease. *Oxid Med Cell Longev,* 2017**,** 5716409.

Santos, D. M. & Tiscornia, G. 2017. Induced Pluripotent Stem Cell Modeling Of Gaucher's Disease: What Have We Learned? *Int J Mol Sci,* 18.

Saunders-Pullman, R., Blau, N., Hyland, K., Zschocke, J., Nygaard, T., Raymond, D., Shanker, V., Mohrmann, K., Arnold, L., Tabbal, S., Deleon, D., Ford, B., Brin, M., Chouinard, S., Ozelius, L., Klein, C. & Bressman, S. B. 2004. Phenylalanine Loading As A Diagnostic Test For Drd: Interpreting The Utility Of The Test. *Mol Genet Metab,* 83**,** 207-12.

Schapira, A. H., Cooper, J. M., Dexter, D., Clark, J. B., Jenner, P. & Marsden, C. D. 1990. Mitochondrial Complex I Deficiency In Parkinson's Disease. *J Neurochem,* 54**,** 823-7.

Schendzielorz, N., Oinas, J. P., Myohanen, T. T., Reenila, I., Raasmaja, A. & Mannisto, P. T. 2013. Catechol-O-Methyltransferase (Comt) Protein Expression And Activity After Dopaminergic And Noradrenergic Lesions Of The Rat Brain. *Plos One,* 8**,** E61392.

Schieber, M. & Chandel, N. S. 2014. Ros Function In Redox Signaling And Oxidative Stress. *Curr Biol,* 24**,** R453-62.

Schmittgen, T. D. & Livak, K. J. 2008. Analyzing Real-Time Pcr Data By The Comparative Ct Method. *Nature Protocols,* 3**,** 1101-1108.

Sian, J., Dexter, D., Lees, A., Daniel, S., Agid, Y., Javoy-Agid, F., Jenner, P. & Marsden, C. D. 1994. Alterations In Glutathione Lveles In Parkinson's Disease And Other Neurodegenerative Disorders Affecting Basal Ganglia. *Annals Of Neurology,* 36**,** 8.

Sidransky, E. & Lopez, G. 2012. The Link Between The Gba Gene And Parkinsonism. *Lancet Neurol,* 11**,** 986-98.

Siegle, I., Fritz, P., Eckhardt, K., Zanger, U. M. & Eichelbaum, M. 2001. Cellular Localization And Regional Distribution Of Cyp2d6 Mrna And Protein Expression In Human Brain. *Pharmacogenetics,* 11**,** 237-45.

Smeyne, M. & Smeyne, R. J. 2013. Glutathione Metabolism And Parkinson's Disease. *Free Radic Biol Med,* 62**,** 13-25.

Stansley, B. J. & Yamamoto, B. K. 2015. L-Dopa And Brain Serotonin System Dysfunction. *Toxics,* 3**,** 75-88.

Stanta, J. L., Saldova, R., Struwe, W. B., Byrne, J. C., Leweke, F. M., Rothermund, M., Rahmoune, H., Levin, Y., Guest, P. C., Bahn, S. & Rudd, P. M. 2010. Identification Of N-Glycosylation Changes In The Csf And Serum In Patients With Schizophrenia. *J Proteome Res,* 9**,** 4476-89.

Stefanis, L. 2012. Alpha-Synuclein In Parkinson's Disease. *Cold Spring Harb Perspect Med,* 2**,** A009399.

Steinberger, D., Weber, Y., Korinthenberg, R., Deuschl, G., Benecke, R., Martinius, J. & Muller, U. 1998. High Penetrance And Pronounced Variation In Expressivity Of Gch1 Mutations In Five Families With Dopa-Responsive Dystonia. *Ann Neurol,* 43**,** 634-9.

Stott, S. R. W. & Ang, S. L. 2013. The Generation Of Midbrain Dopaminergic Neurons. *Patterning And Cell Type Specification In The Developing Cns And Pns: Comprehensive Developmental Neuroscience.*

Sulzer, D., Bogulavsky, J., Larsen, K. E., Behr, G., Karatekin, E., Kleinman, M. H., Turro, N., Krantz, D., Edwards, R. H., Greene, L. A. & Zecca, L. 2000. Neuromelanin Biosynthesis Is Driven By Excess Cytosolic Catecholamines Not Accumulated By Synaptic Vesicles. *Proc Natl Acad Sci U S A,* 97**,** 11869-74.

Takahashi, K. & Yamanaka, S. 2006. Induction Of Pluripotent Stem Cells From Mouse Embryonic And Adult Fibroblast Cultures By Defined Factors. *Cell,* 126**,** 663-76.

Thomas, P. & Smart, T. G. 2005. Hek293 Cell Line: A Vehicle For The Expression Of Recombinant Proteins. *J Pharmacol Toxicol Methods,* 51**,** 187-200.

Torres, G. E., Gainetdinov, R. R. & Caron, M. G. 2003. Plasma Membrane Monoamine Transporters: Structure, Regulation And Function. *Nat Rev Neurosci,* 4**,** 13-25.

Tunbridge, E. M. 2010. The Catechol-O-Methyltransferase Gene: Its Regulation And Polymorphisms. *Int Rev Neurobiol,* 95**,** 7-27.

Tunbridge, E. M., Lane, T. A. & Harrison, P. J. 2007. Expression Of Multiple Catechol-O-Methyltransferase (Comt) Mrna Variants In Human Brain. *Am J Med Genet B Neuropsychiatr Genet,* 144b**,** 834-9.

Vasiliou, V. & Nebert, D. W. 2005. Analysis And Update Of The Human Aldehyde Dehydrogenase (Aldh) Gene Family. *Hum Genomics,* 2**,** 138-43.

Veldman, M. B. & Lin, S. 2008. Zebrafish As A Developmental Model Organism For Pediatric Research. *Pediatr Res,* 64**,** 470-6.

Vielhaber, G., Pfeiffer, S., Brade, L., Lindner, B., Goldmann, T., Vollmer, E., Hintze, U., Wittern, K. P. & Wepf, R. 2001. Localization Of Ceramide And Glucosylceramide In Human Epidermis By Immunogold Electron Microscopy. *J Invest Dermatol,* 117**,** 1126-36.

Volchegorskii, I. A., Shemyakov, S. E., Turygin, V. V. & Malinovskaya, N. V. 2001. Comparative Analysis Of Age-Related Changes In Activities Of Monoamine

Oxidase-B And Antioxidant Defense Enzymes In Various Structures Of Human Brain. *Bull Exp Biol Med,* 132, 760-2.

Vrana, K. E., Walker, S. J., Rucker, P. & Liu, X. 1994. A Carboxyl Terminal Leucine Zipper Is Required For Tyrosine Hydroxylase Tetramer Formation. *J Neurochem,* 63, 2014-20.

Wang, X., Li, J., Dong, G. & Yue, J. 2014. The Endogenous Substrates Of Brain Cyp2d. *Eur J Pharmacol,* 724, 211-8.

Watabe, M. & Nakaki, T. 2008. Mitochondrial Complex I Inhibitor Rotenone Inhibits And Redistributes Vesicular Monoamine Transporter 2 Via Nitration In Human Dopaminergic Sh-Sy5y Cells. *Mol Pharmacol,* 74, 933-40.

Weil, H. & Williams, T. I. 1951. Early History Of Chromatography. *Nature,* 167, 906-7.

Whittaker, J. W. 2016. Intracellular Trafficking Of The Pyridoxal Cofactor. Implications For Health And Metabolic Disease. *Arch Biochem Biophys,* 592, 20-6.

Wider, C., Lincoln, S., Dachsel, J. C., Kapatos, G., Heckman, M. G., Diehl, N. N., Papapetropoulos, S., Mash, D., Rajput, A., Rajput, A. H., Dickson, D. W., Wszolek, Z. K. & Farrer, M. J. 2009. Gch1 Expression In Human Cerebellum From Healthy Individuals Is Not Gender Dependent. *Neurosci Lett,* 462, 73-5.

Winchester, B. 2005. Lysosomal Metabolism Of Glycoproteins. *Glycobiology,* 15, 1r-15r.

Woodard, C. M., Campos, B. A., Kuo, S. H., Nirenberg, M. J., Nestor, M. W., Zimmer, M., Mosharov, E. V., Sulzer, D., Zhou, H., Paull, D., Clark, L., Schadt, E. E., Sardi, S. P., Rubin, L., Eggan, K., Brock, M., Lipnick, S., Rao, M., Chang, S., Li, A. & Noggle, S. A. 2014. Ipsc-Derived Dopamine Neurons Reveal Differences Between Monozygotic Twins Discordant For Parkinson's Disease. *Cell Rep,* 9, 1173-82.

Wu, R. M., Cheng, C. W., Chen, K. H., Lu, S. L., Shan, D. E., Ho, Y. F. & Chern, H. D. 2001. The Comt L Allele Modifies The Association Between Maob Polymorphism And Pd In Taiwanese. *Neurology,* 56, 375-82.

Xicoy, H., Wieringa, B. & Martens, G. J. 2017. The Sh-Sy5y Cell Line In Parkinson's Disease Research: A Systematic Review. *Mol Neurodegener,* 12, 10.

Youdim, M. B. & Bakhle, Y. S. 2006. Monoamine Oxidase: Isoforms And Inhibitors In Parkinson's Disease And Depressive Illness. *Br J Pharmacol,* 147 Suppl 1, S287-96.

Youdim, M. B., Fridkin, M. & Zheng, H. 2004. Novel Bifunctional Drugs Targeting Monoamine Oxidase Inhibition And Iron Chelation As An Approach To Neuroprotection In Parkinson's Disease And Other Neurodegenerative Diseases. *J Neural Transm (Vienna),* 111, 1455-71.

Youdim, M. B. & Weinstock, M. 2001. Molecular Basis Of Neuroprotective Activities Of Rasagiline And The Anti-Alzheimer Drug Tv3326 [(N-Propargyl-(3r)Aminoindan-5-Yl)-Ethyl Methyl Carbamate]. *Cell Mol Neurobiol,* 21, 555-73.

Zhu, M. Y. & Juorio, A. V. 1995. Aromatic L-Amino Acid Decarboxylase: Biological Characterization And Functional Role. *Gen Pharmacol,* 26, 681-96.